Fall 2014

Rock scour in hydraulic laboratory analog scour models

Ali Reza Firoozfar
University of Iowa

ROCK SCOUR IN HYDRAULIC LABORATORY ANALOG SCOUR MODELS

by

Ali Reza Firoozfar

A thesis submitted in partial fulfillment
of the requirements for the Doctor of
Philosophy degree in Civil and Environmental Engineering
in the Graduate College of
The University of Iowa

December 2014

Thesis Supervisor: Professor Larry J. Weber

Professor Athanasios N. Papanicolaou

Graduate College
The University of
Iowa Iowa City, Iowa

CERTIFICATE OF PPROVAL

PH.D. THESIS

This is to certify that the Ph.D. thesis of

Ali Reza Firoozfar

has been approved by the Examining Committee
for the thesis requirement for the Doctor of Philosophy
degree in Civil and Environmental Engineering at the December 2014
graduation.

Thesis Committee:

Larry J. Weber, Thesis Supervisor

Athanasios N. Papanicolaou, Thesis Supervisor

A. Jacob Odgaard

Colby C. Swan

Marian Muste

To my family who have always supported me with infinite love.

ACKNOWLEDGMENTS

First of all, I would like to thank my advisors, Professor & Director Larry Weber and Professor Thanos Papanicolaou, who provided me the opportunity to work under their supervision. I am very grateful for the possibilities that they gave me to perform this research. During the past four years I had the chance to discuss about the research and learn a lot from them through one to one interaction and meetings. This research study was sponsored by Public Utility District No. 2 of Grant County, Washington (GCPUD). I am grateful to GCPUD for the support and cooperation. Special thanks are given to Mr. Duncan Hay of Oakwood Consulting Inc. for his wealth of practical experience to this laboratory study and his contributions to this project. Also, I would like to thank Mr. Andy Craig, Mr. Troy Lyons and Mr. Brandon Barquist for their help towards the completion of this research. Finally, I really appreciate my family for their support and help through all stages of my life.

ABSTRACT

Erosional processes of solid materials have been the focus of many researchers around the world. Erosion can commence within a wide range of material strengths depending on the amount of water-driven energy and material properties. Erosion could also occur due to Aeolian effects as well as chemical weathering but these forcings are not of the focus of this research. Instead, the focus here is on rock erosion in waterways and in particular downstream of dams.

Rock erosion mostly takes place at the downstream of dams where the water conveys through the spillbays from upstream to the downstream during an extreme event. This phenomenon threatens both the structural soundness of the dam with implications to the public safety. It usually occurs when the applied hydrodynamic forces (average and fluctuating) exceed the strength of the rock mass formation. Rock scour at the downstream of dams due to high velocity impinging jet is a complex and highly dynamic process. So a deeper understanding of the process is crucial to determine the rock scour rate and extent.

Hydraulic laboratory models have been employed to investigate hydraulic processes and proved to be reliable tools for testing soil/sediment erosion; however, the study of rock scour remains challenging. The prototype rock formation cannot be utilized in the laboratory models because the flowing water in the scaled model contains much less energy and exerts less forcing. On the other hand, the use of granular sediment (non-cohesive), as a standalone approach to mimic the rock formation is not a precise method, since it will most probably lead to inaccurate results.

The idea of using a mixture of granular and cohesive sediment is investigated here to adequately simulate the rock erosion process in the laboratory scaled models. The granular sediment represents the rock blocks while the cohesive additive is a binder to keep the granular sediment together.

The rock scour process can occur through four mechanisms; fracture failure, block removal, fatigue failure and abrasion. In this study, because the focus is on the hydrodynamic forcing effects on rock erosion, we assume that in the completely and intermittently jointed rock, erosion is mostly governed by fracture, block removal and fatigue failure. Abrasion is triggered by collisional effects and is not the focus here. So, we hypothesize that if the rock formation considered being pre-fractured, it can be simulated using a mixture of non-cohesive sediment with cohesive additive.

This method was utilized to assess the rock scour process at the downstream of the Priest Rapids Dam. The Priest Rapids Dam project was part of a series of projects that was conducted at IIHR-Hydroscience & Engineering at The University of Iowa and sponsored by the Public Utility District No. 2 of Grant County, Ephrata, Washington (GCPUD) to investigate juvenile salmonid migration at the Wanapum/Priest Rapids Development. It is a hydroelectric, concrete gravity, and mid-elevation dam owned and operated by Public Utility District No. 2 of Grant County, Washington (the "District").

To aid the District in their evaluation of fish passage, IIHR-Hydroscience & Engineering constructed comprehensive three-dimensional physical models of the forebay and tailrace of Priest Rapids Dam and a third model of spillbays 19-22 and powerhouse Unit 1 (sectional model).

As part of the last phase of the project, it was crucial to assess the effects of the newly designed fish bypass system on the downstream rock foundation scour. To investigate this process, the 1:64 Froude-based scale tailrace model of the dam was utilized. The mixture of gravel, bentonite clay, and water was employed to mimic the rock formation and simulate the bedrock scour process in the model. Series of preliminary experiments were conducted to find the optimum mixture of gravel, bentonite and water to accurately replicate an existing scour hole observed in the prototype tailrace. Two scenarios were considered. First, tests were conducted to estimate the scour potential downstream of the fish bypass, which is currently under construction. Second, the scour potential downstream of the dam was also assessed for the Probable Maximum Flood (PMF) with the fish bypass system running. Based on the model tests results and observations, the simulated bedrock (mixture of gravel and cohesive bentonite) was able to replicate the rock scour mechanisms, i.e. fracture process, block removal and fatigue observed in nature. During the fish bypass scour tests, it was observed that the erosion process occurs in the form of block removal and fatigue failure.

During the PMF scour test, instead, it was observed that the mixture is eroded in chunks of substrate. This process can be representative of fracture failure in rock which occurs when the induced pressure fluctuation exceeds the fracture strength or equivalently toughness of the rock. In the preliminary phase of this work it was recognized that a prerequisite for replicating the processes in the laboratory is the proper preparation of the mixture. There is limited information available in the literature about how much cohesive additive is required to simulate the erosional strength of the prototype rock formation.

For this reason, in this study the effort has been made to develop a method to simulate the rock formation for studying rock scour process in the laboratory analog scaled models. To simulate the bedrock formation, various combination of granular sediment (gravel), cohesive additive, and water were created and tested. Choosing an appropriate cohesive additive concentration is critical and nearly a balancing act. An appropriate cohesive additive concentration should be cohesive enough to bind the material and not too strong to be eroded by the flowing water in the scaled models. Moreover, its properties should not change over time. Various cohesive additives can be mentioned i.e. kaolin clay, bentonite clay, cement, grease, paraffin wax. Among all of them, bentonite clay was chosen as the appropriate cohesive additive due to its swelling characteristic. When bentonite is mixed with granular sediment, it is restricted by the non-cohesive sediment grains. The bentonite expands to fill the voids and forms a tough, leathery mineral mastic through which water cannot readily move.

In order to assess the erodibility of the mixture the Jet Erosion Test (JET) apparatus was used. The JET apparatus is a vertical, submerged, circular, turbulent impinging jet which is widely accepted and utilized to assess cohesive soil erosion through flow impingement. There are devices such as flumes which could be effectively used for bank erosion where the flow shear action is prevalent. In this study, it was sought important that the forcing replicated in the experiments was of the same nature (normal impinging forcing instead of shear forcing) as observed in the downstream end of a dam. For this reason, JET was chosen as it provided a larger range of stresses (ranging between 100-1000 Pa) comparing to the flume device. The apparatus was

designed based on the device developed by Hanson and Hunt (2007) and built at the IIHR-Hydroscience & Engineering.

Various replicate samples were made with different combinations of gravel, sodium bentonite clay, and water. To determine the erosional strength of the samples (critical stress) they were tested using the JET apparatus. The critical stress was determined as the stress associated with zero eroded mass. The results revealed that the erosional strength of the simulated bedrock mixtures highly depends on the amount of adhesive component (bentonite clay). The mixtures with the higher percentage of bentonite clay are less susceptible to erosion. The erosion threshold plot - similar to Annandale's plot - for the simulated bedrock mixtures was developed.

Using the erosional strength of the simulated bedrock mixtures, a step-by-step systematic method was developed to determine the optimum combination of weakly cohesive substrate in order to simulate the strength of the prototype bedrock. The method is based on the Annandale's erodibility index method and requires information about the prototype bedrock strength (erodibility index). The method is explained in conjunction with the Priest Rapids Dam project example.

The old trial and error method to establish an optimum weakly cohesive substrate is costly and time consuming especially in the case of large scale laboratory models. Also, the applicability of the method would be questionable when there is not enough information or a past data set that can be used as a baseline (witness) test. The new method eliminates these problems and the optimum mixture can be established using the geological information of the prototype bedrock formation.

PUBLIC ABSTRACT

Hydraulic structures safety is a critical aspect in the field of hydraulic engineering. Generally, water-driven erosion threatens the safety of hydraulic structures. Bedrock erosion especially at the downstream of dams due to an impinging jet is a complicated process and needs to be further investigated. Analog hydraulic models have been utilized to evaluate rock scour process in laboratories to gain an improved insight about the key-mechanisms of the rock scour; however, the substrate used in the models has different properties than the ones in the prototype. The use of non-cohesive substrate cannot accurately replicate the rock erosion phenomenon. The idea of utilizing a mixture of cohesive and non-cohesive material is an approach that was adopted here to simulate rock erosion in scaled models. There is limited information about the amount of cohesive additive that is needed to accurately replicate the erosional strength of the bedrock found in the field. To simulate bedrock substrate in the laboratory, mixture samples with different combination of gravel, cohesive bentonite clay, and water were prepared. Series of experiments were conducted using a JET device to determine the erodibility of the samples. The erodibility of the simulated bedrock is formulated to the erosional strength of the prototype bedrock for a specific site project. Using the erodibility of simulated bedrock mixtures, a step-by-step systematic method was developed to determine the optimum combination of weakly cohesive substrate to simulate the strength of the prototype bedrock for use in the laboratory analog scaled models to investigate rock scour process.

TABLE OF CONTENTS

LIST OF TABLES

LIST OF FIGURES

CHAPTER 1 INTRODUCTION

1.1. Introduction

During the last century, the evolution of technology has led to many impressive improvements to dams and their ability to produce energy. Aside from their ability to produce electrical energy as a clean energy source, dams play a key role in controlling extreme flood events. For instance, they are equipped with hydraulic structures such as a spillway, crest weir, etc. that enable them to convey water from upstream to downstream during floods. However, this process generates highly energetic flows that can erode the stream bed and expose the rock underneath it, which can compromise the structural stability of the dams and adversely affect the environment. This energy needs to be dissipated downstream in order to prevent any damage to the structures, i.e., erosion of the downstream foundation (Bollaert, 2002; Annandale, 2006).

The high potential for scour formation represents one of the unavoidable consequences of discharging flow through the spillways into the downstream end of dams. Scour formation and evolution are key agents in the acceleration of bedrock exposure, fractures, and ultimately in foundation failure (Bollaert and Schleiss, 2005). Scour exposes the parent rock material underneath the active layer and leads to rock exposure and the inception of rock erosion. As noted earlier, this phenomenon happens primarily downstream of dams, where the outflow from the spillways contains a significant amount of energy due to the high velocity. Neglecting the bedrock scouring in such events might pose a threat not only to the infrastructure's safety but also to the safety of the general public and property (Annandale, 2006). Consequently, having a better understanding of the process and key parameters are crucial to identifying rock

scour potential and rate. There are many examples of observing large scour holes at the downstream of dams. For instance, at the Malpaso Dam in Mexico, a large scour hole occurred during the release of 3,000 cms water from the weir into the stilling basin over a period of two weeks, while the maximum design flow for the weir was 11,000 cms. This caused severe damage to the stilling basin as well as to the rock foundation (Bribiesca and Viscaino, 1973). Kariba Dam in Zimbabwe (Ramos, 1982), shown in Figure 1-1, is another example.

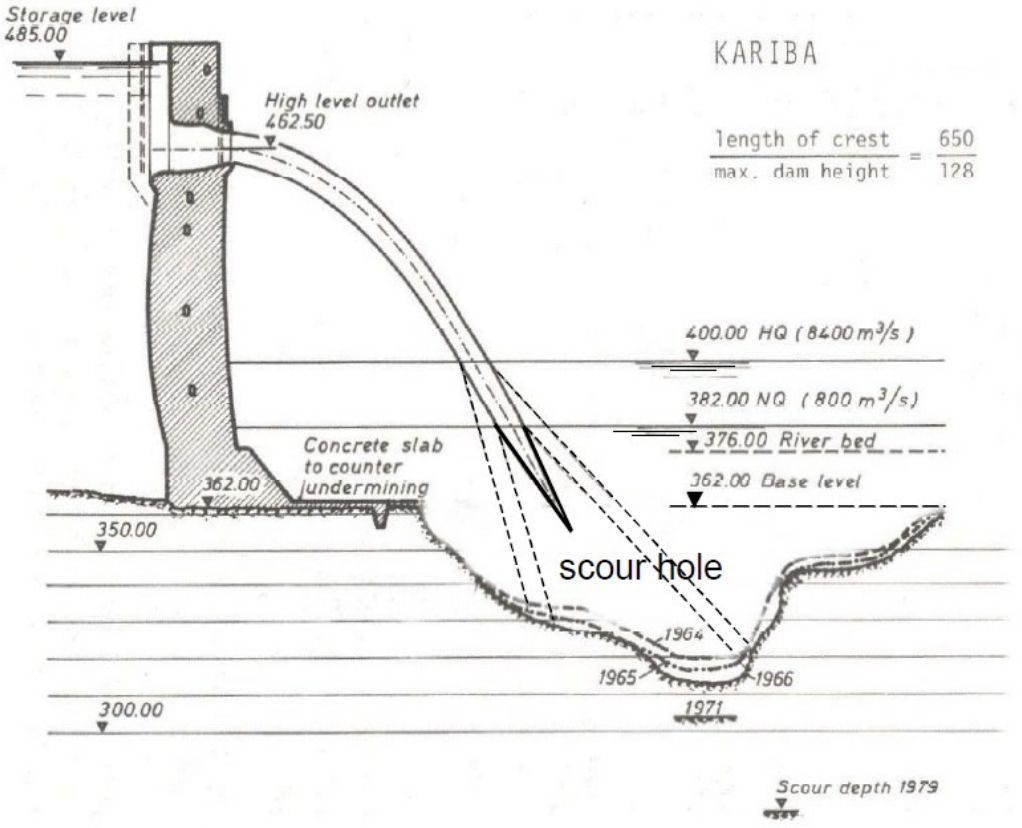

Figure 1-1. Kariba Dam in Zimbabwe, the high level outlet and scour hole at the downstream of the dam (Whittaker and Schleiss, 1984)

Rock scour can occur in both high- and mid-elevation dams. One example is the Priest Rapids Dam in the State of Washington, USA. A full open gate release from spillbay 22 (65,000 cfs) that occurred at the Priest Rapids Project between May 6 and June 5, 2003 resulted in a large scour hole downstream of spillbay 22, as shown in Figure 1-2. The deepest point of the scour hole is at elevation ~357.7 ft. It is unknown whether the scour downstream of spillbay 22 has reached an equilibrium state.

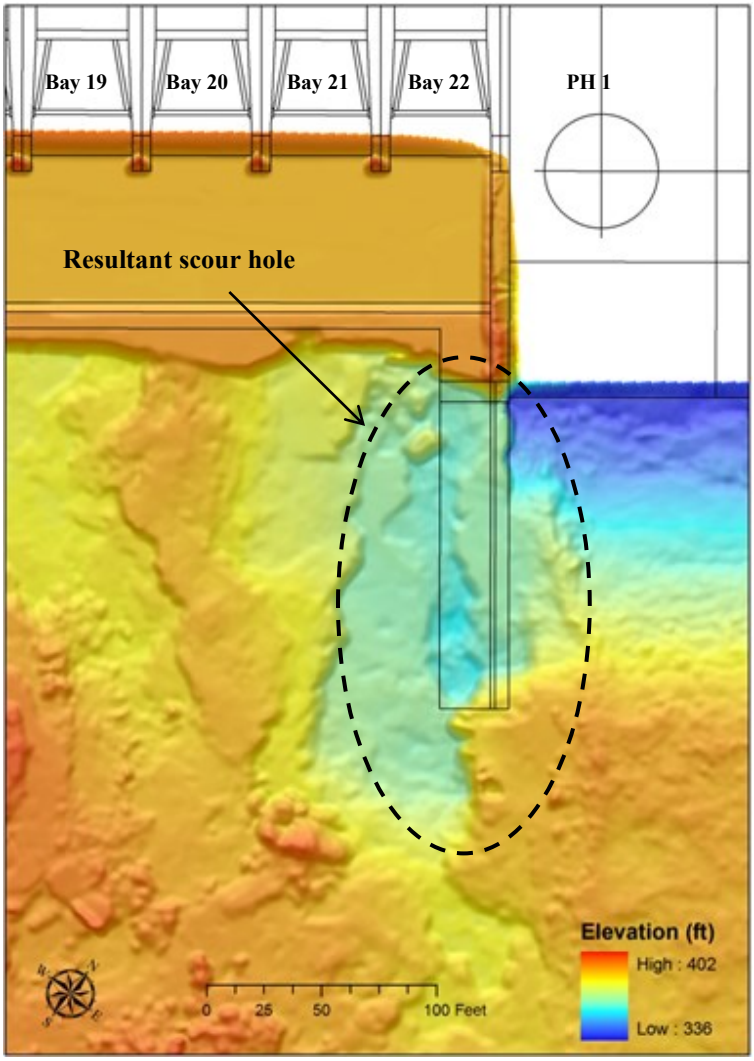

Figure 1-2. Resultant scour hole from spillbay 22 full open gate release (65,000 cfs) at the Priest Rapids Dam (Tetra Tech Inc., 2010)

The highly-dynamic rock scouring process is governed by the interaction among three phases: water, air, and solid (i.e., rock). The two most important physical processes to consider are the hydrodynamic jacking, which fragments or fractures the rock, and the hydrodynamic uplift, which leads to the ejection/dislodgement of the rock from its original position (Bollaert and Schleiss, 2003).

Some empirical and semi-empirical studies of a different nature have been conducted to investigate rock scour mechanisms and to quantify their rate and extent. These studies can be divided into 1) methods that consider only the maximum value of fluctuating pressures exerted on the rock skeleton, 2) methods that are based on the pressure gradient at the top and bottom of the rock, and 3) methods that consider the wave propagation theory for pressure inside of the rock joint (Bollaert and Schleiss, 2003).

Hydraulic modeling has been shown to be a reliable tool to investigate hydraulic phenomena; however, rock scour studies have been proven to pose many challenges. Since flowing water in the scaled models contains much less energy than in the prototype, utilizing the prototype rock in the model is unrealistic for attaining the goal. Furthermore, the use of non-cohesive material leads to unrealistic erosion results, i.e., overestimating the scour extent, underestimating the scour rate, and being unable to simulate the shape and steep side slope of the observed scour holes in the field.

The idea of using a mixture of non-cohesive material with a cohesive additive is an approach that has been adopted to simulate rock erosion in the scaled models. For bedrock scouring simulations, the strength of the substrate in the model is usually lowered in order to assist in generating erosion through a smaller magnitude of erosive

forces (Thompson and Wohl, 2013). However, while the general idea of this approach is clear, there is limited available information about the methods for testing rock erosion and the amount of cohesive additive that is necessary to accurately simulate the strength of bedrock in the field.

In order to gain a deeper insight into rock erosion features and key mechanisms, analog scour models have been utilized to explore the rock scour process. While the materials used in analog models are not similar to the ones in the prototype, they are able to reproduce key features of the phenomenon (Schumm *et al.*, 1987).

Because rock scour is a very complicated process and hydraulic models are robust tools to provide better insight into the hydraulic and sedimentology processes, using analog models to investigate rock scour could yield significant results. Consequently, the use of analog models warrants further investigation in order to develop a method to simulate the existing prototype bedrock in the laboratory.

1.2. Hypothesis

The rock scour process at the downstream of dams that is caused by a high velocity impinging jet results from the following four mechanisms that will be further discussed in CHAPTER 2: brittle fracture failure, block removal, fatigue failure, and abrasion.

In this study, we assume that the rock erosion process in jointed (or equivalently discontinuous) rocks due to an impinging jet is primarily attributable to subcritical failure and block removal rather than to brittle fracture.

Therefore, we suggest that for simulating the jointed rocks for use in the laboratory scaled models, we can assume that the rock is pre-fractured. Based on this assessment, two types of failure may occur, depending on the magnitude of the hydrodynamic forcing relative to rock strength: block removal and fatigue failure, as defined by a network of sub-fractures.

Since the rock was considered to be pre-fractured, we hypothesize that the jointed rock can be simulated using the mixture of non-cohesive sediment, which represents the rock blocks, and cohesive material as a binder that can provide enough force to keep the non-cohesive material particles together.

1.3. Goals and Objectives

The main objective of the current study is to use a mixture of cohesive and non-cohesive materials applicable to analog laboratory scour models in order to develop a laboratory method that can simulate the erosional strength of prototype bedrock. The specific objectives are as follows:

- Validate the aforementioned hypothesis.
- Determine the erodibility of the modeled bedrock and formulate it to the erodibility of the rock in the prototype for the specific site project.
- Develop a step-by-step method for choosing an appropriate weakly cohesive substrate to simulate the prototype rock's erosional strength for use in the scaled laboratory analog scour models.

CHAPTER 2 BACKGROUND

2.1. Conceptual Models of Rock Scour

Akhmedov (1988) developed a conceptual model to describe the scour process in jointed rock formations. The key parameters involved in conceptual models are the erosive force of flowing water and the rock mass properties. The conceptual model consists of the following three stages:

1. The first stage in the rock scour process is the removal of rock fragments, which results from the hydraulic pressure gradient that is induced by the turbulent fluctuation of flowing water in the boundary of flow and rock mass. This stage is mainly affected by the rock joint characteristics. The rock fragments are removed when the hydraulic force exceeds the resistance force of the rock block (i.e., the submerged weight of the block and friction forces).
2. Due to the increase in flow area, the energy of the water flowing over the unit area decreases as the scour process proceeds, but it is powerful enough to remove the rock fragments. In this stage, the smaller rock blocks are disturbed and removed. Moreover, the abrasive force of the flowing water becomes an important factor.
3. In the last stage, the flowing water does not have enough energy to disturb the rock block, but the abrasive force is sufficient to cause scour. In this stage, the strength of the rock mass is considered the most important factor.

Annandale (1995) proposed another conceptual model of the rock scour process that is based on a rational correlation between the energy of flow (i.e., the rate of energy dissipation of flow) and resistance of the earth material to erosion (i.e., the erodibility of

the earth material). Annandale's conceptual model of scour can be summarized in three stages (Figure 2-1): jacking, dislodgement, and displacement.

Induced pressure fluctuation at the boundary results in the jacking out of the rock fragments from the rock mass formation. The jacked out fragment is then dislodged and displaced by the power of flow.

The correlation between the rate of energy dissipation (P) and the resistance of rock formation to erosion can be expressed as:

$$P = f(K_h) \quad \text{(Eq. 2-1)}$$

If $P > f(K_h)$, then the rate of energy dissipation exceeds the resistance to erosion, so the rock formation is expected to be eroded. Otherwise, the erosion process would not be expected to occur.

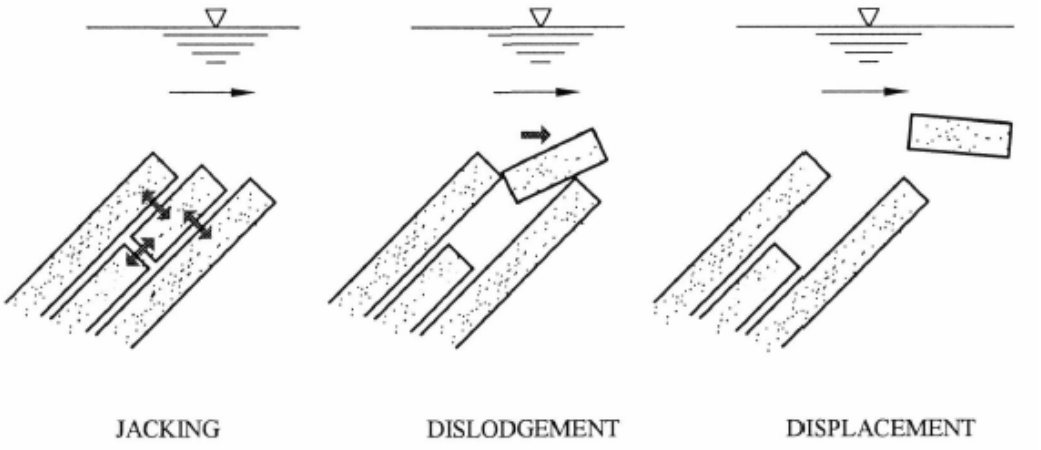

Figure 2-1. Conceptual model depicting the stages in the rock scour process (Annandale, 1995)

2.2. Rock Scouring Mechanisms

There is a misguided belief in the literature that, in the case of turbulent flows, rock erosion is due to the applied shear stress caused by flowing water. Annandale (2006) demonstrated that the fluctuating pressure (normal stress) leads to the erosive capacity of water and suggested using this concept instead of the shear stress concept to investigate rock erosion (Annandale, 2006). Rock scour can occur through four processes: brittle fracture, block removal, fatigue failure, and abrasion. Figure 2-2 depicts the physical-mechanical processes that are responsible for the rock formation scour that is due to high velocity impinging jets.

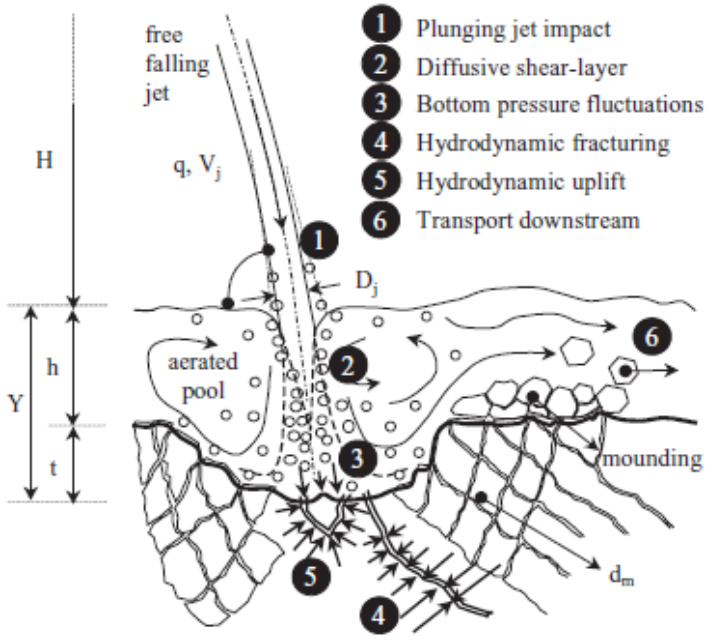

Figure 2-2. Processes responsible for a rock formation's scour phenomenon (Bollaert and Schleiss, 2003)

The first three processes are the result of fluctuating pressure (Bollaert, 2002). The abrasion type of rock scour is due to the effects of suspended rock fragments in the water column or of removed rock sliding on the surface of bed rock, which is considered minimal here (Annandale, 2007). The different rock scour mechanisms are detailed in the following sections in which they are presented in a sequential mode that begins with the processes corresponding to the largest magnitude of hydrodynamic forcing. Abrasion is included, but it is primarily derived from collisional effects.

Scour in general is a function of time and the magnitude of hydrodynamic forces. This becomes pronounced in the scour of rocks' elements. It is not only the magnitude of hydrodynamic forces that can lead to the fracturing of rock and the further evolution of the scour hole, but it is also the frequency of the events that exceed threshold conditions. In several instances, the magnitude may not be much higher than the resistance, but that rock element may experience fatigue, which explains why intermittently joint rocks in some instances may fracture at magnitudes that are less than those corresponding to uplift. In some ways, it is not only the magnitude that matters but also the pulsing and resonance character of the phenomenon. Figure 2-3 illustrates the sequence of the rock mass formation failure process.

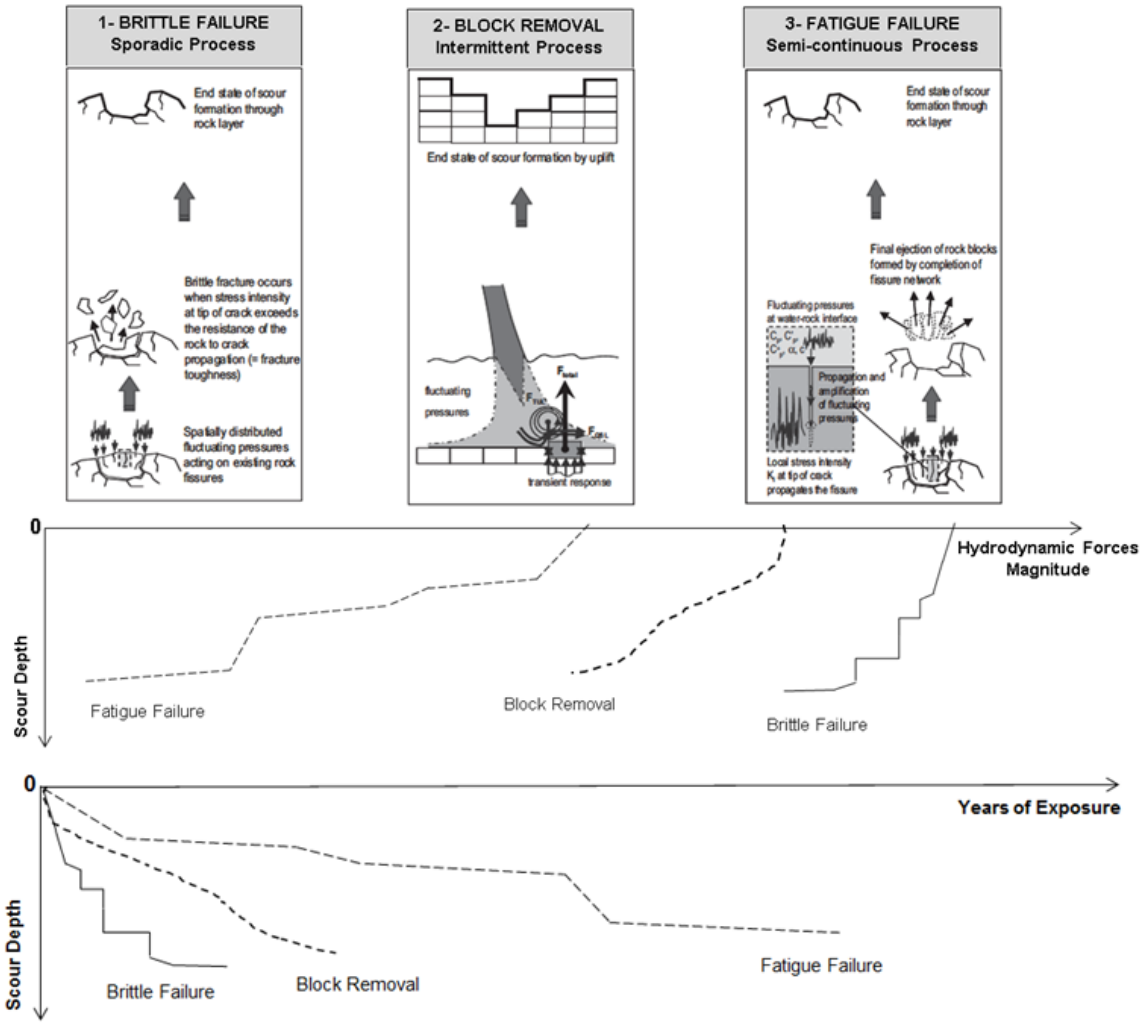

Figure 2-3. Sequence of the rock mass formation failure phenomenon (top schematic from Bollaert, 2010)

2.2.1. Brittle Fracture

A brittle fracture failure occurs when the stress intensity, K, at the tip of the close-ended fissures exceeds the fracture toughness of the rock, K_I:

$$K \geq K_I \qquad \text{(Eq. 2-2)}$$

With respect to the fracture mechanisms, three loading modes are possible: the opening, sliding, and tearing modes (Figure 2-4). The opening mode of fracture is

dominant in a rock mass fracture that is caused by hydrodynamic forces. However, a combined fracture mode is also possible (Bollaert, 2002).

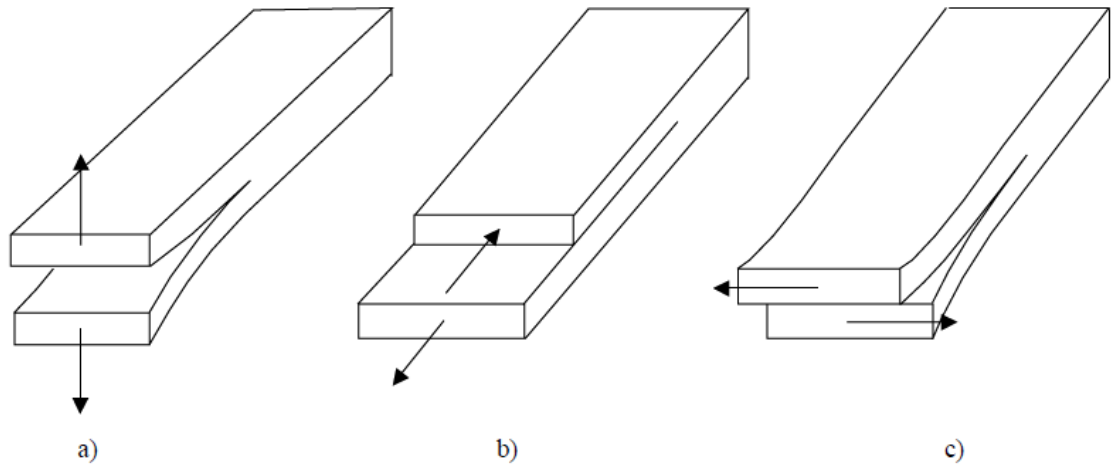

Figure 2-4. Three modes of the fracture : a) mode I, opening mode, b) mode II sliding mode, and c) mode III, tearing mode

The turbulent fluctuating pressure in the flowing water creates fluctuating pressure at the tip of the close-ended fissures in the rock, which causes the rock to fracture into the opening mode (mode I) (Annandale, 2006). Atkinson (1987) developed an equation to calculate the stress intensity:

$$K = \sigma_{water} \sqrt{\pi\, a\, f} \qquad \text{(Eq. 2-3)}$$

where K is the stress intensity (MPa $\sqrt{m}$), a is the crack length (m), σ_{water} is the pressure at the tip of crack, and f is a function that accounts for the geometry of the rock block as well as the crack extension, loading conditions, and edge effects. The value of f can be calculated through the formulas that are provided by Bollaert (2002).

Bollaert (2002) developed the regression functions for computing the fracture toughness of rock (K_I) using the rock's tensile strength, Unconfined Compressive Strength (UCS), and confining stress.

In this type of failure, the fluctuating turbulent pressure results in the shear intensity. A brittle fracture causes the rock to explode into small pieces (Figure 2-5). As with block removal, the brittle fracture is also an instantaneous failure that occurs as soon as the shear intensity becomes larger than the fracture roughness of the rock.

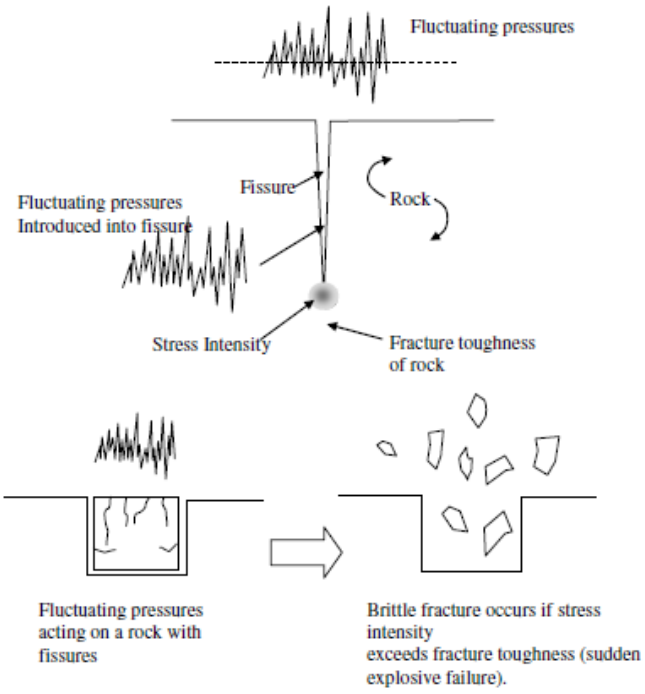

Figure 2-5. Brittle fracture failure (Annandale, 2006)

2.2.2. Block Removal

Applied force induced by fluctuating pressure (F_{down}) causes an increase in the magnitude of pressure at the base of the rock block (F_{up}) because of the transient and

resonance phenomenon in the joint of the rock block (Annandale, 2006; Schmitt *et al.,* 2012).

As soon as the upward force exceeds the submerged weight of the block and the friction force on the sides of block, rock block removal, which is an intermittent mechanism of failure in jointed rock, will occur. Figure 2-6 shows a schematic of rock block and its acting forces.

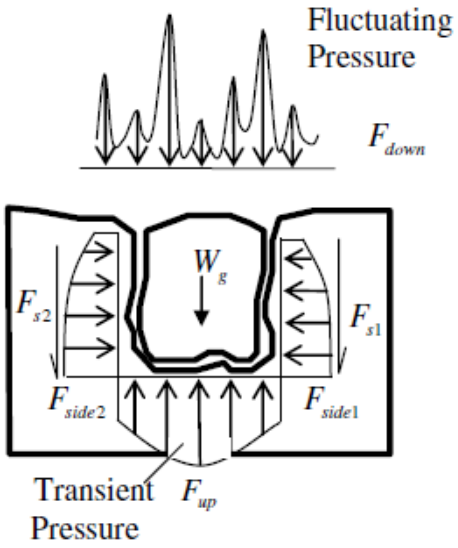

Figure 2-6. Block removal failure (Annandale, 2006)

For computing the block removal possibility, the forces acting on a single block, taking into consideration all of the effective forces and integrating them over the pulse period, should be considered in a simple form of the momentum equation (Bollaert, 2002):

$$\int_0^{\Delta t}\left(F_{up} - F_{down} - W_g - F_{s1} - F_{s2}\right)dt = F_{\Delta t} = m\,V_{\Delta t} \qquad \text{(Eq. 2-4)}$$

where F_{up} is total upward forces due to the transient pressure in the joint, F_{down} is the total downward forces due to the fluctuating pressure at the top of the block, W_g is the submerged weight of the block, F_{s1} and F_{s2} are the friction forces on the sides of the block, $F_{\Delta t}$ is the net applied force over the time period Δt, m is the mass of block, and $V_{\Delta t}$ is the velocity of the block. It can be concluded that the height at which the block will be displaced can be calculated using (Bollaert, 2002):

$$h = \frac{V_{\Delta t}^2}{2g} \quad \text{(Eq. 2-5)}$$

If the calculated block displacement, h, exceeds the height of the block, then it will be removed. Also, the required power to move the block is:

$$\frac{E}{\Delta t} = F_{\Delta t}\ \frac{h}{\Delta t} = F_{\Delta t}\ V_{\Delta t} \quad \text{(Eq. 2-6)}$$

2.2.3. Sub-Critical Failure (Fatigue)

When the stress intensity caused by the fluctuating turbulent pressure does not exceed the fracture toughness of rock, fatigue failure occurs after a period of time (Figure 2-7). When the fluctuating pressure acts continuously on the close-ended fissures, it will eventually break the rock. This kind of failure is apparently time dependent (Annandale, 2007).

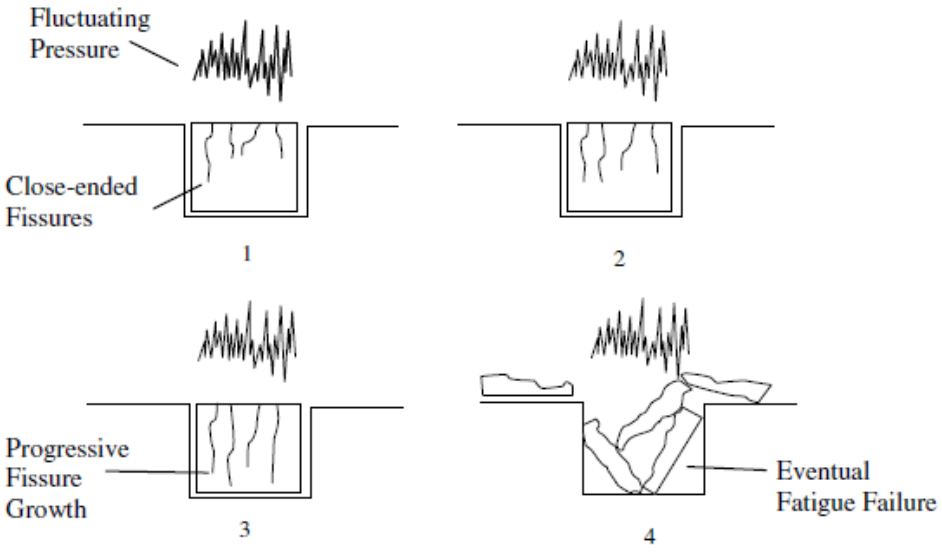

Figure 2-7. Fatigue failure of rock (Annandale, 2006)

2.2.4. Abrasion

Failure due to abrasion usually occurs when the flow is abrasive enough relative to the rock formation's resistance to scour. In this type of failure, two possibilities exist: first, the suspended pieces of rock affect the bed rock formation and lead to failure by breaking off into small pieces and, second, the removed block slides over the bed formation and removes the rocks layer by layer. The research on failure due to abrasion is relatively new, beginning only in the past decade, and more works need to be done in this area (Annandale, 2007). Figure 2-8 illustrates the abrasion type of rock formation failure.

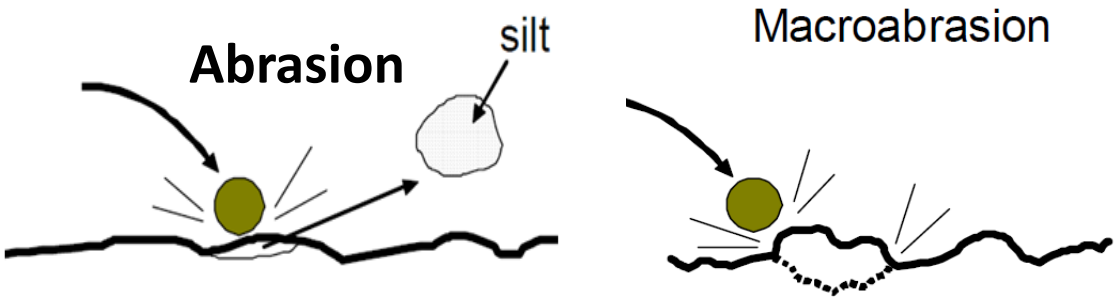

Figure 2-8. Schematic diagram illustrating the abrasion and macroabrasion (Sketch courtesy Gary Parker) (Chatanantavet, 2007)

2.3. Rock Mass Properties

The type of rock material and its discontinuities are two important aspects that affect the rock mass behavior in the scour process. Most of the properties can be determined by field observation and borehole testing (Bollaert, 2002).

Based on the rock mass discontinuities, the rocks can be classified as intermittently jointed, completely jointed, and intact. Figure 2-9 depicts the two most commonly-encountered rock mass situations. In terms of rock scour mechanisms, it is obvious that the hydrodynamic fracturing and fatigue are responsible for the scour process in intermittently jointed rocks. The resistance of the intermittently jointed rock to scour depends on the magnitude and degree of fluctuation of the hydrodynamic forces and rock properties, which determine whether or not the joint will propagate and break the rock mass (Bollaert and Schleiss, 2001).

In the case of completely jointed rock, hydrodynamic uplift plays an important role in the scour process. The resistance of completely jointed rock to scour depends on hydrodynamic uplift force, dimension, size, shape, weight of the blocks, and the friction forces along the joint.

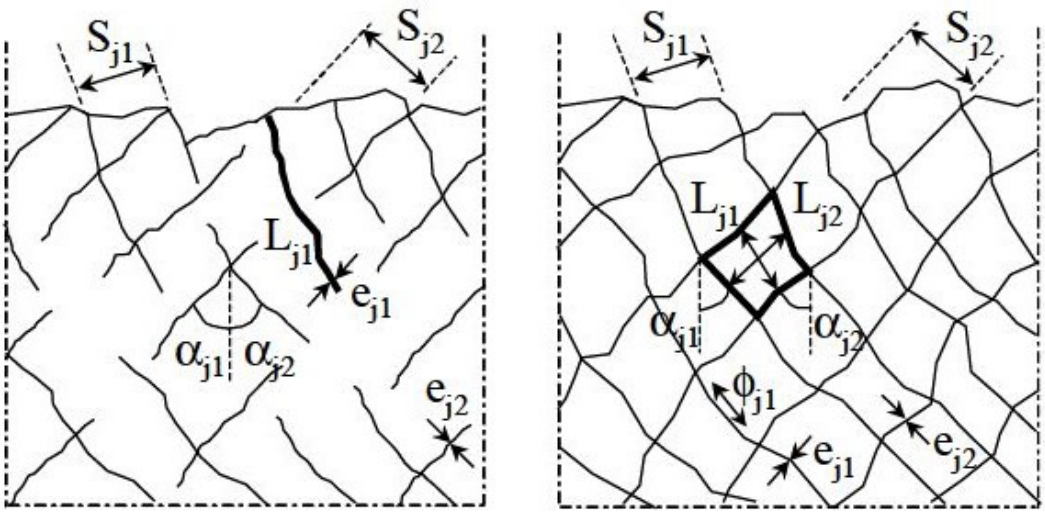

Figure 2-9. Rock mass layer situations: a) intermittently jointed rock, and b) completely jointed rock (Bollaert and Schleiss, 2001)

2.4. Bed Rock Scouring Methods

A general overview of the existing formulas to evaluate rock scour reveals that they can be broadly divided into two categories: the empirical formulas and the semi-analytical approaches (Bollaert and Schleiss, 2003). For the sake of comparison, an empirical method and two analytical-empirical methods are described in this section.

2.4.1. General Scour Expression for Plunging Flows

A series of empirical formulas have been developed to evaluate the scour of rock in the plunge pools, downstream of dams, etc. that was caused by the impinging jet into a plunge pool (see Breusers and Raudkivi (1991)). It should be noted that empirical formulas are site-specific and were developed using model tests and field observations.

The first method described here is an empirical formula to determine the extent of scour in the plunge pool. Mason and Arumugam (1985) developed a general expression

for the scour in the plunge pool by comparing different formulas and testing for many different cases. Their best fit to the model and prototype data resulted in the following expression (see Figure 2-2 for parameters definition):

$$Y = t + h = K \frac{H^y q^x h^w}{g^v d_m^z} \quad \text{(Eq. 2-7)}$$

where Y is the equilibrated scour depth (m), t is the scour depth beyond the original bed level (m), h is the tailwater depth (m), q is the discharge per unit width of the plunging jet (m^2/s), and d is the mean grain size (m). The K= (6.42-3.1 $H^{0.1}$), v= 0.3, w= 0.15, x= (0.6- H/300), y= (0.15-H/200), and z= 0.1.

This formula is also applicable to the free jets from the flip buckets, pressure outlets, and over flows.

2.4.2. Erodibility Index Method-Resistance to Scour

The second method described here is an analytical-empirical method to evaluate rock scour. Annandale (1995) developed the Erodibility Index Method (EIM) in order to investigate the scour threshold of the earth material ranging from granular sediment to rock mass formation. This method is based on the earth material's geo-mechanical characteristics and the flow's erosive capacity. This method can help predict whether or not the rock formation will scour. Moreover, it can approximate scour depth. Parameter K_h, which is known as the Erodibility Index and was defined by Kirsten (1982), was used to quantify the geo-mechanical characteristics of rock. This parameter represents the rock's ability to resist the erosive capacity of water (Annandale, 1995).

The mean Erodibility Index K_h can be computed by:

$$K = M_s \,.\, K_b \,.\, K_d \,.\, J_s \quad \text{(Eq. 2-8)}$$

where K = Erodibility Index; M_s = material strength; K_b = particle or block size; K_d = shear strength; and J_s = orientation and shape factor.

Material strength number represents the rock's potential for brittle fracture or fatigue failure. The particle or block size number represents the potential for block removal. The shear strength, the orientation, and shape numbers, respectively, represent the strength of the eroded rock and the block orientation. These parameters can be easily determined in the field using investigation and the simple tests detailed in the following sections.

2.4.2.1. Mass Strength Number (M_s)

The mass strength number can be derived using the Unconfined Compressive Strength (UCS) as a relevant indicator parameter.

Table A-1 shows the mass strength number related to rock, and it is important to keep in mind that weathering can affect the mass strength values because it weakens the rock formation. Assigning an appropriate value to the M_s for a rock formation that is exposed to weathering requires expertise and can be accomplished by testing similar weathered rock in the laboratory or by considering a reduction coefficient for the actual M_s (Annandale, 2006).

2.4.2.2. Particle Size Number (K_b)

The particle size number for the rock is a function of the rock joint spacing and the number of joint sets. The rock joint spacing is estimated using the borehole data, or the Rock Quality Designation (RQD), which is a parameter in drill core logging that is

defined as the ratio of the sums of the lengths of pieces of rock that are longer than 0.1 m to the total length of the core (Annandale, 1995).

A schematic representation of the rock joint set (J_n) is provided in Figure 2-10, and the value for the J_n parameter is available in Table A-2.

Figure 2-10. Schematic presentation of rock joint set (left to right: one joint set, one joint set with random joints, two joint sets)

The value for the particle size number will be calculated using:

$$K_b = \frac{RQD}{J_n} \quad \text{(Eq. 2-9)}$$

The value of K_b varies from 5 to 100, with 5 denoting the lowest and 100 denoting the highest quality of rock.

2.4.2.3. Shear Strength Number (K_d)

The shear strength value for the rock is related to the rock's different surface characteristics that comprise the discontinuities. Shear strength represents the relative resistance with respect to the discontinuities in the rock and will be determined as the ratio between the joint wall roughness (J_r) and the joint wall alteration (J_a). J_r represents

the degree of roughness of opposing faces of rock discontinuity, and J_a represents the degree of the material's alteration that forms the faces of the discontinuity (Annandale, 2006). The J_r and J_a values can be found in Table A-3 and Table A-4.

By determining the value of J_r and J_a, one can calculate the shear strength number of the rock as follows:

$$K_d = \frac{J_r}{J_a} \quad \text{(Eq. 2-10)}$$

2.4.2.4. Orientation and Shape Number (J_s)

This parameter represents the relative ability of rock to resist erosion due to the structure of the rock formation and its direction to the flow. This parameter is a function of the angle between the horizontal plane and the plane of discontinuity and also of the ratio of joint spacing (Annandale, 1995). Table A-5 provides the orientation and shape.

After determining the Erodibility index, it is necessary to define the erosive capacity of water. To quantify the erosive capacity of water, it was crucial to choose a method that both accurately represents the strength of the fluctuating turbulent pressure and that can be easily computed. Consequently, Annandale (1995) selected the rate of energy dissipation as the parameter to use in the case of an impinging jet (Annandale, 1995). The stream power of the flow can be calculated from:

$$P = \gamma\, q\, h \quad \text{(Eq. 2-11)}$$

where P is the stream power per unit width, γ is the specific weight of the fluid, q is the unit discharge, and h is the total head.

The rate of energy dissipation versus the calculated Erodibility Index was plotted for a comprehensive set of data, and the scour threshold condition was defined according to the observation of data sets.

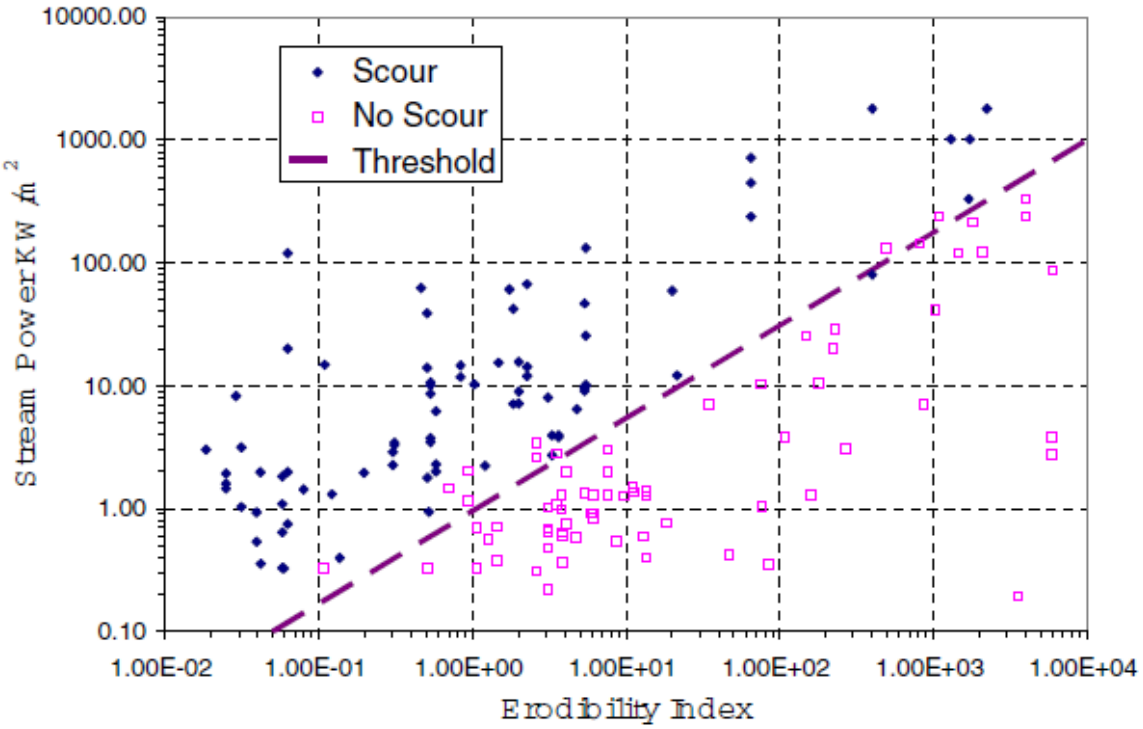

Figure 2-11. Erosion threshold relating stream power and the Erodibility Index (Annandale, 1995)

It can be observed from Figure 2-11 that as long as the available stream power exceeds the required stream power for erosion, the bed rock will begin to scour. While investigation of the bed rock scouring and the scour extent is a well-accepted and reliable method, it is unable to provide any information about the scour rate.

The scour threshold line can be described with the following equations:

$$P_c = 0.48\,K^{0.44} \quad \text{for} \quad K \leq 0.1 \qquad \text{(Eq. 2-12)}$$

$$P_c = K^{0.75} \quad \text{for} \quad K > 0.1 \qquad \text{(Eq. 2-13)}$$

where K is the erodibility index and P_c is the critical stream power (Kw/m^2) (Annandale, 2006).

This method is also able to predict the scour extent of the rock formation. The scour extent can be determined by calculating the available stream power at different elevations and the stream power that is required to scour the rock. The ability of rock to resist scour induced by flow is space dependent, since the rock formation changes by changing the elevation. Therefore, it needs to be determined for different elevations in order to estimate the ultimate scour depth (Annandale, 2007).

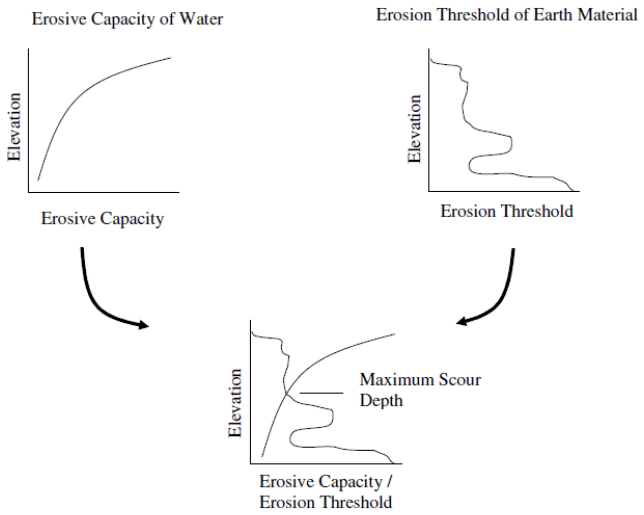

Figure 2-12. Estimating the scour extent using the erodibility index method (Annandale, 2007)

2.4.3. Van Schalkwyk's Method

The third method is an analytical-empirical approach similar to the previous method. Van Schalkwyk *et al.* (1994) developed a method to evaluate rock scour in unlined spillways. The method was developed based on the field observation of eighteen unlined spillways as well as through some laboratory tests. Similarly to the Annandale's (1995) Erodibility Index Method, their approach formulated the extent of rock erosion relative to the energy of flowing water and characteristics of the rock mass formation. They utilized the unit stream power of the flow and the Kirsten excavation index (K_h) as representative of the water-driven energy and geo-mechanical characteristics of rock mass, respectively (see Section 2.4.2).

Van Schalkwyk *et al.* (1994) classified the extent of rock erosion into four categories based on the erosion depth, as depicted in Table 2-1. Van Schalkwyk's chart to evaluate rock scour is depicted in Figure 2-13.

Table 2-1. Extent of erosion classification for
Van Schalkwyk's method
(Van Schalkwyk *et al*., 1994)

Erosion Depth (m)	Class of Erosion
0	Non (O)
0-1	Little (L)
1-5	Moderate (M)
>5	Excessive (E)

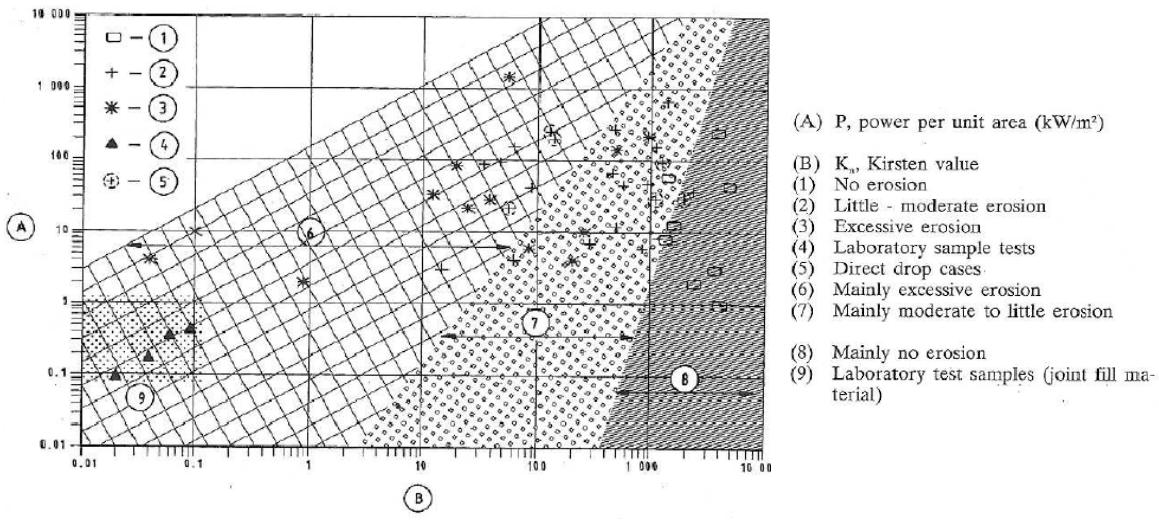

Figure 2-13. Van Schalkwyk's chart for rock scour evaluation (Van Schalkwyk *et al.*, 1994)

2.5. Analog Scour Models

The role of analog models to investigate rock scour could be significant since rock scour is a very complicated process, and hydraulic models are robust tools to provide better insight into the hydraulic and sedimentology processes. Analog models have been utilized to investigate the rock scour process in order to gain a deeper insight into rock's erosional features and key mechanisms. While the material used in the analog models is not similar to the ones in the prototype, they are able to reproduce some important features of the phenomenon (Schumm *et al*., 1987).

The approach that uses a mixture of non-cohesive material with a cohesive additive has been explored to simulate rock erosion in scaled models (i.e., Johnson (1977), Shepherd and Schumm (1974), Wohl and Ikeda (1997), Barani *et al*. (2008)). For bedrock scouring simulation, the strength of the substrate in the model is usually lowered in order to produce erosion via smaller erosive forces (Thompson and Wohl, 2013).

However, there is limited information available about the testing procedures and the amount of cohesive additive that is needed to accurately simulate the strength of bedrock in the field. A methodological approach to accurately simulate the erosional strength of prototype bedrock for use in the laboratory models is needed.

2.6. Rock Scouring in Analog Laboratory Models

- Johnson (1977)

Johnson (1977) tried to develop a trial and error method to study the rock scour in laboratory models. Various mixtures of non-cohesive material and binders were tested to replicate an observed scour hole downstream of an undisclosed dam and investigate the scour hole's evolution in a laboratory model. Clay, cement, a mixture of cement and sawdust, grease, and paraffin wax were added as a binder to the non-cohesive material in order to replicate the steep side slope of the observed scour hole in the rock formation. Finding a weak binder that maintains its characteristics over time was difficult. The mixture they ended up with was comprised of 30% China clay and 10% water that was added to a uniform gravel. This mixture allowed them to reproduce a scour hole in the model that showed good agreement with the one observed in the field.

For another flood spillway design, the scour process for a large area of weak rock at the downstream of spillway was studied and led to the development of another technique used to replicate the rock. In this study, the mixture was comprised of 50 parts chalk powder (kaolinite), 1 part cement, 80 parts water, and 300 parts crushed gravel (2 to 3 mm, clean and dry) by volume.

The mixture could produce steep side slopes over a height of 50 cm under the erosion process. The scour process was observed to start by means of a local shear flow velocity of between 0.7 m/s-1.0 m/s.

This is a useful technique to study rock scour in laboratory models, in which a broad range of strength adjustments is made possible via varying the size of the gravel and the amount of binder that is added to the mixture. However, it is necessary to produce a homogenous mixture because the accumulation or lack of cohesive material leads to underestimating or overestimating the scour. This can be avoided by utilizing a dense granular material and good compaction.

- Shepherd and Schumm (1974)

Shepherd and Schumm (1974) used the analog laboratory model to study river incision in bed rock rivers. Their objective was to determine the bedrock channel morphology during the incision process. They simulated a bed rock river in a laboratory flume using a mixture of fine sand with silt-clay and kaolinite, which provided a uniform, cohesive, isotropous material. The final mixture was chosen as 1 part kaolinite with 14 parts sand. Mixtures with a higher percentage of sand were determined to be too erodible, while mixtures with a higher amount of kaolinite proved to be more resistant. After preparing the mixture in a cement truck, they poured it as slurry into the flume and allowed it to dry for two weeks. The water content of the mixture varied from 21.5% from the bottom to 18.3% at the top. A direct shear test of the mixture showed strength of 1.6 psi. The mixture was impermeable due to its high percentage of clay. The mixture's resistance to scour seemed to qualitatively simulate homogenous bedrock,

which was confirmed by the resultant erosional bed forms that were similar to those observed in the field.

- Wohl and Ikeda (1997)

Wohl and Ikeda (1997) used a mixture of fine sand and bentonite clay to investigate erosional bed forms and channel incision into a cohesive, homogeneous substrate with gradients that varied from 1% to 20% while other variables were kept constant (flow discharge, sediment discharge, and run time). After a series of initial tests and calibration experiments, they chose a substrate of 70% fine sand (median diameter = 0.15 mm) and 30% bentonite by weight. The substrate was mixed in a mixer, placed in the channel, and tamped down to achieve the highest possible degree of homogeneity. At the range of slopes investigated, this substrate was non-erodible under flows of clear water. The final experiment results revealed that the erosional bed forms shift from longitudinal grooves to a wide, shallow undulating channel as the gradient varies. The results showed that the simulated bedrock channel that used the substrate could replicate the erosional bed forms and the channel incision process.

- Barani *et al.* (2008)

Barani *et al*. (2008) used an analog model to simulate the scour resistance of stone materials in the plunge pool of the Karoon-III dam on the Karoon River in south eastern Iran. They conducted a series of experiments to find the appropriate mixture of cohesive and non-cohesive materials in order to simulate the scour resistance of the rock. They utilized a 1:70 scale laboratory model of the dam to investigate the rock scour

phenomenon. The Erodibility Index (EI) of the rock in the prototype ranged from 103 to 530 downstream of the dam. Cement and bentonite clay were added to granular material to produce the mixture, but the cement was removed due to its high resistance to erosion and its changing properties over time. Bentonite clay appeared to be an appropriate binder and was chosen as the final additive. They found that the best mixture to simulate the stone material was gravel, sand, water, and bentonite. Through a series of experiments, in which they tested mixtures in a flume under different flow conditions, they determined the most effective amount of clay bentonite to use in order to replicate the erodibility index of the prototype rock. The rate of energy dissipation was determined using measured water surface profile, calculated water surface profile using the standard step method, and the normal depth for the initiation of the scour flow condition. The erodibility index of the mixture was determined based on the measured and calculated rate of energy dissipation for the initiation of scour and by utilizing Annandale's erodibility threshold plot for rock (Annandale, 1995). Table 2-2 shows the final test mixture, velocity, and stream power at the initiation of scour, and Figure 2-14 depicts the erodibility index of the simulated bedrock for various classes of bentonite.

Table 2-2. Various tested mixture to simulate the scour resistance of the bedrock at the Karoon dam-III (Barani *et al*., 2008)

Sample	Class of Bentonite	Gravel (Kg)	Sand (Kg)	Bentonite (Kg)	Water (Kg)	$V_{critical}$ (m/s)	Stream Power (KW/m^2)
A4	7.5	47.2	9.5	4.7	10.7	1.55	16.0
D4	8.5	47.2	9.5	5.4	10.7	1.88	36.0
B4	10	47.2	9.5	6.3	10.7	1.97	50.0
E4	11.5	47.2	9.5	7.2	10.7	2.16	71.0

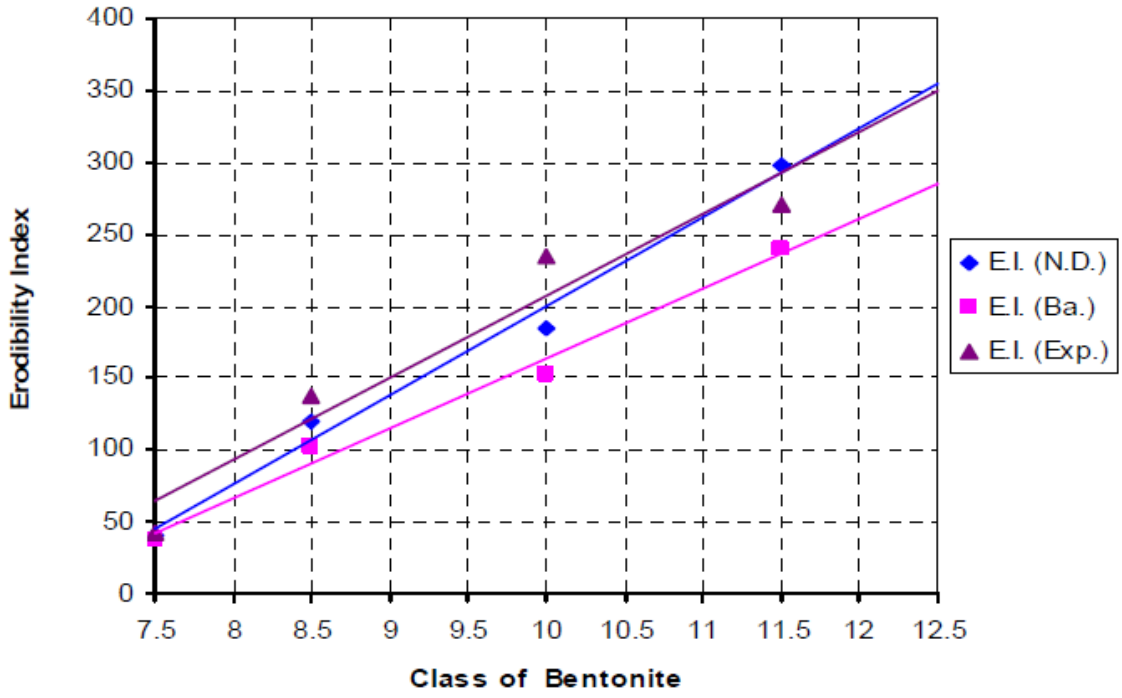

Figure 2-14. Erodibility index of the simulated bed rock using the normal depth method (N.D.), standard step method (Ba.) and experimental method (Exp.) (Barani *et al*., 2008)

2.7. Erodibility of Cohesive Soils

The present study focuses on using a weakly cohesive substrate to simulate bedrock scour in the laboratory analog models. Consequently, a deeper insight into the erodibility of cohesive soil is required. This section focuses on past studies on the erodibility of cohesive soils. Assessing the erodibility of cohesive material is crucial for investigating rill, gully, earth dam, spillway, etc. erosion processes. Various methods, such as open-channel flume tests (Hanson, 1990; Papanicolaou *et al,*. 2007), the Erosion Function Apparatus (Briaud *et al.*, 2001), the Hole Erosion Test (HET) apparatus (Wan and Fell, 2002), the Coutte Flow Device (CFD) (Moore and Masch, 1962), and the

vertical impinging jet (Jet Erosion Tests) (Hanson, 1991; Mazurek, 2001; Hanson and Cook, 2004), have been utilized to study the erodibility of cohesive soils.

In this study, we used the JET apparatus to assess the erodibility of the simulated bedrock because it replicates the process that is responsible for rock scour downstream of dams, i.e., an impinging jet. Moreover, the device can produce higher velocity jets and, consequently, greater stresses than flume devices. This section focuses on the past works that used the vertical impinging jet to address the erodibility of cohesive soils. In the following section, the JET apparatus- a submerged, circular, turbulent impinging jet- which is more widely accepted and utilized to assess cohesive soil erosion resistance is discussed in detail.

2.7.1. Jet Erosion Test (JET)

The JET approach is based on the assumption that the rate of erosion of cohesive materials changes linearly with shear stress (Hanson, 1991). By monitoring the time development of a scour hole in the soil sample, Hanson and Cook (2004) presented an analytical procedure to assess the erodibility of cohesive soil using the JET apparatus.

The JET device, in which a submerged jet vertically attacks the soil specimen beneath the jet and scour depth is measured at different times with a point gauge, can be used both in the field and in the laboratory. The laboratory JET device consists of a jet tube, nozzle, point gauge, and submergence tank. The jet tube connects to the jet submergence tank and has an orifice plate at the other end that produces the jet. The point gauge is also mounted at the top of the jet tube and is aligned with an orifice plate that measures the depth of scour. When the point gauge passes the jet nozzle to measure

the scour depth, it shuts off the flow effectively. There is an adjustable deflector plate under the orifice plate which initially protects the soil specimen surface during the period in which the submergence tank is filled. Figure 2-15 shows the in-situ and laboratory JET Apparatus.

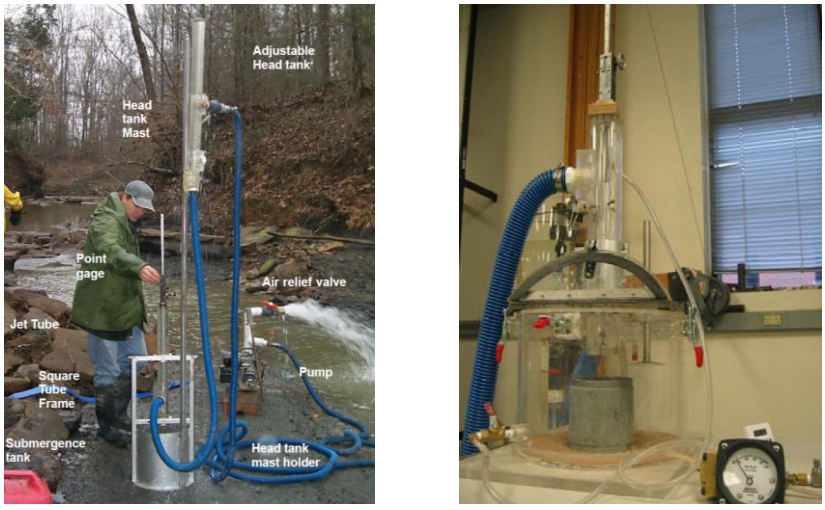

(a) (b)

Figure 2-15. Jet Erosion Test (JET) apparatus; a) *In-situ* version (Hanson and Cook, 2004); and b) Laboratory version (Wahl, 2010)

The soil specimen is positioned and centered in the submergence tank beneath the jet nozzle, and the jet attacks perpendicular to the specimen surface. The initial elevation of the soil surface is measured using the point gauge. The deflection plate is adjusted to cover the soil surface while the submergence tank is filling up. When the submergence tank is full, the deflector plate is rotated and the test begins. The depth of scour is then measured and recorded at specific time intervals until the scour hole reaches equilibrium.

2.7.1.1. Governing Equations and Calculations

Four zones of flow have been defined (Hanson *et al.,*1990) for a circular impinging jet. The first is the "flow establishment zone," through which the potential jet core extends. In this region, the velocity of the jet remains constant. The second zone occurs when the jet is fully developed and is called the "established flow zone." The third zone is the "deflection zone," where the normal jet acting on the flat surface changes to a horizontal wall jet. The last zone is called the "wall jet zone," where the jet is parallel to the boundary layer.

The jet core is a very important region of the jet. Key experimental and theoretical studies that have investigated the extension of this region (Bollaert, 2002) are presented in Table 2-3. The potential core jet length is calculated by multiplying the constant K times the jet's diameter (d_0) for circular jets or by the jet width (b) for rectangular jets.

Table 2-3. Studies on the constant K to determine the potential jet core length (Bollaert, 2002)

Author	Year	K	Jet Type	Analysis
Albertson *et al.*	1950	6.2	Circular	2D jet diffusion- Experimentally
Homma	1953	4.8	Circular	Experimentally
Cola	1965	7.2	Rectangular/Submerged	Conserv. Eq.-Experimentally
Poreh and Hefez	1967	9.0	Circular	2D jet diffusion
Hartung and Hausler	1973	5.0	Circular/Impinging	Estimation of diffusion angle
Beltaos and Rajaratnam	1973	8.3	Rectangular	Momentum flux of the jet
Beltaos and Rajaratnam	1974	5.8-7.4	Circular	Momentum flux of the jet
Chee and Yuen	1985	3.3	Circular/Impinging	Dimensional analysis of momentum
Ervine and Falvey	1987	4.0	Circular/Impinging	Momentum jet- Experimentally
Ervine and Falvey	1987	6.2	Circular/Submerged	Experimentally
Bormann and Julien	1991	3.2	Rectangular/Impinging	Jet diffusion coefficient Cd
Ervine *et al.*	1997	4.0	Circular/Impinging	Experimentally

Beltaos and Rajaratnam (1973) conducted one of the first studies on the circular impingement of a jet on a flat and smooth bed. They investigated the characteristics and behavior of the jet based on experiments and dimensional analysis. They defined three zones of flow for the circular impingement jet: the free jet region, the impingement region, and the wall jet region. They investigated key parameters of the flow field such as time- averaged velocity, pressure, and the shear stress field. Figure 2-16 shows the 2-D jet impingement on a flat and smooth bed.

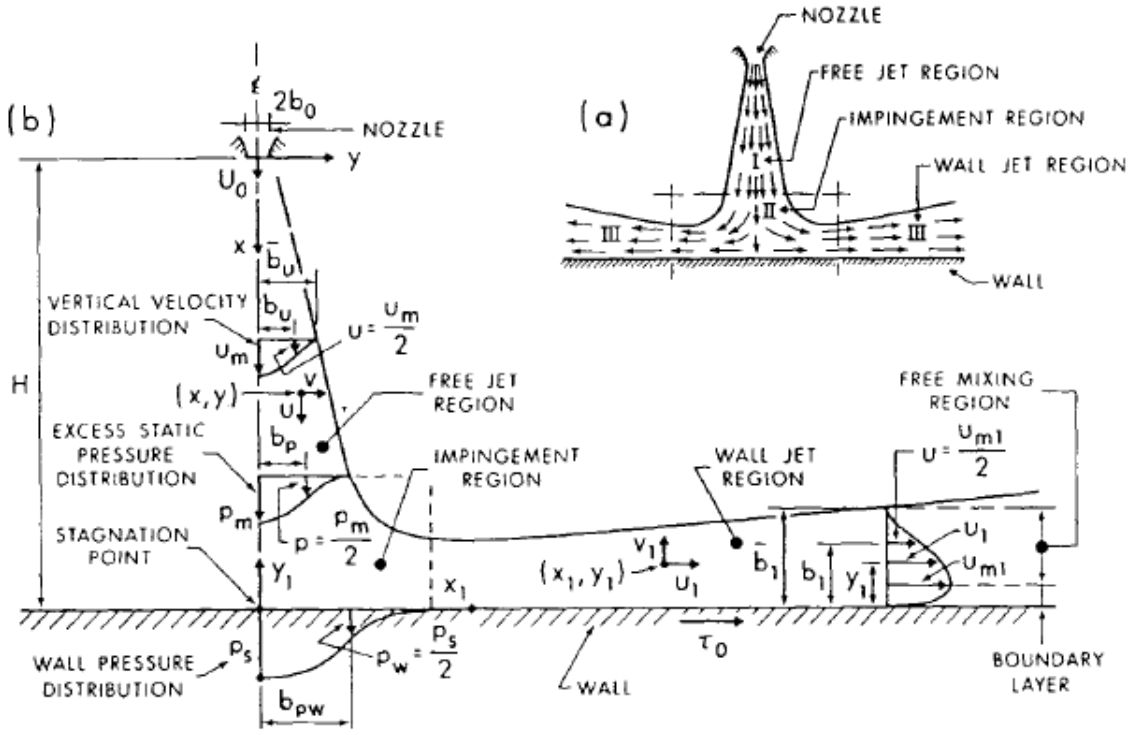

Figure 2-16. Jet impingement and diffusion on a flat and smooth bed; a) three jet regions, and b) velocity and pressure distribution (Beltaos and Rajaratnam, 1973)

An impingement jet has been utilized by researchers to study the scour of cohesionless and cohesive soils (Rajaratnam 1981, Hanson 1991, Mazurek 2001, Hanson and Cook 2004).

Rajaratnam (1981) studied the characteristics of sand bed scour using impingement turbulent jets. Through his dimensional analysis and experiments, he developed a method to relate the maximum depth of scour $\varepsilon_{m\infty}$ in a sand bed that was formed by the turbulent impinging jet to the jet characteristics, bed material, and liquid properties.

$$\varepsilon_{m\infty} = \emptyset(M_0, \rho, H, g\Delta\rho, d) \quad \text{(Eq. 2-14)}$$

where M_0 is the jet momentum flux at the nozzle, ρ is the density of the fluid, H is the jet impingement height, Δρ is the difference between the densities of the fluid and bed material, and d is the median diameter of the bed material.

Using the Buckingham PI theorem results in:

$$\frac{\varepsilon_{m\infty}}{H} = \emptyset\left(\frac{F_0}{\sqrt{\frac{H}{2b_0}}}\right) \quad \text{(Eq. 2-15)}$$

$$F_0 = \frac{U_0}{\sqrt{gd\frac{\Delta\rho}{\rho}}} \quad \text{(Eq. 2-16)}$$

where F_0 is the densimetric Froude number, and U_0 is the velocity of jet. The bed profile of the scour hole in a sand material bed was found to be:

$$\left(\frac{\varepsilon}{\varepsilon_m}\right)_\infty = e^{-0.693\left(\frac{x}{b}\right)^2} \quad \text{(Eq. 2-17)}$$

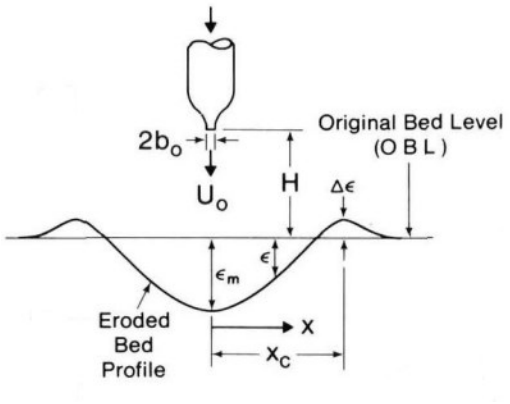

Figure 2-17. Scour hole by a vertical impinging-parameter definition (Rajaratnam, 1981)

In the last equation, ε is the depth of erosion in meters, x is the longitudinal distance from the jet nozzle (m), and b the value of x where the scour depth is half of the maximum ultimate scour depth (m). The sketch in Figure 2-17 includes the parameter definitions.

Mazurek (2001) conducted an experimental study to investigate the scour of clay soil using a submerged vertical impinging jet. The objectives of this study included: first, to examine the properties of scour in the clay soil by the jet and, second, to relate the scour hole properties of the clay soil to the jet hydraulic characteristics and soil properties in order to develop a method to predict the scour hole's dimensions. The study revealed that the ultimate scour hole dimensions are a function of the jet's characteristics (i.e., jet momentum flux and impingement height), properties of the fluid (i.e., viscosity and density), and the soil's properties (i.e., critical shear stress). It was stated that the scour hole grows linearly as a function of the logarithm of time except at the start of the erosion process and near equilibrium. This study showed that the scour experiments of cohesive soil using the submerged vertical jet are repeatable. Using the jet mechanic concepts and

the soil critical shear stress as the soil's resistance to erosion, the ultimate scour hole depth can be expressed as a function of:

$$\varepsilon_{m\infty} = f_1(M_0, \rho, H, \mu, \tau_c) \quad \text{(Eq. 2-18)}$$

where M_0 is the jet momentum flux at the nozzle ($M_0 = \frac{\pi}{4}\rho U_0^2 d^2$), ρ is the density of the fluid, H is the jet impingement height, U_0 is the jet velocity at the nozzle, d is the nozzle diameter, μ is the dynamic viscosity of the fluid, and τ_c is the critical shear stress of the clay.

Using the Buckinghum PI theorem will result in a dimensionless function:

$$\frac{\varepsilon_{m\infty}}{H} = f_1\left\{\frac{\rho U_0}{\tau_c}\left(\frac{d}{H}\right)^2, \frac{U_0 d}{\vartheta}\right\} \quad \text{(Eq. 2-19)}$$

Hanson and Cook (2004) utilized a submerged circular turbulent vertical jet (JET apparatus) to investigate the cohesive bed scour. The JET apparatus determines the erodibility of cohesive soils based on the assumption that the rate of erosion of material is a linear function of the shear stress, which was expressed by Hanson and Cook (2004) as:

$$\varepsilon_r = k_d(\tau_e - \tau_c) \quad \text{(Eq. 2-20)}$$

where ε_r is the rate of erosion (m/s), k_d is the erodibility coefficient (m^3/Ns), τ_e is the effective stress (Pa), and τ_c is the critical stress (Pa). Figure 2-18 depicts the schematic view of the jet acting on the soil surface and the parameter's definition.

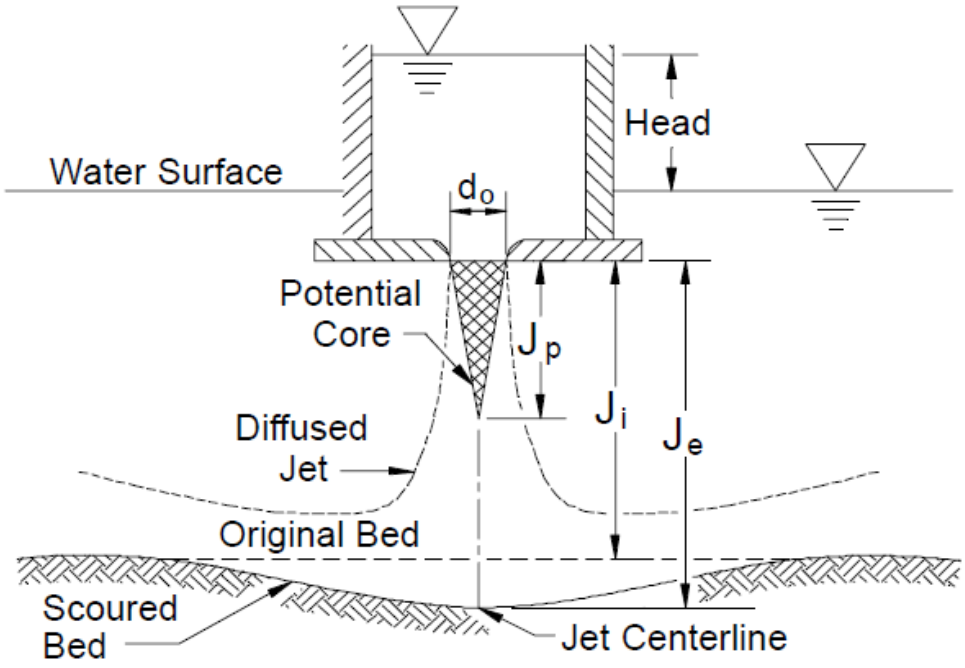

Figure 2-18. Schematic view of the jet and parameters definition (Hanson and Cook, 2004)

Hanson and Cook (2004) presented that the maximum shear stress at the center of the jet for an impinging submerged circular jet is determined by:

$$\tau_i = \tau_0 \left(\frac{J_p}{J_i}\right)^2 \quad \text{for} \quad J_i \geq J_p \qquad \text{(Eq. 2-21)}$$

$$\tau_0 = C_f \rho U_0^2 \qquad \text{(Eq. 2-22)}$$

$$U_0 = \sqrt{2gh} \qquad \text{(Eq. 2-23)}$$

$$J_p = C_d \, d_0 \qquad \text{(Eq. 2-24)}$$

where τ_i is the maximum shear stress at the soil water surface, C_f is the friction coefficient that is equal to 0.00416, U_0 is the jet velocity at the exit, $J_p$is the potential core length of the jet, C_d is the diffusion constant equal to 6.3, d_0 is the jet diameter, and J_i is the distance between the jet exit and the soil surface.

An analytical method was developed by Hanson and Cook (1997) to determine the critical shear stress and erodibility of cohesive soil. This method is based on the principles of the submerged jet and the scour hole progression caused by the jet. The procedure is based on the technique developed by Stein *et al.* (1993) for a planar jet at an overfall.

The critical shear stress is the stress that corresponds to the scour hole equilibrium condition. It is difficult to achieve the equilibrium condition since it might take a long time to reach the equilibrium state. The scour progression was observed to continue for 14 months in non-cohesive sand material (Blaisdell *et al.*, 1981).

To address this issue and predict the equilibrium scour hole depth, Hanson and Cook (2004) used an approach that was proposed by Blaisdell *et al.* (1981), in which they proposed that scour progression as a function of time is a logarithmic- hyperbolic function. The method to compute the critical shear stress and erodibility of the cohesive soil is well described in Hanson and Cook (1997).

2.8. Summary

The rock erosion process is a crucial concern in the safety of a hydraulic structure. Ignoring this phenomenon poses a threat to the public and to property. While hydraulic laboratory models can help researchers study hydraulic processes, a rock erosion study using laboratory scaled model is really challenging due to the scaling issue. The prototype rock formation cannot be employed for studying rock erosion in the scaled models since the flowing water does not have enough energy to simulate the erosion process. Moreover, utilizing granular sediment to simulate the rock erosion is inaccurate

and leads to unrealistic results. The idea of using a weakly cohesive substrate (a mixture of granular sediment and cohesive additive) has been employed to study rock erosion in scaled models.

To study the jointed rock erosion process in the laboratory scaled models, the rock formation can be considered as pre-fracture. Therefore, we hypothesize that the jointed rock formation can be simulated using the mixture of non-cohesive, which represents the rock blocks, and cohesive material as binder to provide enough force and to keep the non-cohesive material particles together.

Trial and error method has been utilized to achieve an appropriate weakly cohesive substrate in a qualitative manner in order to simulate the bed rock. Choosing a proper cohesive additive was critical. China clay (Johnson, 1977), kaolinite (Shepherd and Schumm, 1974), and bentonite clay (Wohl and Ikeda, 1997) (Barani *et al.*, 2008) are some of the cohesive additives that have been utilized in the past studies. Compared to the number of studies that have been done on rock erosion in the laboratory analog scaled models, there has not yet been a study to systematically and dynamically simulate the strength of prototype rock formation. The proper amount of cohesive additive was determined by the researchers in order to achieve a homogenous, sufficiently erodible substrate. This provided the motivation to investigate and develop a method to simulate the prototype bed rock formation for use in laboratory analog scaled models.

In order to simulate the strength of the prototype rock formation using a weakly cohesive mixture, the strength and resistance of the mixture to erosion must be examined. Various devices and methods were developed to determine the erodibility of the cohesive soils. Among all of the developed methods used to assess the erodibility of cohesive

soils, we selected the JET apparatus, which is a submerged, circular, turbulent impinging jet that replicates the process responsible for rock scour downstream of a dam. This device is also capable of producing sufficient stress and a high velocity jet.

CHAPTER 3 EXPERIMENTAL SETUP AND EXPERIMENTS

This chapter explains the experimental setup, which includes the Priest Rapids Dam rock scour simulation that uses the laboratory scaled model, the development of the weakly cohesive substrate to mimic the rock formation for the fundamental experiments, the Jet Erosion Test (JET) device, and the experiments.

3.1. Priest Rapids Dam Rock Scour Simulation

3.1.1. Introduction

This project is part of a series of projects at IIHR that was sponsored by the Public Utility District No. 2 of Grant County, Ephrata, Washington (GCPUD) in order to investigate juvenile salmonid migration at the Wanapum/Priest Rapids Development. Three physical models were constructed and employed to test the design of the Priest Rapids Dam's fish bypass. Priest Rapids Dam is located at river mile 397.1 on the Columbia River and bridges Yakima and Grant Counties in Washington State. It is a hydroelectric, concrete gravity dam that is owned and operated by Public Utility District No. 2 of Grant County, Washington (the District). The dam is 24 miles south of the town of Vantage and 47 miles northeast of the town of Richland. Construction of the dam began in 1956 and was completed in 1961. The dam creates the Priest Rapids Lake, which extends 18 miles upstream to the spillway of the Wanapum dam. Figure 3-1 shows the project site and offers an aerial view of the dam, which consists of a ten unit powerhouse and twenty-two spillway bays. The total powerhouse capacity is 955.6 MW.

To aid the District in their evaluation of fish passage, IIHR-Hydroscience & Engineering (IIHR) constructed comprehensive three-dimensional physical models of the

forebay and tailrace of Priest Rapids Dam and a third model of spillbays 19-22 and powerhouse Unit 1 (sectional model). The purpose of these models is to provide tools that the District can use to assist in the design, evaluation, and implementation of fish bypass methods at the Priest Rapids project.

The models are housed in buildings that are owned by The University of Iowa. The 1:64 scale Priest Rapids tailrace model and the 1:20 scale sectional model are located in the James Street Laboratory in Coralville, Iowa.

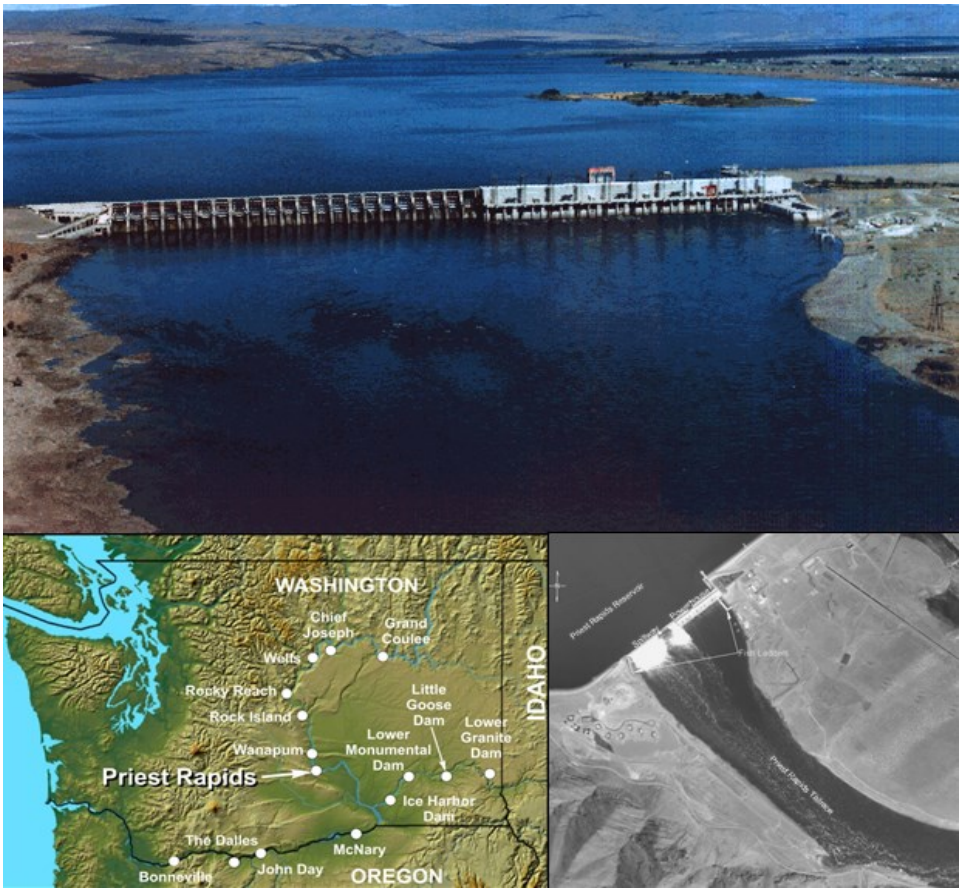

Figure 3-1. Priest Rapids dam project site

As part of the last phase of the project, it was crucial to determine the effect that the newly designed fish bypass system had on the downstream rock foundation scour. To assess the scour process, we used the 1:64 Froude scale tailrace model of the dam.

This section summarizes a series of scour tests that were conducted using the 1:64 scale Priest Rapids Tailrace model. We performed three scour tests as follows:

- Full open gate release from spillbay 22

This test simulated the full open gate release from spillbay 22 that occurred from May 6 – June 5, 2003 at the Priest Rapids Project, which resulted in the formation of a large scour hole in the field downstream of spillbay 22. The objective of the model scour test was to establish the appropriate gravel/bentonite mixture that would yield a maximum depth of the model scour hole that matched the observed maximum depth in the field over an acceptable time frame.

- Priest Rapids Fish Bypass (PRFB) scour potential

In the tailrace model, we assessed the scour potential downstream of the PRFB that was associated with the 90% tailwater exceedance and 50% headwater exceedance values found during the fish outmigration season. This was a conservative test condition since it utilized a low tailwater elevation and represented an estimate of the erosion that could occur in the project over an extended period of time.

- Probable Maximum Flood (PMF) scour potential

We assessed the scour potential downstream of the Priest Rapids Dam spillway for the PMF with the PRFB in operation. The total spillway flow on the model was set at a PMF of 1.33 million cubic feet per second (cfs).

3.1.2. Project Site Geology

This section summarizes the geology of the Priest Rapids Dam project site. The geologic and hydrogeologic study of the Priest Rapids dam was conducted by GeoEngineers, Inc. in 2005 to support the Juvenile Fish Bypass system project (GeoEngineers, Inc., 2005).

The bedrock in the vicinity of the Priest Rapids Dam is basalt and is considered to be part of the Yakima basalt subgroup. Basalt bedrock formations in this area are categorized as Priest Rapids Members of the Wanapum basalts formation. The Priest Rapids Member consists of a series of four basalt flows that are identified at the project site from oldest to youngest as: PR-I, PR-II, PR-III, and PR-IV (Harza Engineering Company 1959, Mackin 1961, Geoengineers, Inc., 2005). The thickness of each flow is typically PR-I 25-30 ft, PR-II 35-45 ft, PR-III 55-65 ft, and PR-IV 80-100 ft, respectively.

The Priest Rapids Member is characterized as medium- to coarse-grained and contains a high percentage (approximately 15-20%) of angular shaped spaces between networks of small mineral crystals within the basalt. Based on the field observation and underwater videos, the upper surface of the PR-IV in the vicinity of the dam is nearly planar to slightly rounded by erosion from a glacial burst or the Columbia River flood.

While the bedrock surface away from the dam construction zone tends to be smooth and planar, there are some areas of irregularity with small steps. In the vicinity of the dam construction zone, the bedrock surface is observed to be more irregular and angular. The area is affected by the high velocity jet discharging through the spillbays.

The Priest Rapids Member is a strong and dense rock. Based on the field observation and evaluation of the exploration logs, the Priest Rapids Member in the vicinity of the Dam can be classified, using the Unified Rock Classification System (URCS), as BBEAe to CBEAe- Basalt, black to reddish-brown with a visually fresh to stained-state, medium to coarse grained, vesicular to non-vesicular, pit quality, containing open three dimensional planes of separation estimated to form blocks of 0.5-1'x 1-2'x 1-3' with no fillings, having breaks parallel to open planes, and having an approximate field weight of 175 pounds per cubic feet.

Based on the sample recovery data found in logs completed by the Washington Irrigation Development (1922), the rock core recovery in vesicular zones versus non-vesicular zones was estimated. The sample recovery data show that recovery was greater in non-vesicular rock than in vesicular zones, with an average of 85% and 68%, respectively. The Rock Quality Designation (RQD) of the Priest Rapids Member is not available, but it can be estimated from rock core recovery as ranging from fair to good quality (GeoEngineers, Inc., 2005). Figure 3-2 shows the Priest Rapids Member (PR-IV) rock at the project site.

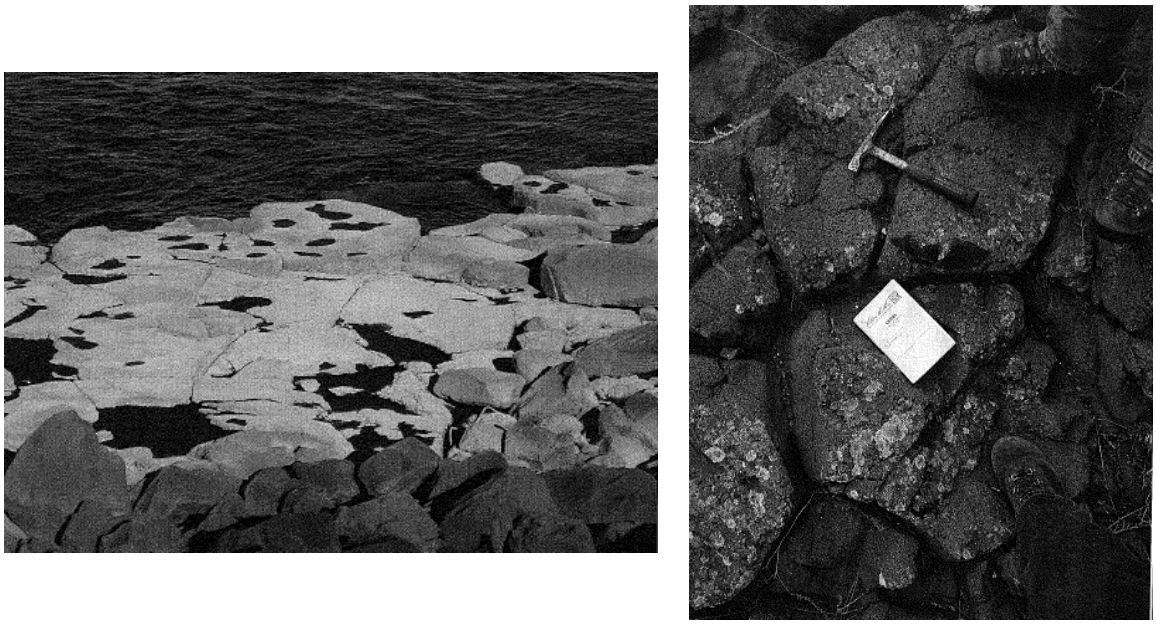

Figure 3-2. Left: View of the top of the columns of the Priest Rapids Member (PR-IV) on the right bank downstream of the Priest Rapids Dam; Right: Priest Rapids Member (PR-IV)-Columns with vesicles (GeoEngineers, Inc., 2005)

Using underwater videos finished by GeoEngineers, Inc. (2005), the river bed was categorized to differentiate the bedrock condition and size and to determine the range of overburden material at the project site. The substrate geology in the vicinity of the dam is depicted in Figure 3-3. The river bed is categorized into "Gravel, Cobbles, and Boulders," "Bedrock Surface with Boulders," Flat Bedrock," "Irregular Bedrock," and "Depressions and Benches in Bedrock." The "Gravel, Cobbles, and Boulders" category pertains to the areas that are typically covered with gravel- to boulder-sized deposits. The "Bedrock Surface with Boulders" category generally consists of the boulder-sized material that is lying on the bedrock at a shallow depth and may include local deposits of cobble- and gravel-sized material. The "Flat Bedrock" unit consists of a relatively smooth and flat bedrock surface, while the "Irregular Bedrock" unit represents the areas

with exposed bedrock and small to large steps. The "Depression and Benches in Bedrock" unit is the area where the bedrock surface has been scoured. This unit is located downstream of spillbays 20 through 22 where the proposed juvenile fish bypass units are supposed to be constructed.

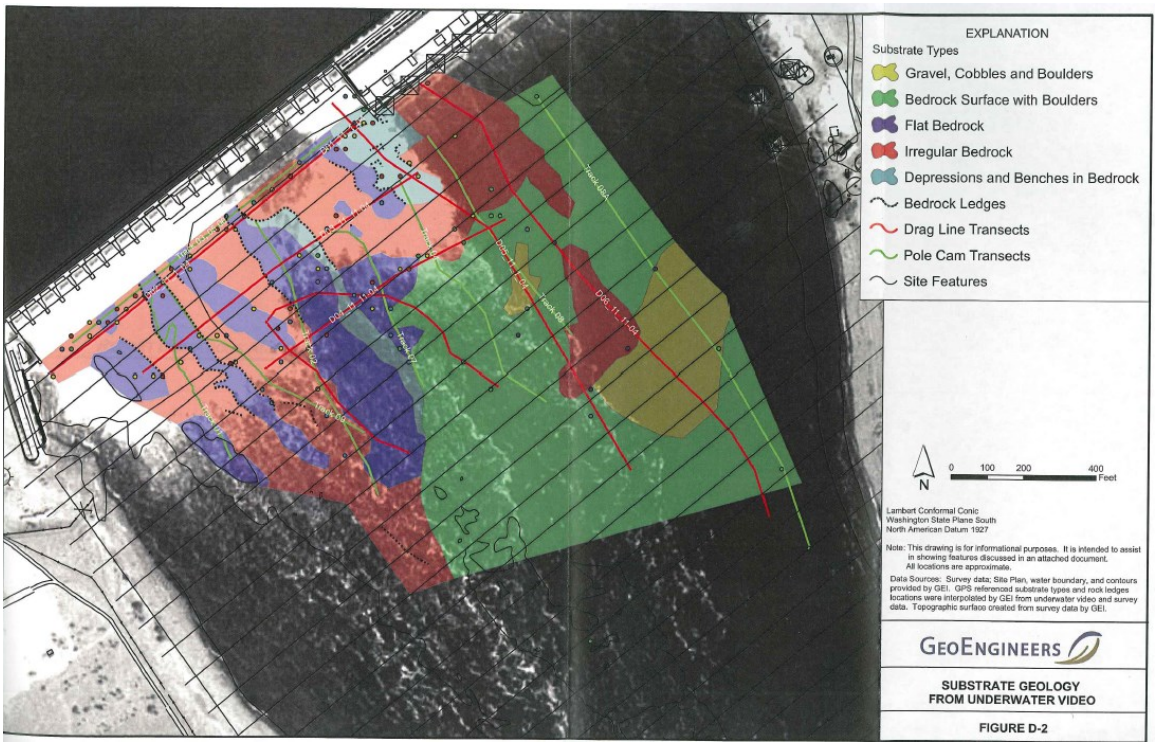

Figure 3-3. Substrate geology of the project site area from underwater video (GeoEngineers, Inc., 2005)

3.1.3. Modeled Bedrock

According to GeoEngineers (2005), the size of rocks that are eroded or plucked from the bedrock outcrops on the river bottom are variable (Table 3-1). In areas where platy partings are present and are moderately to strongly developed, the plucking of small slabs of rock typically [0.5'x1'x1'] to [1.5'x3'x3'] - nominally 11.76 to 35.4 inches in

diameter is likely to occur. Once loosened, the thinner slabs are likely to break down into more equidimensional particles that are estimated to be [0.5'x0.5'x0.5'] to [1.5'x1.5'x2'] - nominally 7.44 to 24.58 inches in diameter. Large particles may also be dislodged, as evidenced by the larger boulders downstream of spillways 17 and 22. The median particle sizes are estimated to be [2'x2'x3'] to [3'x3'x4'] - nominally 34.08 to 49.16 inches in diameter with an estimated maximum of [4'x4'x6'] - nominally 68.17 inches in diameter.

Table 3-1. Fractured bedrock size

Fractured bedrock type		Estimated size	Nominal diameter inches	
			prototype	model
1		[0.5'×1'×1'] to [1.5'×3'×3']	11.76 to 35.4	0.184 to 0.55
2		[0.5'×0.5'×0.5'] to [1.5'×1.5'×2']	7.44 to 24.58	0.11625 to 0.384
3	Median size	[2'×2'×3'] to [3'×3'×4']	34.08 to 49.16	0.5325 to 0.768
	maximum	[4'×4'×6']	68.17	1.065

Based on this information, the bedrock was modeled with nominally 0.45 inch washed angular gravel (a range of approximately 1/16 inch to 1 inch). Sieve analysis data is provided in Figure 3-4.

Bentonite was mixed with the rock matrix in a rotary mixing drum in order to reduce void spaces and increase cohesion. Various gravel:bentonite:water ratios were tested and ranged from 3:1:1 to 12:1:1 (expressed in term of the volume). The bentonite

and gravel mixture was placed and compacted from the laboratory floor upwards to the bed surface. The final lift was screeded and smoothed to match surveyed grade stakes.

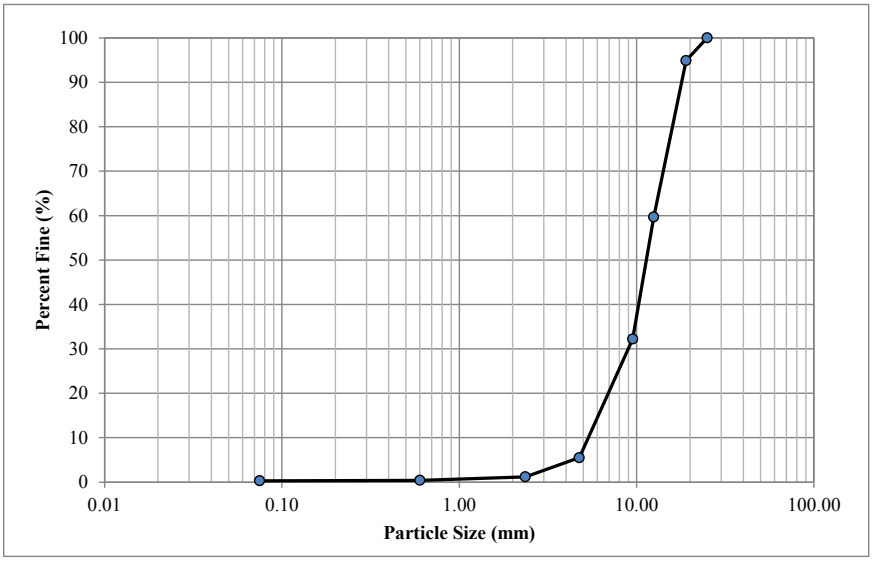

Figure 3-4. 3/4 inch concrete stone sieve analysis (model dimensions)

3.1.4. Full Open Gate 22 Scour Test

The first test in this series of scour tests replicated the full open gate release from spillbay 22 that occurred at the Priest Rapids Project between May 6 and June 5, 2003. The release resulted in a large scour hole downstream of spillbay 22 in the field, as shown in Figure 3-5 (Tetra Tech Inc., 2010). The deepest point of the scour hole is at elevation ~357.7 ft. It is unknown whether the scour downstream of spillbay 22 reached stability in the field.

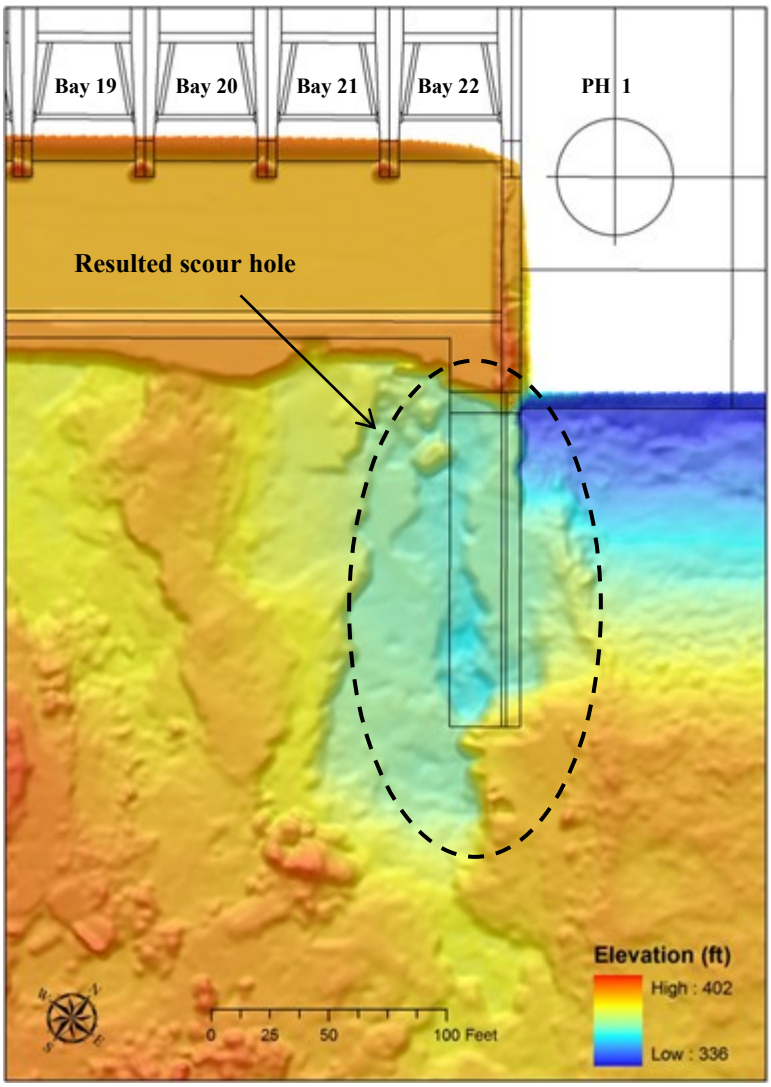

Figure 3-5. Resultant scour hole from spillbay 22 full open gate release

It is known that prior to the full open release in the field, the training wall downstream of spillbay 22, shown in Figure 3-5, was intact and that it was eroded and washed downstream at an unknown time during the 427.5 hours release. The training wall is thought to have influenced the location and shape of the resultant scour hole. The goal of the model scour test, therefore, was to begin the release with the training wall in place, successfully erode the training wall at some point during the release, and create a

scour hole of equal depth and similar shape to that existing in the field. Several gravel-bentonite-water ratios and model training walls were tested. The final training wall consisted of 24 concrete filled PVC pieces, each anchored with a 1 inch screw into the bed. The final erodible bed mixture was 9 parts gravel to 1 part bentonite to 1 part water by volume (85.60% Gravel, 7.70% bentonite Clay, and 6.70% water by weight). Mixtures tested with larger fractions of bentonite failed to reach the target scour depth in a reasonable time frame, while mixtures with smaller fractions of bentonite reached the target scour depth unrealistically quickly.

Model settings were calculated by averaging District data over the entire release period (Table 3-2).

Table 3-2. Model river conditions for spillbay 22 full open gate scour test

Elevation (ft)		**Flow Rate (Kcfs)**			
HW (ft)	**TW (ft)**	Q_{River}	Q_{PH}	Q_{22}	$Q_{13\text{-}21}$
486.8	410.0	148.1	81.0	63.5	0.4 each; 3.6 total

The initial bathymetry for the full open gate scour test was comprised of a combination of available data sets that included: 1993 ENSR single beam hydrographic data, 1998 ENSR fathometer data, March and December 2009 Tetra Tech multibeam hydrographic data, and construction design data. Figure 3-6 shows the test area and the extents of the data that were used to create the initial bathymetric surface. Figure 3-7 shows the initial bathymetry that was created with 177 surveyed grade stakes. Figure 3-8 shows photographs of the initial bathymetry (Note: The original test domain was significantly reduced in size for the final scour test). Figure 3-9 shows the test underway.

Figure 3-10 is a photograph of the final location of the training wall segments and the developed scour hole. The training wall first started to erode after 1.3 model hours and was completely eroded after 1.8 model hours. Figure 3-11 is the final bathymetry after 10.25 model hours, when the target scour depth of ~358 ft was reached. Figure 3-12 is a difference plot of the final model bathymetry minus the initial model bathymetry. Figure 3-13 is a difference plot of the final bathymetry minus the December 2009 multibeam bathymetry from the field. Although the locations of the deepest scour were close in the model and field, a longer and generally deeper scour hole was observed in the model than the one that occurred in the field. This could indicate that the model rock was too small to build up and hold a bar in the location where the scour occurred in the model.

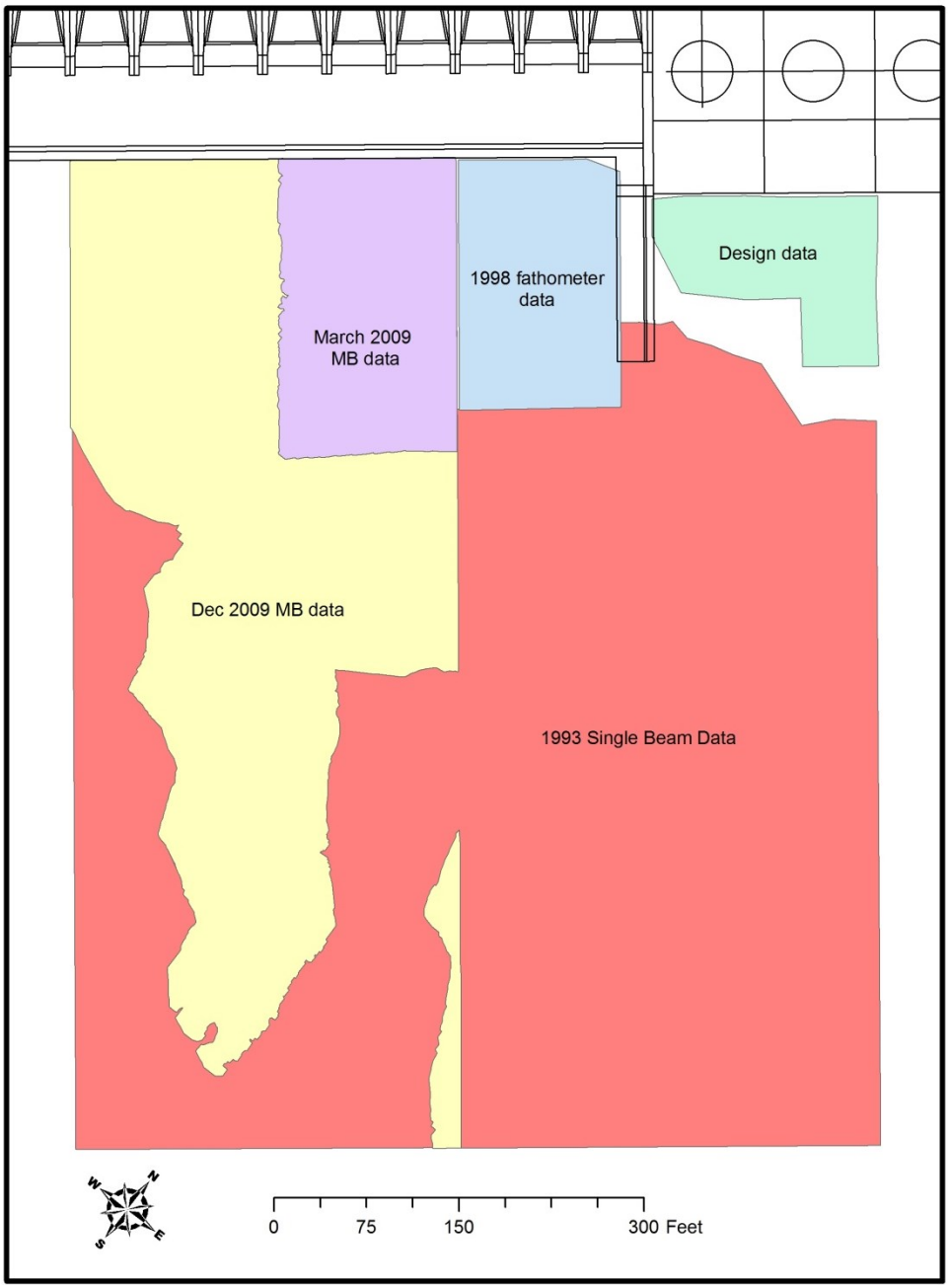

Figure 3-6. Data sets used to create initial bathymetric surface for spillbay 22 full open gate scour tests

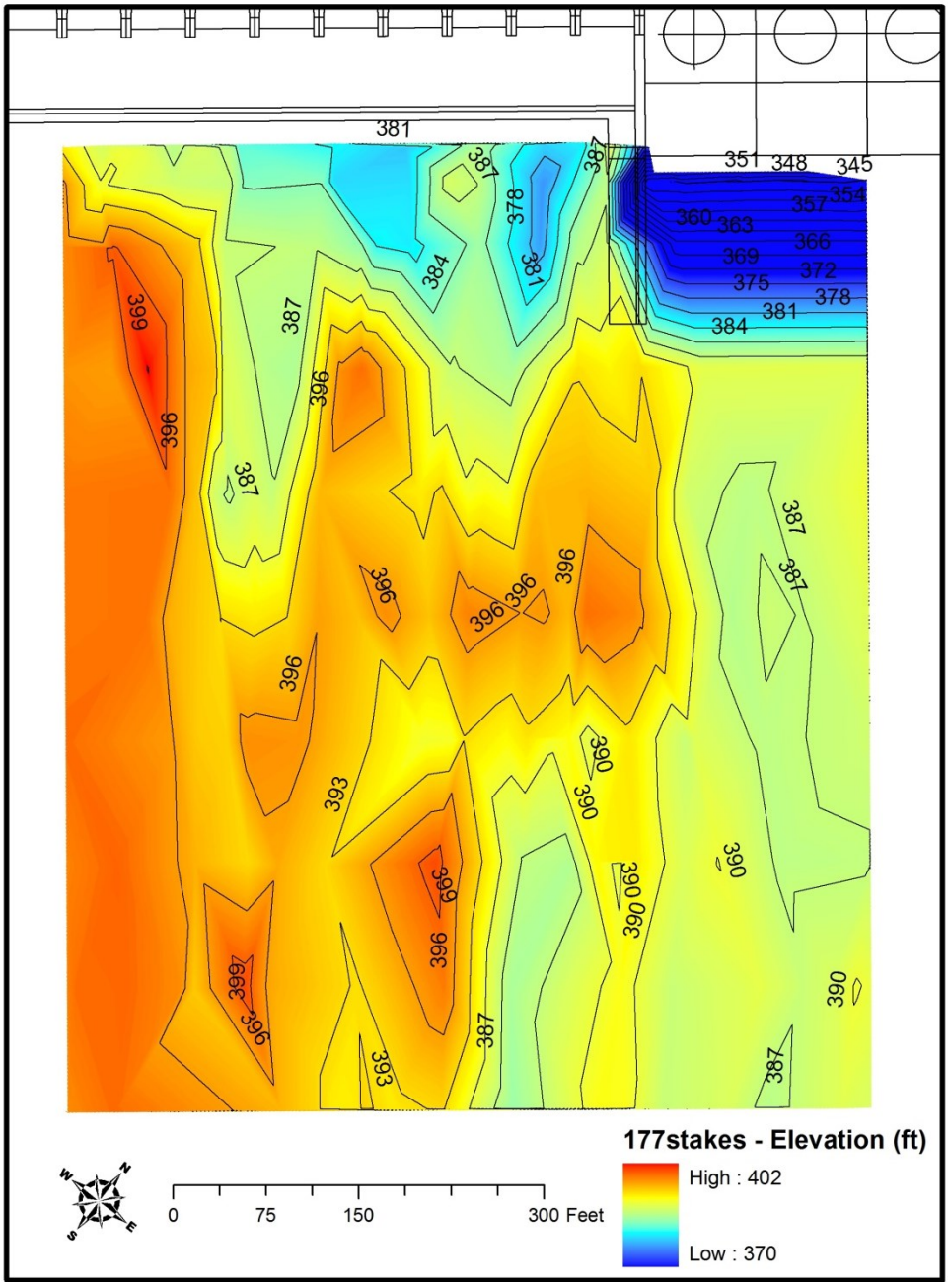

Figure 3-7. Initial bathymetric surface for spillbay 22 full open gate scour test

Figure 3-8. Photographs of the initial bathymetry and segmented training wall for the spillbay 22 full open gate scour test

Figure 3-9. Full open gate 22 scour test underway

Figure 3-10. Resultant scour hole and final positions of training wall segments

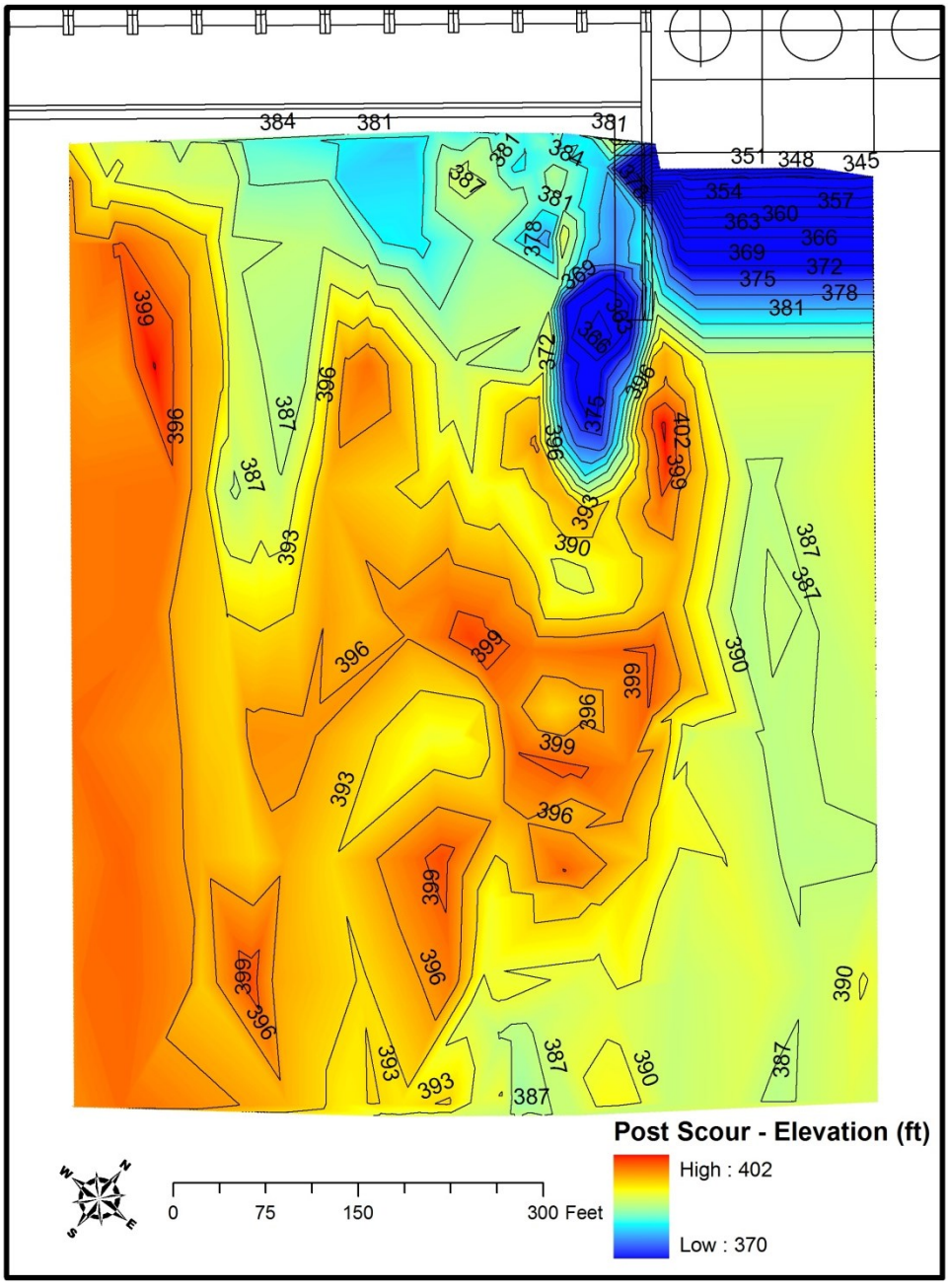

Figure 3-11. Final bathymetric surface for spillbay 22 full open gate scour test

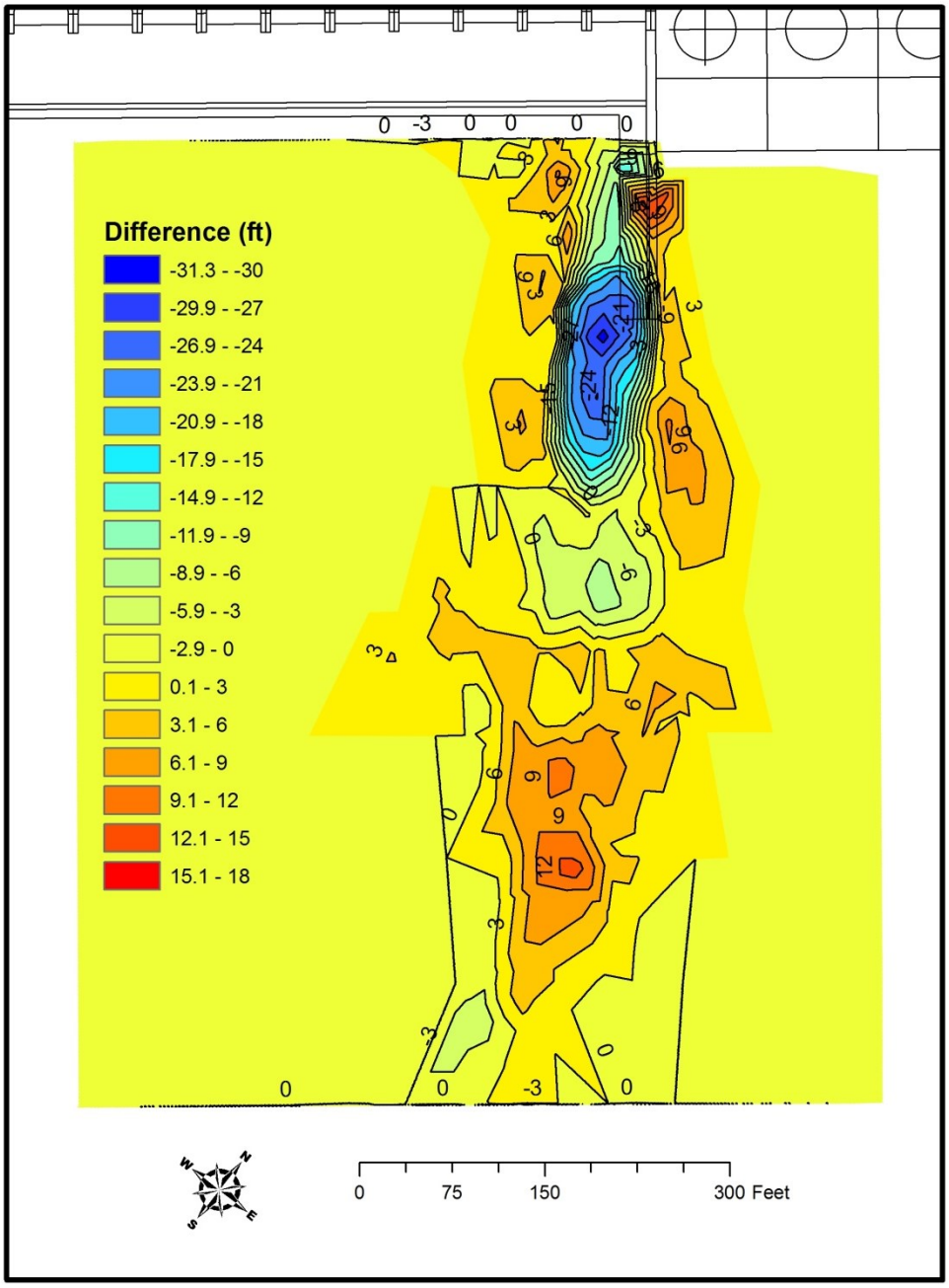

Figure 3-12. Difference plot – final bathymetry minus initial bathymetry for spillbay 22 full open gate scour test

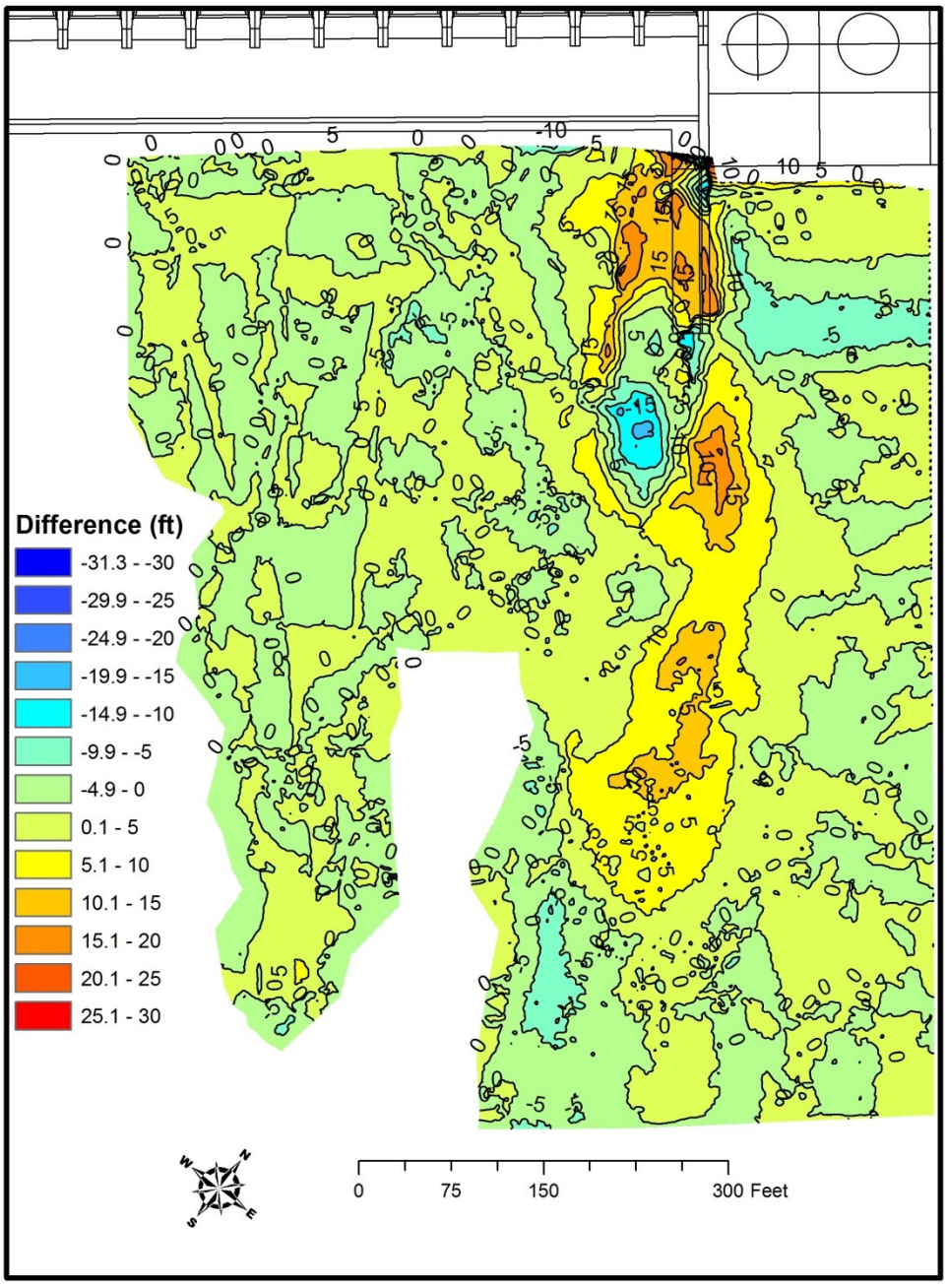

Figure 3-13. Difference plot – final model bathymetry minus December 2009 multibeam bathymetry

3.1.5. PRFB Scour Test

We conducted the second test in the series to assess the scour potential downstream of the PRFB. This was a conservative test in that the 90% exceedance tailwater elevation of 405.2 ft and the 50% exceedance headwater elevation of 486.6 ft were utilized. The results of this scour test represent an estimate of the erosion that could occur at the project over an extended period of time. The gravel:bentonite:water mixture of 9:1:1 was again used for this test. Flow conditions are outlined in Table 3-3. The model was operated until erosion in the tailrace stabilized, which occurred after approximately 43 model hours.

Table 3-3. Model river conditions for PRFB scour test

Elevation (ft)		Flow Rate (Kcfs)		
HW (ft)	**TW (ft)**	**Q_{River}**	**Q_{PH}**	**Q_{bypass}**
486.6	405.2	64.3	37.2	27.1

The initial bathymetry for the PRFB scour test was created with the use of 101 grade stakes set to December 2009 Tetra Tech multibeam data inflection points. Figure 3-14 shows the initial bathymetric surface for the PRFB scour test. Figure 3-15 shows photographs of the initial bed. Figure 3-16 is a photograph of the test underway. A plunging jet was observed in the bay 20 bypass, while skimming jets were observed in bays 21 and 22. The plunging jet in bay 20 caused a significant amount of erosion. There was a tendency for the pier extensions to be undermined during the test, particularly with pier 20. Figure 3-17 shows the final bathymetry after ~43 model hours. Figure 3-18 shows photographs of the final scoured bed. In general, the existing scour

hole migrated upstream and towards the right bank. The largest amount of erosion was observed 70 feet downstream of bypass bay 20, where 17 feet of scour occurred. Figure 3-19 is a difference plot of the final bathymetry minus the initial bathymetry. During the PRFB scour test, we observed that the simulated bedrock was eroding in the form of block removal and fatigue failure.

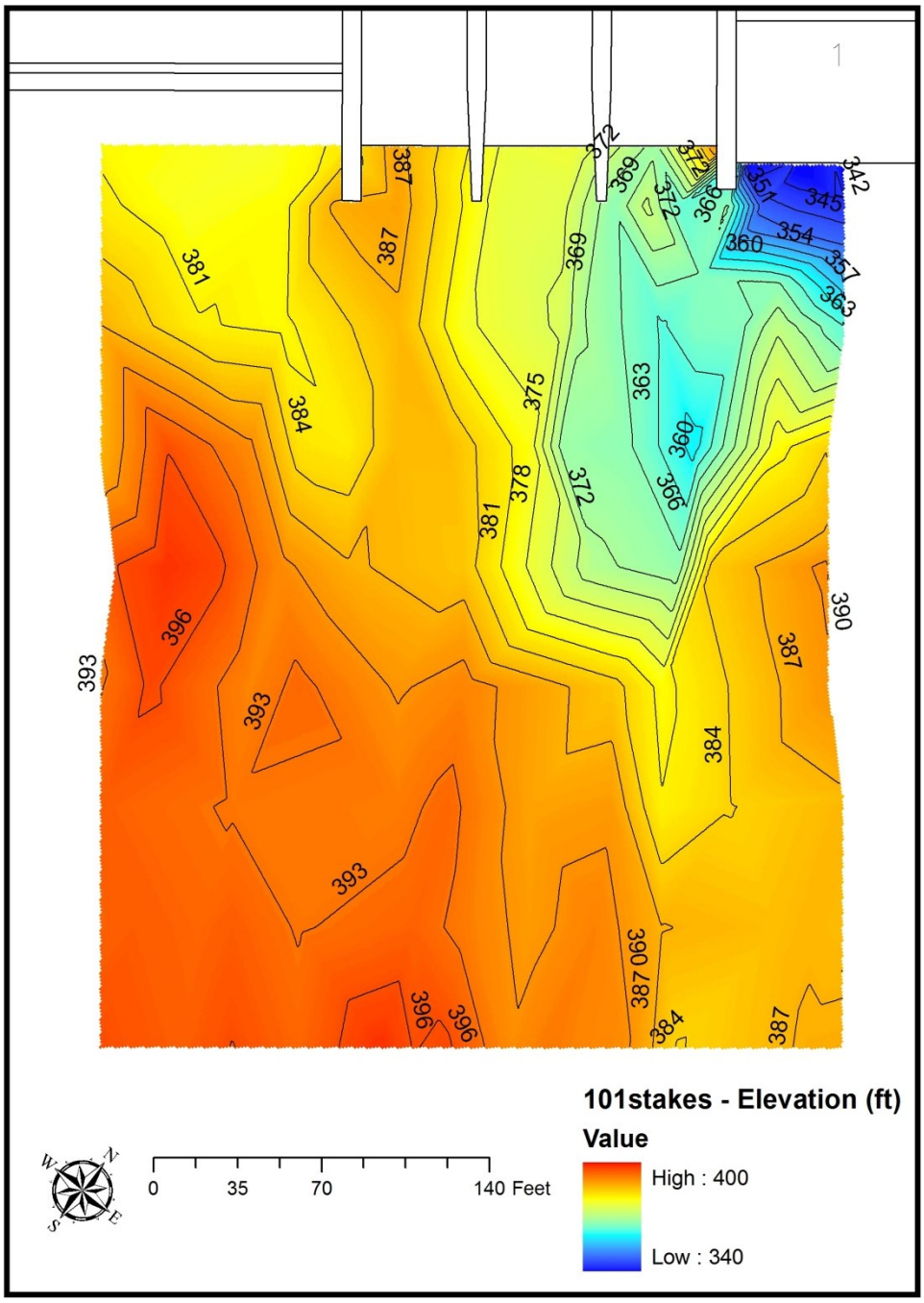

Figure 3-14. Initial bathymetric surface for PRFB scour test

Figure 3-15. Photographs of the initial bathymetry for the PRFB scour test

Figure 3-16. PRFB scour test underway

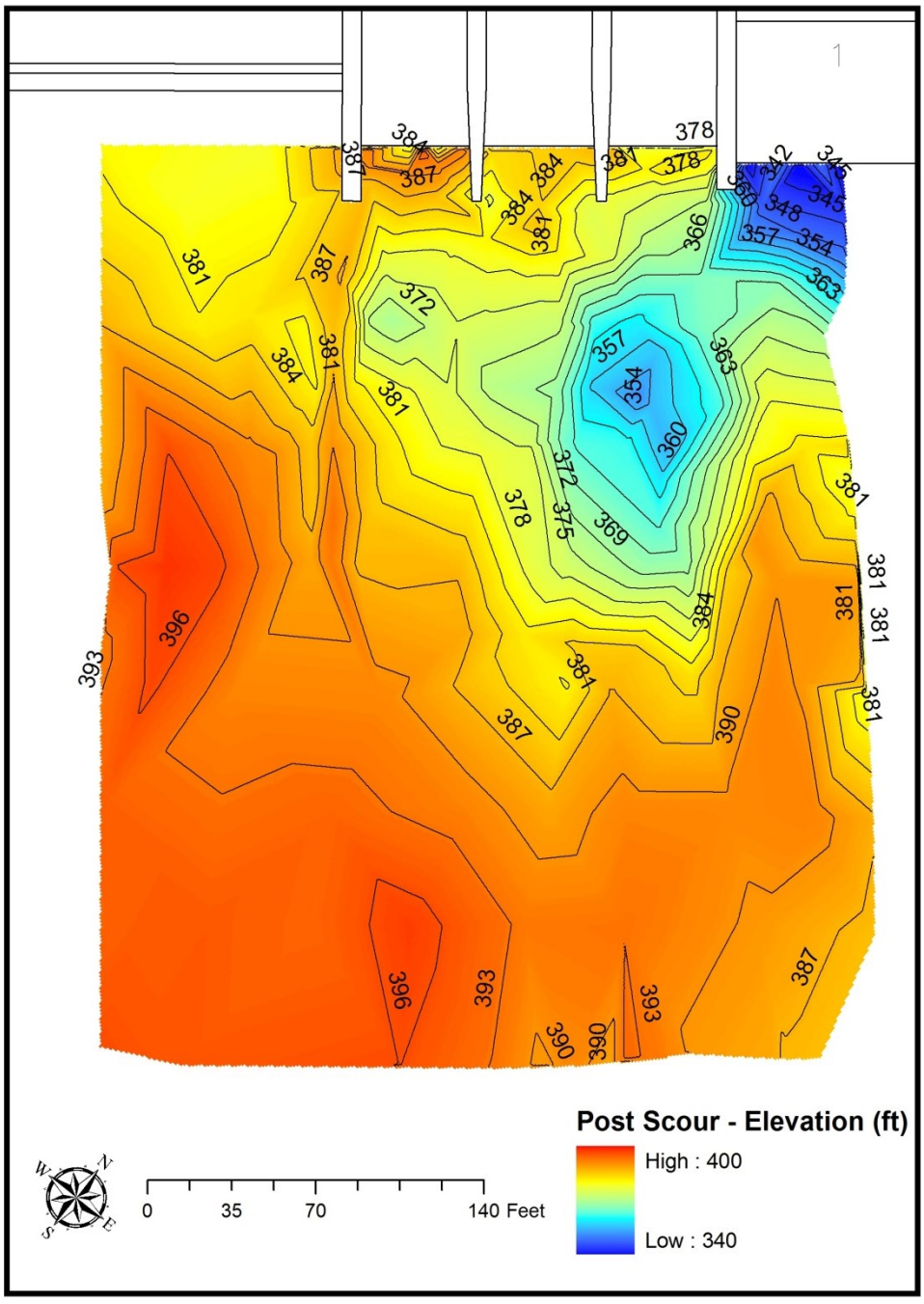

Figure 3-17. Final bathymetric surface for PRFB scour test

Figure 3-18. Photographs of the final scoured bathymetry for the PRFB scour test

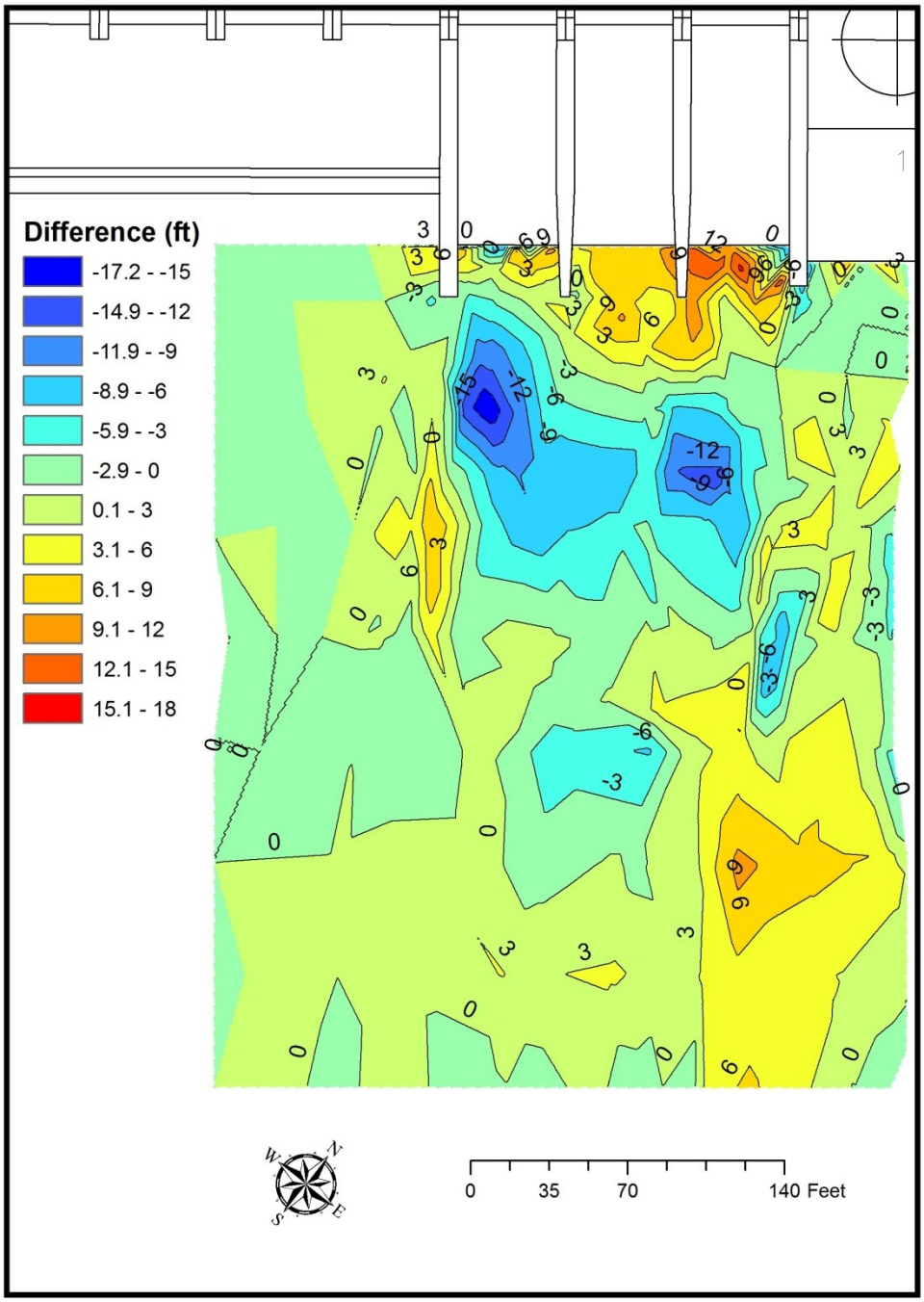

Figure 3-19. Difference plot – final bathymetry minus initial bathymetry for PRFB scour test

3.1.6. PMF Scour Test

Scour potential downstream of the Priest Rapids Dam spillway for the PMF with the PRFB in operation was assessed in the tailrace model. The total spillway flow in the model was set at a PMF of 1.33 million cubic feet per second (cfs). The initial bed condition was created using a combination of 1993 ENSR single beam hydrographic survey data, 1998 ENSR fathometer data, March and December 2009 Tetra Tech multibeam hydrographic survey data, PRFB scour test resultant bed survey data, and construction design data. The combined data set was used to select 179 grade stake locations in order to define the initial bathymetric condition for the PMF scour test. The extent of the erodible bed for the PMF scour test was from the right bank model wall through powerhouse unit 2 and 800 feet downstream of the existing endsill.

Two line-of-sight laser rangefinders were used to scan the erodible bed before and after the scour test. Figure 3-20 shows photographs of the completed initial bathymetry, and Figure 3-21 shows the scanned initial bathymetry.

Eighteen locations were monitored until a stable bed was achieved after a run time of 158.5 model hours. Large areas of scour were observed downstream of the spillway and near the fish bypass downstream of bays 18 and 19. The greatest erosion took place approximately 350 feet downstream of spillbays 12 and 13, where 54 feet of scour was observed. Figure 3-22 shows the scanned final bathymetry.

Figure 3-23 through Figure 3-25 show streamwise sections of the initial and final bathymetry. Figure 3-26 is a difference plot of the final bathymetry minus the initial bathymetry. Figure 3-27 shows photographs of the final scoured bed. Two areas of significant undermining were observed under the pier 20 training wall and to the right of

the existing endsill along the right bank fish facilities (Figure 3-27). There was no tendency to undermine the main spillway apron except near spillbays 1, 19, and 20.

The laser scanners were validated with the total station on the final bathymetric surface. 230 points were surveyed, with the total station throughout the scour test domain and the elevations compared to those from the Laser scanners**.** The average difference was -0.586 feet (-0.110 inches model) with a standard deviation of +/- 2.436 feet (+/- 0.457 inches model). The average difference and standard deviation are within the grain size distribution of the gravel used to make up the erodible bed.

During the PMF scour test, it was observed that the mixture is eroded in chunks of substrate. This process can be representative of fracture failure in rock, which occurs when the induced pressure fluctuation exceeds the fracture strength or equivalent toughness of the rock.

Figure 3-20. Photographs of completed initial bathymetry for PMF scour test

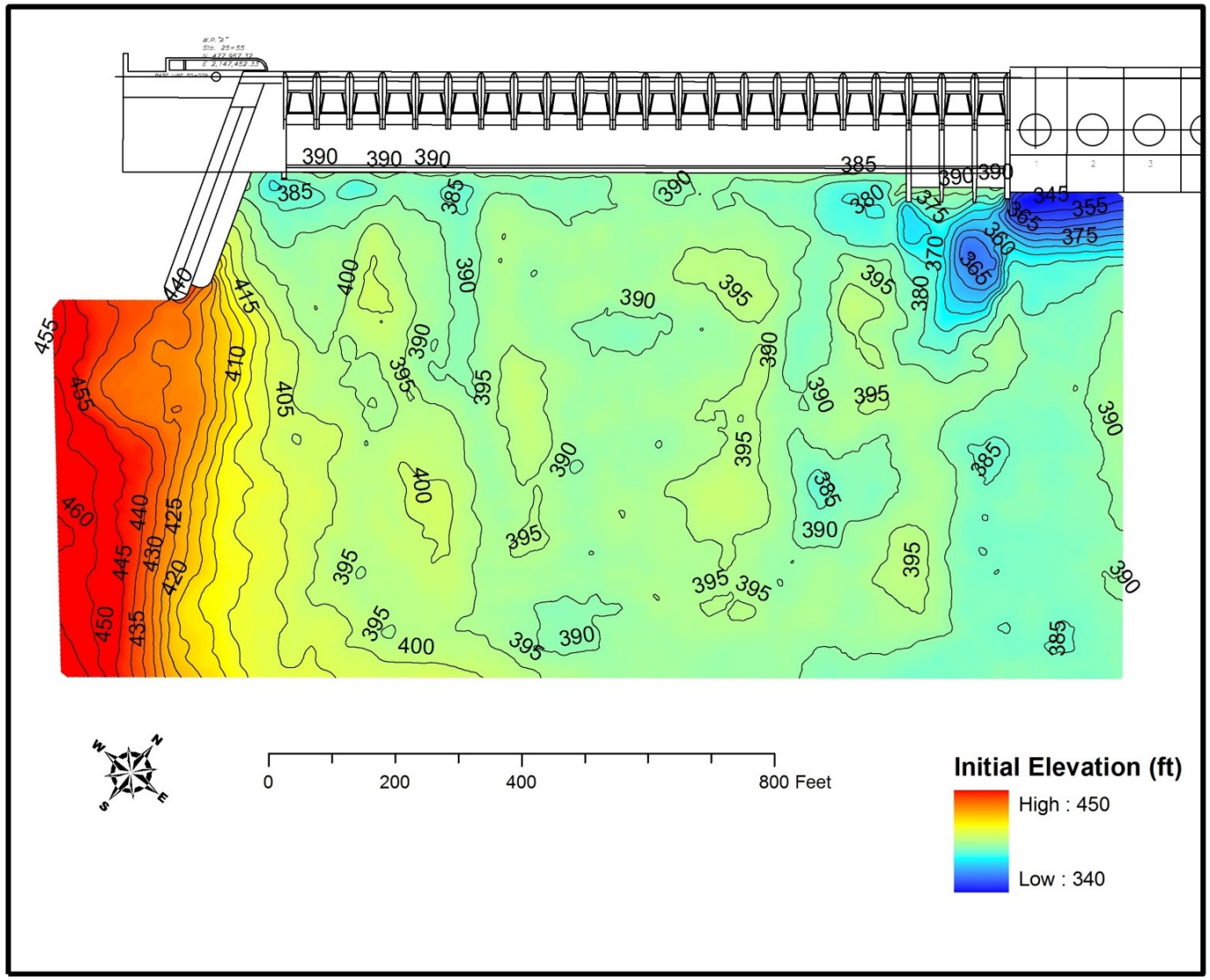

Figure 3-21. Laser scanned initial bathymetry for PMF scour test

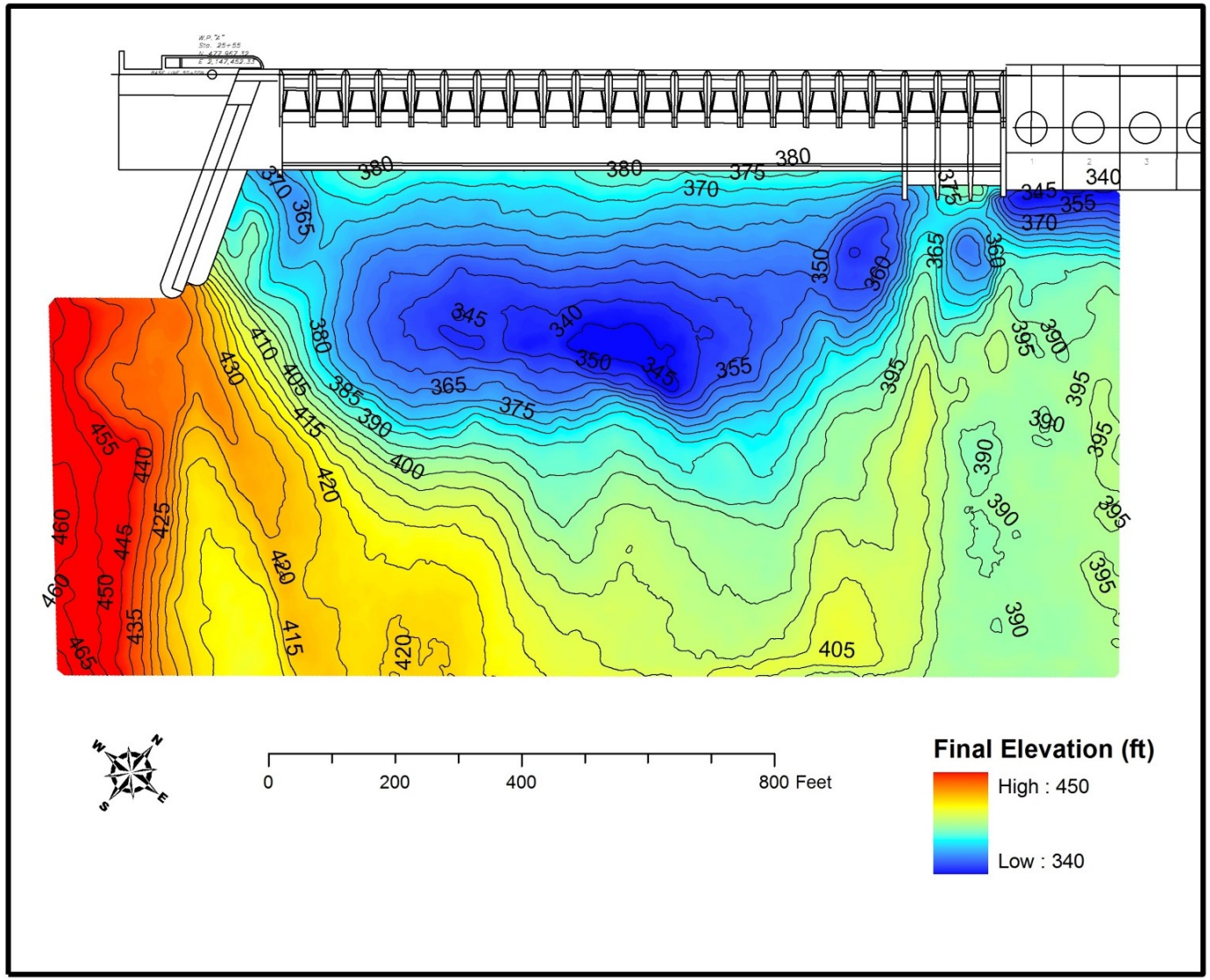

Figure 3-22. Laser scanned final bathymetry for PMF scour test

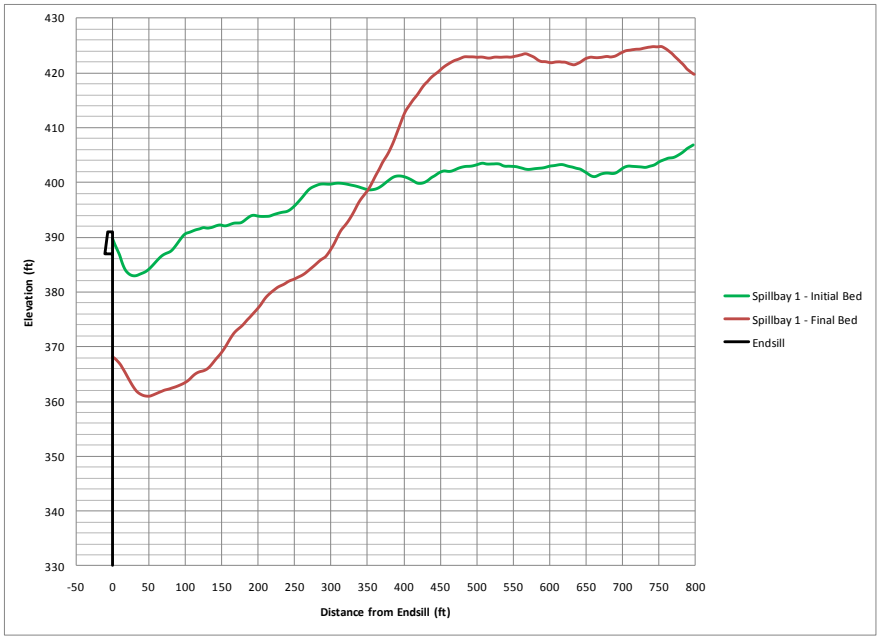

a)

b)

Figure 3-23. Streamwise sections of initial and final PMF scour test bathymetry downstream of the centerlines of: a) Spillbay 1; b) Spillbay 7

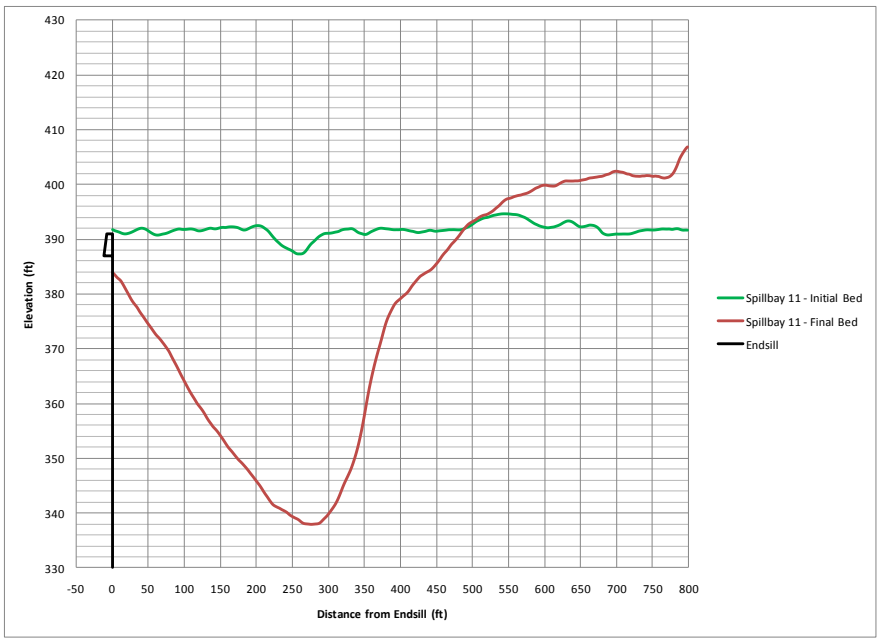

a)

b)

Figure 3-24. Streamwise sections of initial and final PMF scour test bathymetry downstream of the centerlines of: a) Spillbay 11; b) Spillbay 12

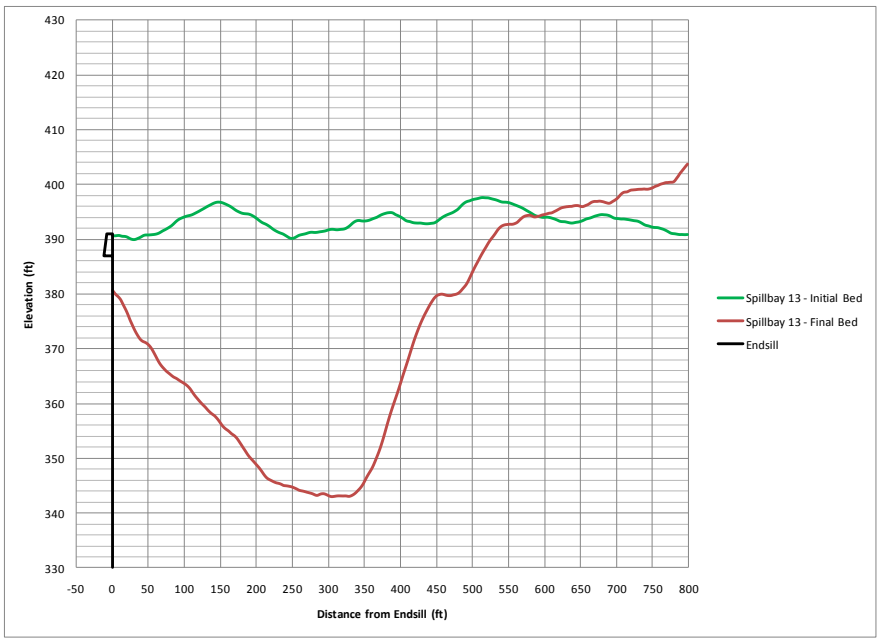

a)

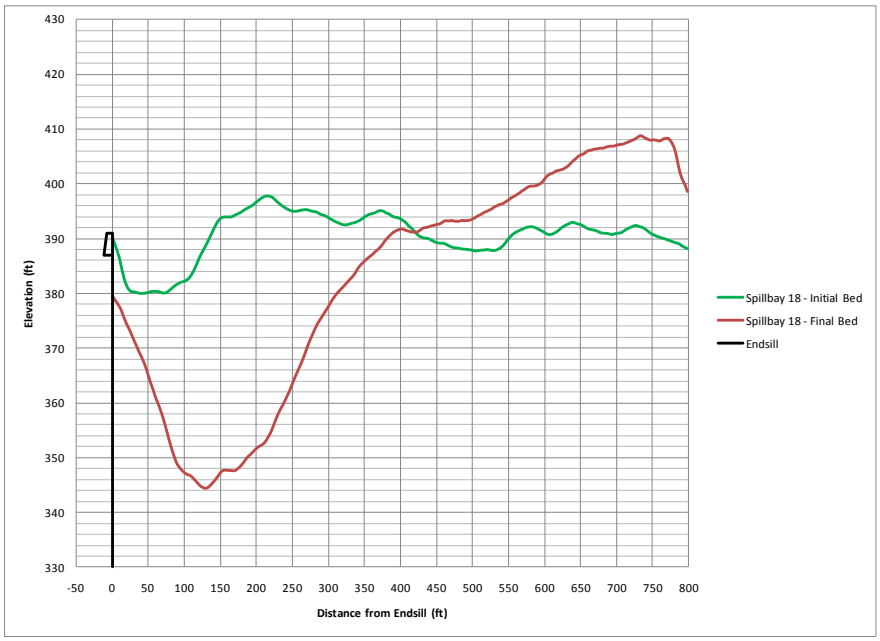

b)

Figure 3-25. Streamwise sections of initial and final PMF scour test bathymetry downstream of the centerlines of: a) Spillbay 13; b) Spillbay 18

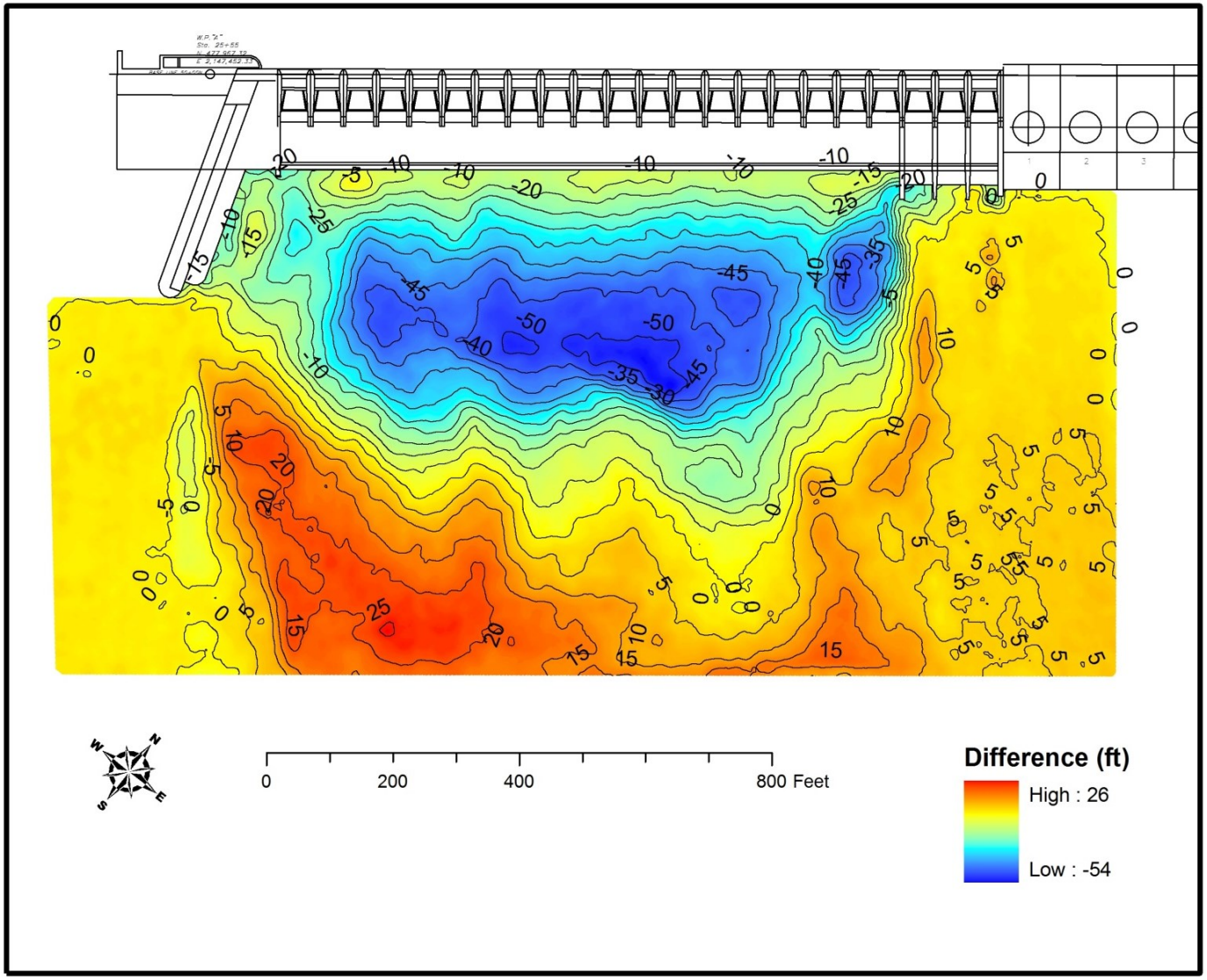

Figure 3-26. Difference plot – final bathymetry minus initial bathymetry for PMF scour test

Figure 3-27. Photographs of final scoured bed from PMF scour test

3.2. Substrate Development

To simulate the bedrock substrate in the laboratory, we prepared mixture samples with various combinations of gravel, cohesive bentonite clay, and water. Gravel was used as a non-cohesive component, and sodium bentonite was added to the mixture as a binder.

Any material that is primarily composed of the smectite group of minerals and whose physical properties are dictated by the smectite minerals is known as "Bentonite" (Grim and Guven, 1978). Large cation-exchange capacity, large specific surface area, high swelling potential, and low hydraulic conductivity to water are some characteristics of the smectite minerals. Most bentonite is either sodium or calcium bentonite. Sodium bentonite has a larger swelling capacity and lower hydraulic conductivity as compared to calcium bentonite (Gleason *et al.*, 1997).

This study used feed grade sodium bentonite #90. The Atterberg's limits, Liquid Limit (LL), and Plastic Limit (PL) of the sodium bentonite are provided in Table 3-4.

Table 3-4. Atterberg's limits of the sodium bentonite #90 feed grade

Liquid Limit	392
Plastic Limit	46
Plasticity Index	346

The particle size distribution of sodium bentonite clay was determined using the SediGraph III 5120 (Figure 3-28). The SediGraph method of particle size analysis is based on Stokes Law. Parallel X-ray beams are used in SediGraph to determine

concentration of sediment in the water column. Figure 3-29 shows the particle size distribution of the bentonite clay.

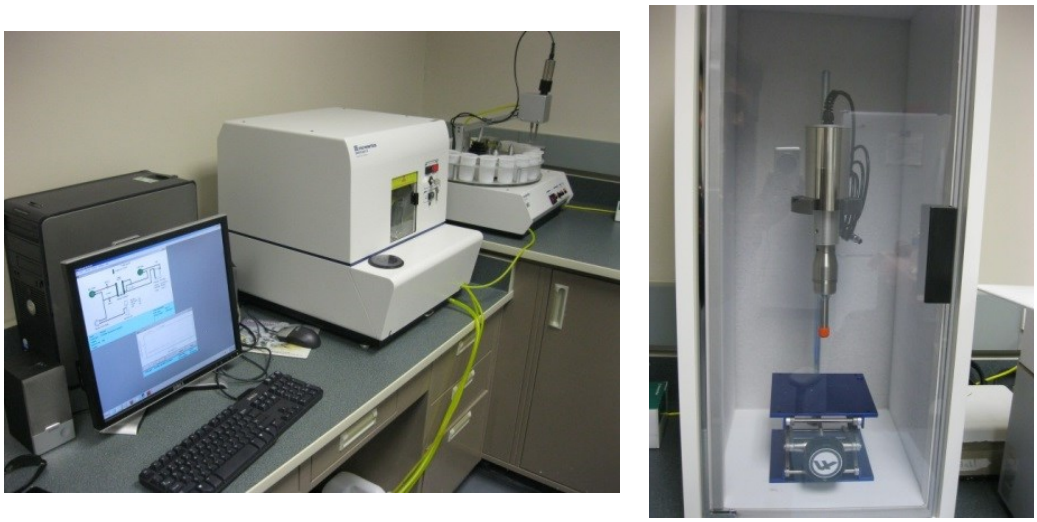

Figure 3-28. Sedigraph III5120 with Master Tech Carousel and ultrasonic stirrer

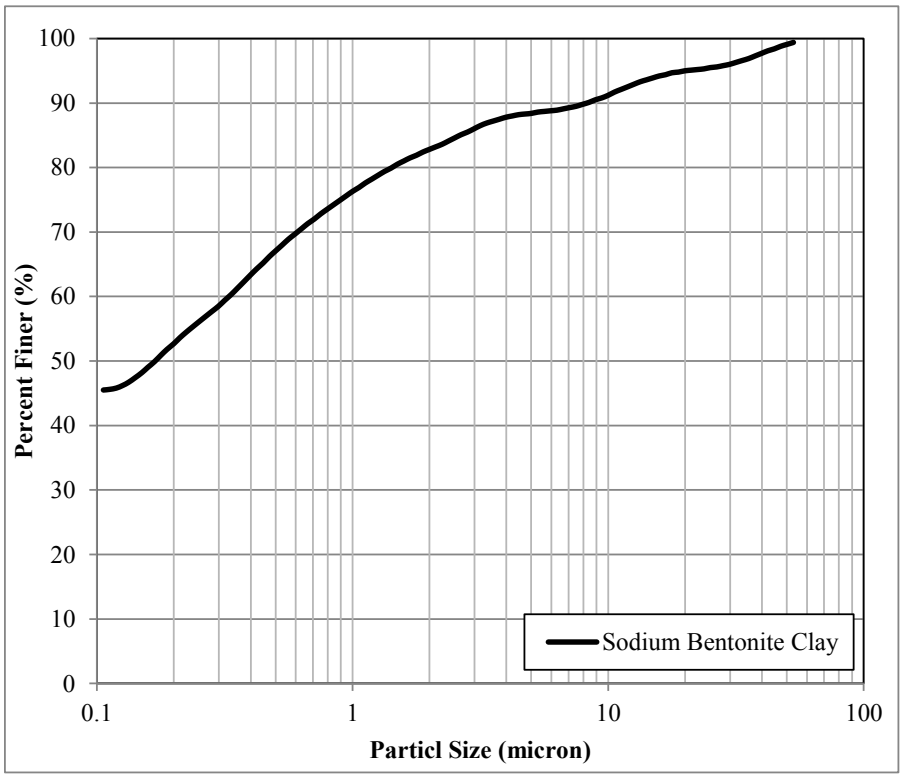

Figure 3-29. Particle size distribution of sodium bentonite clay

The same type of gravel that was used in the Priest Rapids Tailrace model scour tests was utilized here to develop the substrate. Figure 3-30 and Table 3-5 show the gravel particle size distribution and properties.

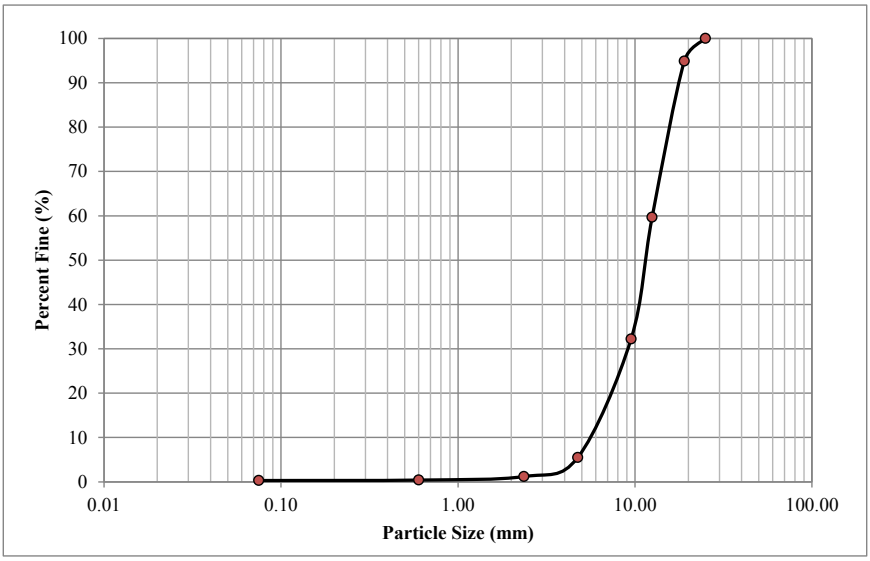

Figure 3-30. Particle size distribution of the gravel material

Table 3-5. Gravel material properties

d_{16} (mm)	d_{50}(mm)	d_{84} (mm)	d_g (mm)	σ_g
6.62	11.44	16.99	10.60	1.60

3.3. Jet Erosion Tests

3.3.1. Experimental Setup

The JET apparatus was designed based on the JET device developed by Hanson and Hunt (2007) and was built at the IIHR-Hydroscience & Engineering, The University of Iowa. The device consists of two main parts: the jet tube and the submergence tank. The jet tube was made of 76.2 mm ID acrylic pipe. A well-designed orifice plate with an opening size of 12.7 mm was built and attached to the bottom of the jet tube in order to

produce a vertical turbulent jet. A vertical vernier point gauge was installed on the jet tube to measure the scour depth in the mixture sample. The jet tube was attached to the lid and positioned at the center of the submergence tank. A stainless steel deflector plate was installed on the lid in order to protect the mixture sample surface from any disturbance prior to the beginning of the scour test. The submergence tank is 457.2 mm tall and is made of a 450.85 mm ID acrylic pipe. 219.07 mm, 171.45 mm, and 117.60 mm ID acrylic rings were installed co-centroid with the submergence tank to align the sample container with different sizes with the jet. Figure 3-31 and Figure 3-32 depict a 3-D perspective and drawing views of the JET apparatus. A photograph of the JET device setup in the laboratory is shown in Figure 3-33.

A 1 HP pump supplies water to the device. Water was pumped through a 50.80 mm I.D. flexible tubing from the sump under the laboratory floor. Control of the device flow rates was provided by butterfly valves in the feed line. Flow was measured with weigh-tank calibrated orifice flow meters. The flow meters were installed to ASME standards (Standard, A.S.M.E., 1995). Flow meter pressure differentials were measured with a precision two tube manometer that was accurate to +/- 0.00015 meters. Two orifice flow meters were installed in parallel lines to support high and low flows. Flow rates for the inlet pipes were calculated using the equations provided below. Q is discharge in cubic feet per second (cfs), and Δh is head differential in feet of water. These equations were developed from a statistical regression of the orifice calibration data.

High flows → 38.1 mm inlet: $$Q_{1.5-inch} = 0.0426 \cdot \Delta H^{0.5}$$ (Eq. 3-1)

Low flows → 25.4 mm inlet: $$Q_{1.0-inch} = 0.0210 \cdot \Delta H^{0.5}$$ (Eq. 3-2)

Maximum discharge, jet velocity, the Reynolds parameter, and the initial stress were computed for three various orifice sizes. Table 3-6 provides the jet characteristics for different orifice sizes. The JET apparatus is capable of producing a range of velocity up to 15.2 m/s. The calculated Reynolds number indicates that the jet is fully turbulent (Re>>2300). The apparatus is also capable of producing stress up to 962 Pa within the potential core jet region and 471 Pa in the developed region.

Table 3-6. Maximum jet velocity, initial stress and Reynolds number for various jet orifice sizes

Pump	d_0 (inch)	Q_{max}		$V\ jet_{max}$		Re	J_p (m)	$J_i<J_p$		$J_i>J_p$		
		(cfs)	(gpm)	(ft/s)	(m/s)			$J_i=4d_o$ (m)	$\tau_o=\tau_i$ (Pa)	$J_i=9d_o$ (m)	τ_o(Pa)	τ_i (Pa)
1/2 HP	0.313	0.020	8.97	37.51	11.43	9.1E+04	0.050	0.032	543.89	0.071	543.89	266.51
	0.500	0.034	15.30	24.99	7.62	9.7E+04	0.080	0.051	241.43	0.114	241.43	118.30
	0.750	0.041	18.34	13.32	4.06	7.7E+04	0.120	0.076	68.55	0.171	68.55	33.59
1.0 HP	0.313	0.024	10.64	44.53	13.57	1.1E+05	0.050	0.032	766.39	0.071	766.39	375.53
	0.500	0.068	30.53	49.89	15.21	1.9E+05	0.080	0.051	961.94	0.114	961.94	471.35
	0.750	0.090	40.56	29.46	8.98	1.7E+05	0.120	0.076	335.32	0.171	335.32	164.31

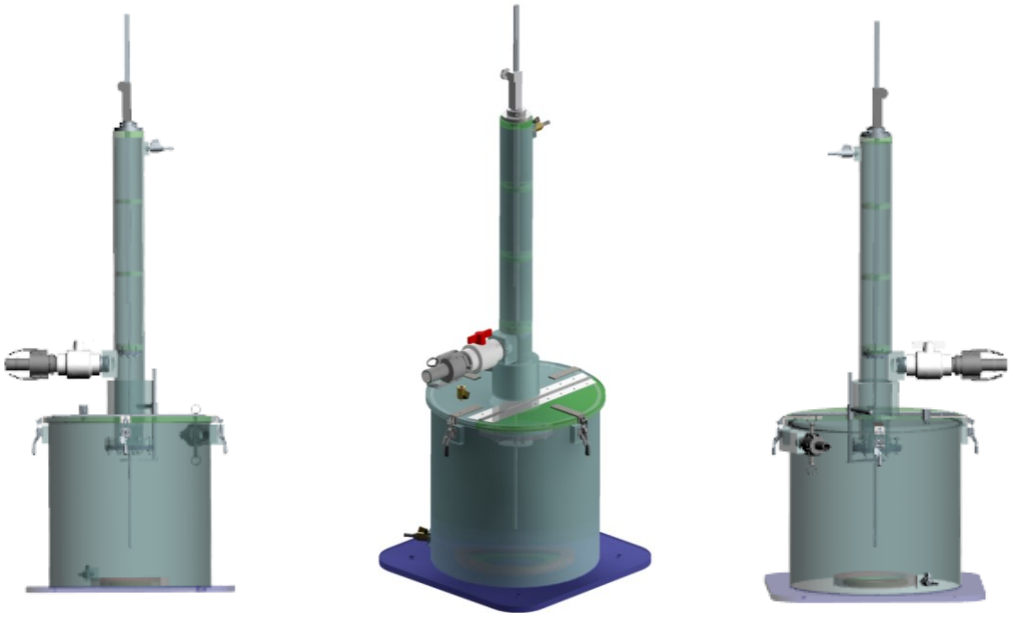

Figure 3-31. JET apparatus 3D perspective views

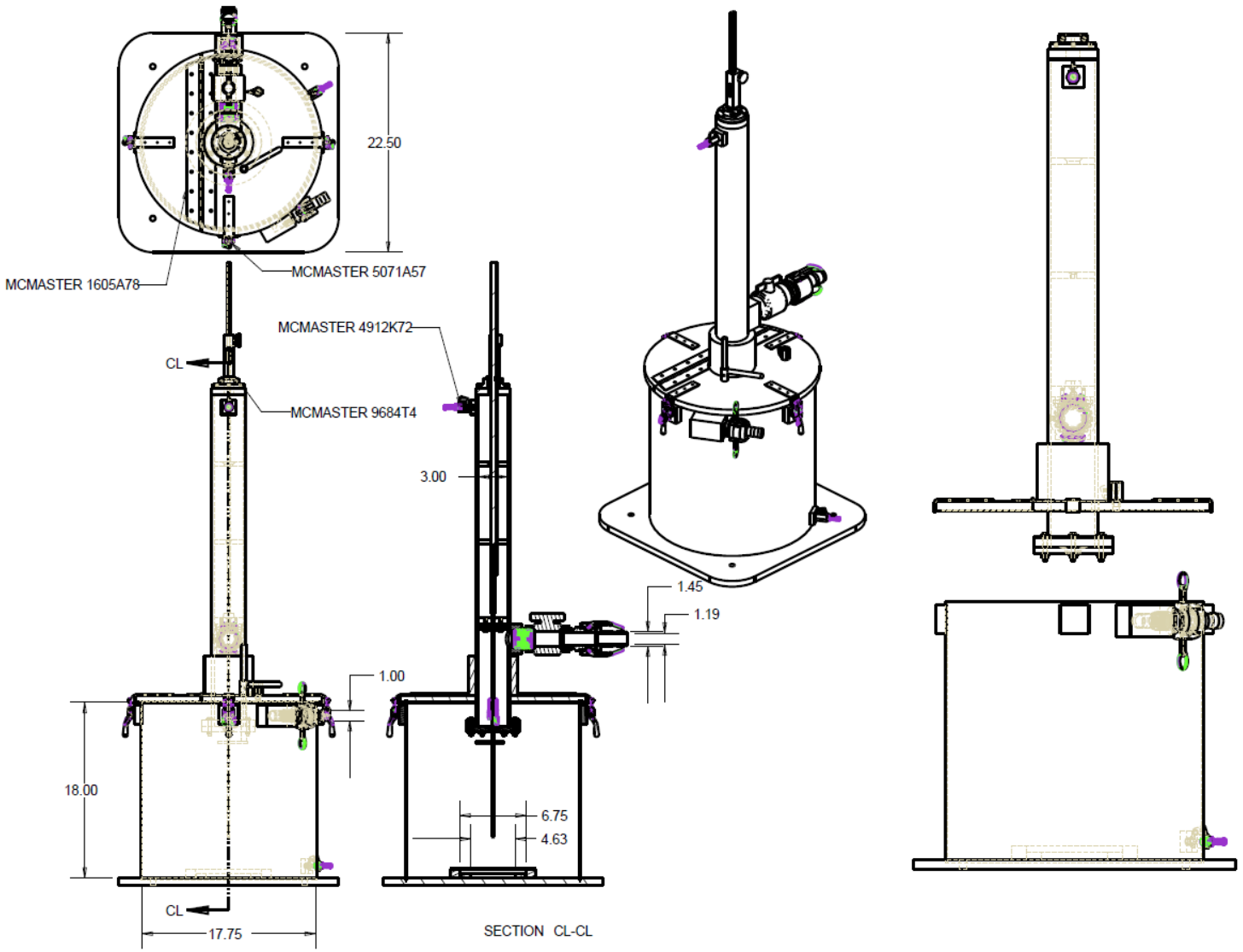

Figure 3-32. The JET apparatus drawing views

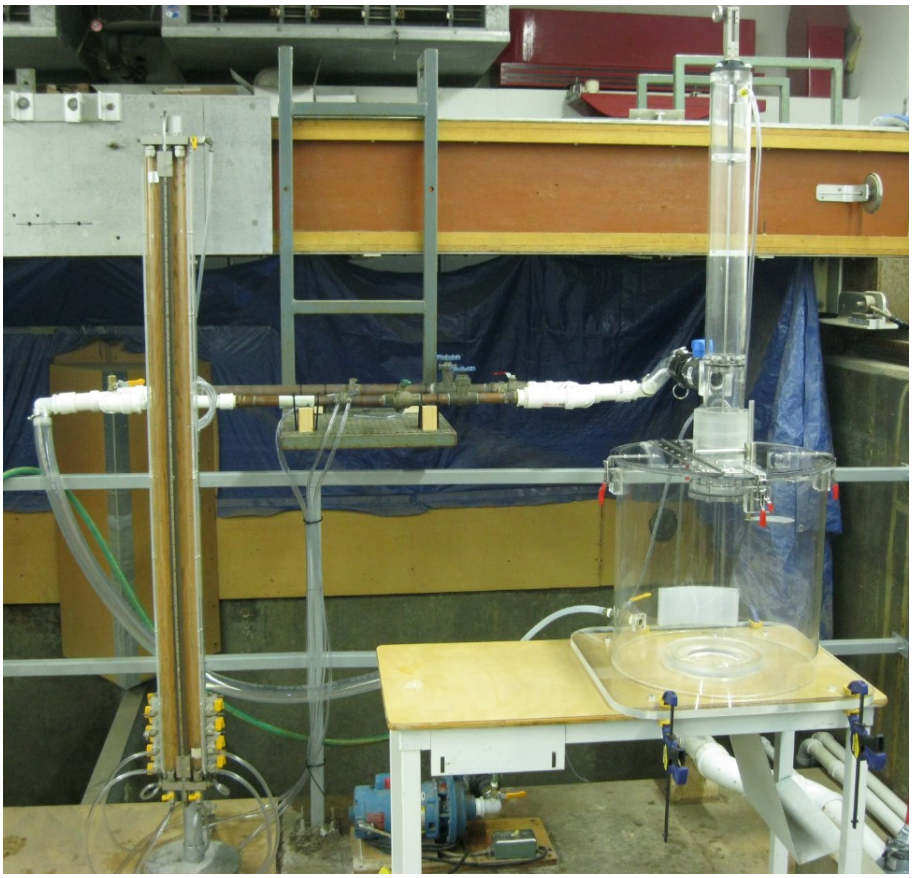

Figure 3-33. Photograph of the JET apparatus setup

3.3.2. Sample Preparation

Various replicate samples were made with different combinations of gravel, sodium bentonite clay, and water. In a rotary mixer, water was added and mixed with gravel to ensure that the entire surface of the gravel particles becomes wet. The sodium bentonite clay was slowly added to create a homogenous mixture.

A sample container was built using a 202.2 mm I.D. PVC pipe, which was cut lengthwise in half, hinged on one side, and clamped on the other side. The mixture was placed in the sample container in 3 layers (each layer approximately 50 mm thick). Each layer was compacted with 16 blows using a manual rammer in order to keep consistency

in the sample preparation procedure and to achieve maximum possible homogeneity. The manual rammer was a 50.8 mm diameter cylinder with a weight of 24.5 N and was dropped from a height of 304.8 mm, which produces a compaction effort of 600 kN.m/m^3 (ASTM-D698-07, 2007). Finally, the sample was removed from the sample container and placed into the test container in order to be tested in the JET device. Figure 3-34 shows the mixture and prepared sample for the test. An example of the test container with a sample mixture is shown in Figure 3-35.

Figure 3-34. Sample container and manual rammer

Figure 3-35. Test container with sample mixture prior to testing

3.3.3. Test Procedure

Tests were conducted using the submerged jet device with a nozzle diameter of 12.7 mm. Cylindrical samples had a diameter and height of 202.1 mm and 146.05 mm, respectively. To investigate the erodibility of the simulated bedrock, five different mixtures were made with various combinations of gravel, bentonite clay, and water. Table 3-7 presents the simulated bedrock mixtures where the fraction of materials is expressed in term of mass. It should be noted that all of the samples were created using one type of gravel. The procedure of choosing an appropriate gravel type is site specific and was not investigated in the present study. The mixtures with various bentonite clay contents and a constant water content were tested to investigate the effect of the bentonite clay content on the erodibility of simulated bed rock. Mixture (GB-13) which consisted of 85.6% gravel, 7.70% bentonite clay, and 6.70% water (expressed in term of mass) was used as the baseline mixture. This is the mixture utilized as the final simulated bedrock mixture for the Priest Rapids Dam scour tests (See Section 3.1.4). For each mixture, four samples were prepared to be tested using the JET device for various initial stresses. Individual tests were conducted for 60 minutes. Data collection was performed in 10 minutes elapsed time. Data collection includes center scour depth, maximum scour depth, eroded material, and photographs. Eroded materials were collected, washed, dried, and weighed. The eroded mass for each test case was plotted versus the average stress that was applied to the sample. Figure 3-36 shows an example of the JET test underway.

Table 3-7. Mixture with varying bentonite clay content

Mixture	Material (%)*		
	Gravel	Bentonite	Water
GB-15	89.45%	3.85%	6.70%
GB-14	87.52%	5.78%	6.70%
GB-13	85.60%	7.70%	6.70%
GB-12	83.68%	9.62%	6.70%
GB-16	81.75%	11.55%	6.70%

*Expressed in term of mass

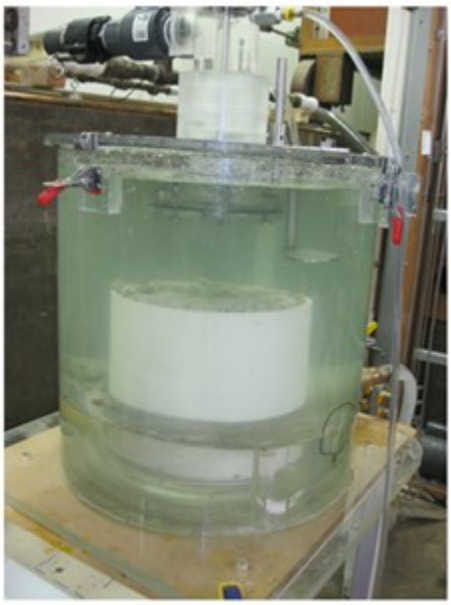

Figure 3-36. JET test underway

3.3.4. Test Results

3.3.4.1. Simulated Bedrock Critical Stress

The critical stress of the simulated bedrock was determined using the experiments conducted with the JET device. In order to examine the critical stress of the cohesive soil

using the JET device, different methods have been utilized. These methods are: the Hanson and Cook (2004) method, visual assessment of the critical stress, an equilibrium state assessment of the critical stress, and an assessment of the critical stress from the JET tests erosion rate plot (Cossette *et al.*, 2012).

In the present study, the critical stress of the simulated bedrock was assessed from the eroded material plot. The eroded material was collected, washed, dried and weighed for each time interval measurement during the scour test. Then, the eroded mass was plotted against the average stress applied to the sample on that time interval. The critical stress of the sample was determined as the stress value associated with zero eroded mass.

To calculate the average stress applied to the sample surface, we employed the method developed by Hanson and Cook (2004).

Hanson and Cook (2004) determined that the maximum stress applied to the boundary of soil and water for the impingement submerged circular jet is determined by:

$$\tau = C_f \rho U_0^2 \left(\frac{J_p}{J}\right)^2 \quad \text{for} \quad J \geq J_p \qquad \text{(Eq. 3-3)}$$

$$J_p = C_d \, d_0 \qquad \text{(Eq. 3-4)}$$

where τ is the maximum stress at the soil water surface, C_f is friction coefficient, U_0 is the jet velocity at the exit, $J_p$is the potential core length of the jet, C_d is the diffusion constant equal to 6.3, d_0 is the jet diameter, and J is the distance between the jet exit and the soil surface.

The value of the friction coefficient ($C_f = 0.00416$) was determined by Hanson *et al.* (1990) through a series of experiments on a circular submerged jet acting on a flat and smooth surface.

The average applied stress was computed as follow:

$$\tau_{ave} = \frac{\tau_i + \tau_f}{2} \quad \text{(Eq. 3-5)}$$

where τ_i and τ_f are the initial and final applied stresses at each measurement time interval, respectively.

The plot of the eroded mass against the average applied stress was developed for each mixture. To determine the critical stress of the mixture, a linear function was fitted to the data and extended to the zero eroded mass.

Figure 3-37 shows an example of an eroded mass-average applied stress plot in order to determine the critical stress for mixture GB-12. The original plot refers to the plot in which all of the measurements were used. As can be observed in figure 3-37, the fitted linear function does not show a high regression coefficient (R^2=0.0676). The data corresponding to the first measurement time interval does not follow a clear pattern (circled with a dashed line).

We revised the plot by eliminating the data corresponding to the first measurement time interval. Figure 3-38 shows the revised plot for mixture GB-12. The regression coefficient of the linear function was dramatically improved (R^2=0.5837). This pattern was observed through the rest of datasets as well. Thus, for examining the critical stress of the mixtures using the eroded mass-average applied stress plot method, the above mentioned revision was applied to all of the datasets. The revised eroded mass-stress plots for mixtures GB-13 through GB-16, are provided in Appendix A (Figure B-1 through B-4).

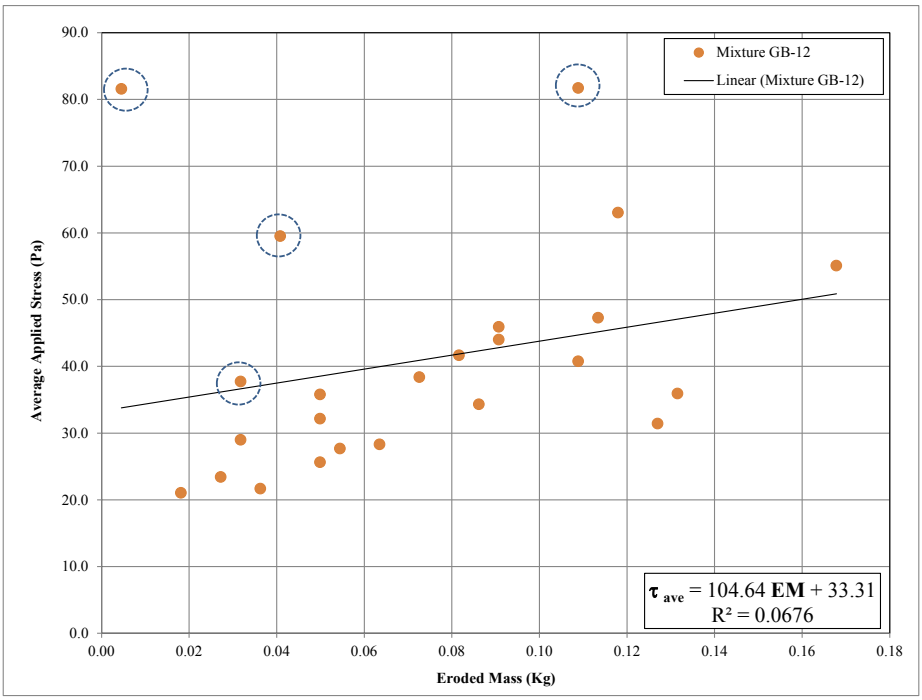

Figure 3-24. Eroded mass vs. average applied stress for mixture GB-12 (original plot)

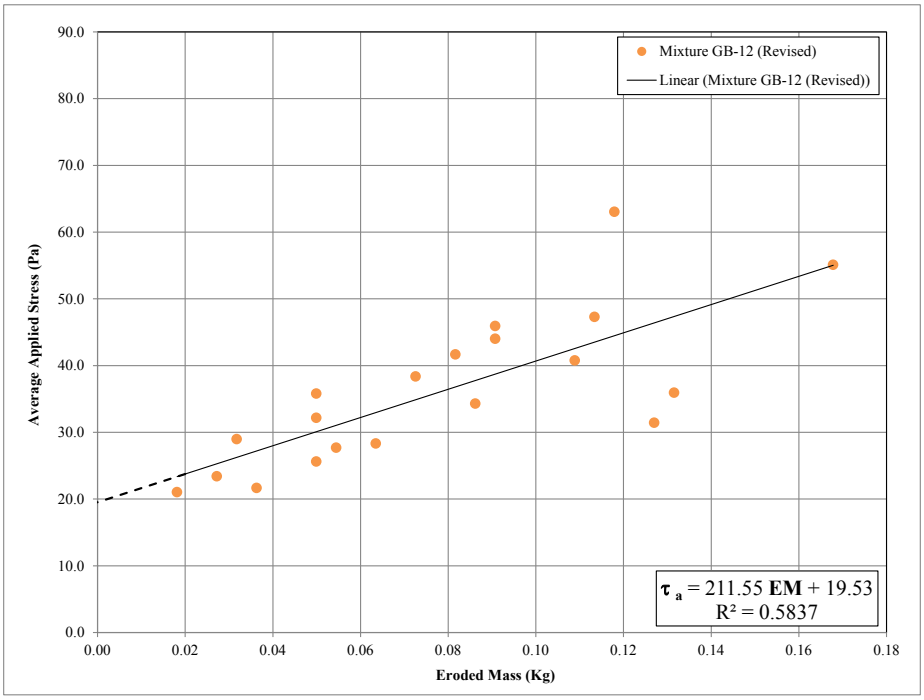

Figure 3-25. Eroded mass vs. average applied stress for mixture GB-12 (revised plot)

The critical stress of the simulated bedrock samples was determined. Table 3-8 show the critical stress of the simulated bedrock mixtures with various bentonite clay contents. The general information of the JET tests is presented in Table 3-9.

At first glance, the results reveal that the critical stress of the mixture positively correlates with the bentonite clay content. In other words, mixtures with larger bentonite clay contents are more resistant to erosion.

Table 3-8. Critical stress of the simulated bedrock mixtures with various bentonite clay contents

Mixture	**Gravel**	**Bentonite**	**Water**	τ_c **(Pa)**
GB-15	89.45%	3.85%	6.70%	5.99
GB-14	87.53%	5.78%	6.70%	8.95
GB-13	85.60%	7.70%	6.70%	16.94
GB-12	83.68%	9.63%	6.70%	19.53
GB-16	81.75%	11.55%	6.70%	27.39

Table 3-9. Simulated rock mixtures- JET experiments

Mixture	Material (%)			Test	Date	d_0 (mm)	Q(lit/s)	U_0 (m/s)	Re	τ_0 (Pa)	τ_i (Pa)
	Gravel	Bentonite	Water								
GB-15	89.45%	3.85%	6.70%	GB-15-1	8/11/2014	12.7	0.46	3.64	46179	55.00	21.28
				GB-15-2	8/11/2014	12.7	0.57	4.48	56871	83.42	42.22
				GB-15-3	8/11/2014	12.7	0.52	4.09	51973	69.67	34.14
GB-14	87.52%	5.78%	6.70%	GB-14-2	7/29/2014	12.7	0.57	4.53	57493	85.25	45.84
				GB-14-3	7/29/2014	12.7	0.69	5.41	68754	121.92	61.37
				GB-14-4	7/29/2014	12.7	0.81	6.40	81307	170.51	93.23
				GB-14-5	8/1/2014	12.7	0.44	3.51	44613	51.34	26.55
GB-13	85.60%	7.70%	6.70%	GB-13-1	7/30/2014	12.7	0.57	4.51	57338	84.79	46.36
				GB-13-2	7/31/2014	12.7	0.69	5.42	68831	122.20	64.97
				GB-13-3	7/31/2014	12.7	0.81	6.37	80869	168.67	97.65
				GB-13-4	7/31/2014	12.7	0.89	7.00	88927	203.97	109.05
GB-12	83.68%	9.62%	6.70%	GB-12-1	8/1/2014	12.7	0.57	4.49	56965	83.69	45.25
				GB-12-2	8/1/2014	12.7	0.69	5.43	69012	122.84	64.24
				GB-12-3	8/1/2014	12.7	0.81	6.41	81416	170.96	88.43
				GB-12-4	8/2/2014	12.7	0.90	7.07	89822	208.09	98.78
GB-16	81.75%	11.55%	6.70%	GB-16-1	8/7/2014	12.7	0.58	4.55	57739	85.99	43.99
				GB-16-2	8/7/2014	12.7	0.69	5.43	69012	122.84	58.62
				GB-16-3	8/7/2014	12.7	0.82	6.44	81851	172.80	86.97
				GB-16-4	8/10/2014	12.7	0.89	7.06	89624	207.17	93.38

In the present study, Annandale's method is utilized to link the strength of the simulated bedrock to the prototype bedrock. After determining the critical stress of the simulated bedrock mixture, it is necessary to examine the critical stream power. To link the critical stress value of the mixtures to the stream power, we employed the universal distribution of turbulence production near-bed region.

The universal distribution of energy supply, turbulence production, and the direct dissipation near-bed region in the case of turbulent flow were provided and verified experimentally by Schlichting and Gersten (2000). It is indicated that distributions shown in Figure 3-39 are universal and applicable to any type of turbulent flow. The applied stream power to the bed is actually the turbulence production ($\tau \frac{du}{dy}$) near the bed region. The dimensionless term of turbulence production is defined by $\tau^+ \frac{du^+}{dy^+}$.

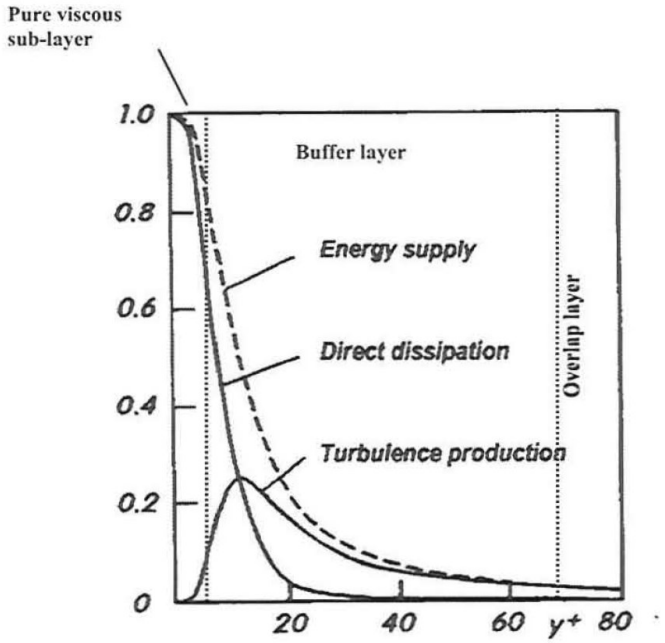

Figure 3-26. Universal energy balance of the mean motion in the near-bed region (Schlichting and Gersten, 2000)

By integrating the dimensionless turbulence production term with respect to the dimensionless depth near –bed region ($0 \leq y^+ \leq 70$), Annandale (2006) showed that the applied unit stream power in the near-bed region along a boundary can be expressed as:

$$P_{applied} = \tau_t \bar{u} = 7.853 \frac{\bar{\tau}_w^{1.5}}{\sqrt{\rho}} \quad \text{(Eq. 3-6)}$$

where τ_t is the turbulent shear stress at the boundary, $\bar{u}$ is average velocity, and $\bar{\tau}_w$ is the average wall shear stress. The pressure fluctuation, which is the main cause of the erosion process, is a result of the applied stream power that is generated by the turbulence production near the bed region (Annandale, 2006).

The critical stream power of the mixtures associated with the critical stresses, as determined by the experiments, can be computed using (Eq. 3-6). Eventually, the erodibility index of the simulated bedrock mixtures was calculated using Annandale's

Erodibility Index Method (Eqs. 2-12 and 2-13). Table 3-10 shows the erodibility index of the simulated bedrock mixtures.

Table 3-10. Erodibility index of the simulated bedrock mixtures

Mixture	Gravel	Bentonite	Water	τ_c (Pa)	P_c (KWatt/m^2)	K
GB-15	89.45%	3.85%	6.70%	5.99	3.64E-03	1.52E-05
GB-14	87.52%	5.78%	6.70%	8.95	6.65E-03	5.97E-05
GB-13	85.60%	7.70%	6.70%	16.94	1.73E-02	5.26E-04
GB-12	83.68%	9.62%	6.70%	19.53	2.14E-02	8.54E-04
GB-16	81.75%	11.55%	6.70%	27.39	3.56E-02	2.70E-03

The erodibility index associated with gravel particle size (D_{84}=16.99 mm) was also compared with the results of the simulated bedrock mixtures. Two approaches were employed: the shields diagram and the erodibility index method.

The critical stress to the incipient motion of the gravel particle size of D_{84}=16.99 mm was determined using the shields approach (τ_c=14.93 N/m^2). By inserting the critical stress into (Eq. 3-6) and then utilizing (Eq. 2-12), the critical stream power and erodibility index of the gravel particles were determined as 0.0143 Kw/m^2 and 0.00034, respectively.

Also, an effort was made to determine the erodibility index of the gravel particles using Annandale's erodibility index method. As previously mentioned, the erodibility index method is applicable to a wide range of earth materials ranging from very fine soils to bedrock. The method was employed here to calculate the resistance of the gravel particles to erosion (erodibility index).

The average mass strength number for gravel was considered to be M_s=0.105 (See Table A-6), which is the average value of very loose and dense material. The particle size number was calculated using the following equation:

$$K_b = 1000D^3 \quad \text{(Eq. 3-7)}$$

where D is the characteristic particle size (m).

The particle size number for the characteristic gravel size (D_{84}=16.99 mm) was computed to be (K_b= 0.0049). The shear strength number or the inter-particle bond shear strength of the granular soil is estimated by the friction angle using the following equation:

$$K_d = \tan\varphi \quad \text{(Eq. 3-8)}$$

Assuming a friction angle of 35 degrees for the gravel, the shear strength number will be (K_d= 0.7). The relative ground structure number for the non-cohesive granular earth material is considered to be unity (J_s=1.0).

Consequently, the erodibility index of the gravel can be calculated using (Eq. 2-8). The erodibility index of gravel is equal to 0.00036.

The erodibility index of the simulated bedrock mixtures were plotted against the bentonite clay contents (Figure 3-40). Also, the erodibility index of the gravel material, calculated using the shields and erodibility index methods, was added to the plot (zero bentonite clay content). As can be seen in Figure 3-40, the erodibility index of the gravel material is higher than those of the GB-15 and GB-14 mixtures, with 3.85% and 5.78% bentonite clay content, respectively. This means that the gravel material is less susceptible to erosion than the simulated bedrock mixtures. This finding contradicts the

visual observation conducted during the experiments, in which it was observed that adding bentonite clay to the gravel material increases its resistance against erosion.

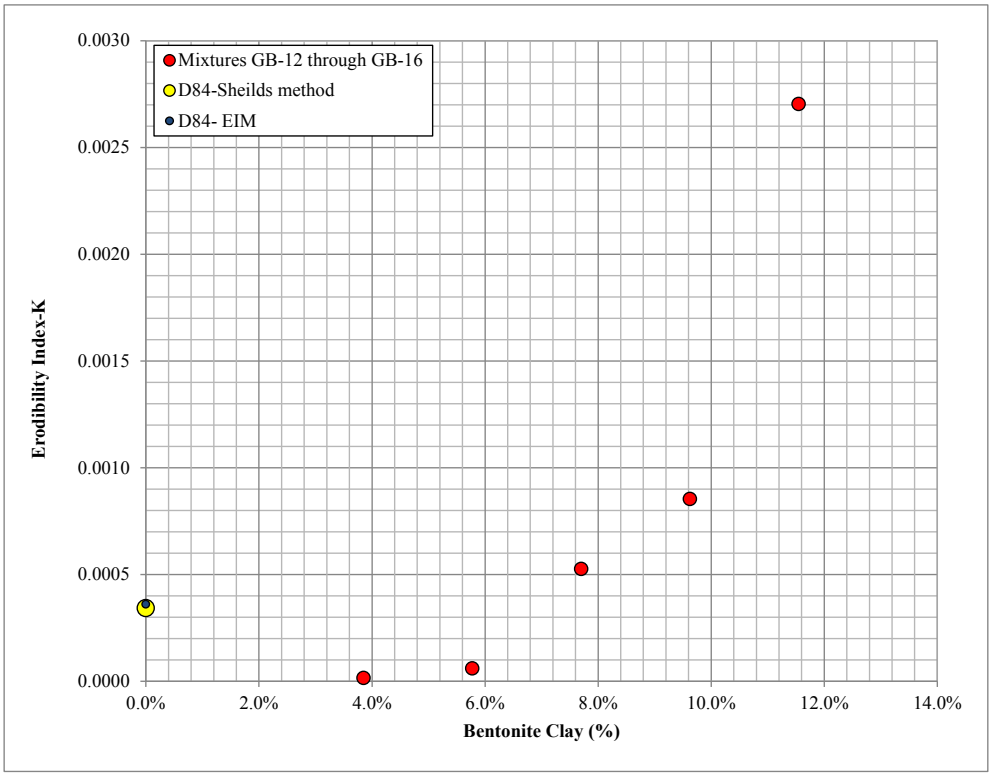

Figure 3-40. Variation of erodibility index with bentonite clay content

The erodibility index of the simulated bedrock mixture was calculated using the critical stress that was obtained through a series of experiments conducted with the JET device. To calculate the applied stress to the sample, Hanson and Cook (2004) used a friction coefficient equal to 0.00416 (C_f= 0.00416). Annandale (2006) disputed the value of the friction coefficient used by Hanson and Cook (2004).

The unit Stream power and shear stress induced by an impinging jet can be determined using the following equations:

$$P = \tau U \quad \text{(Eq. 3-9)}$$

$$\tau = \rho C_f U^2 \quad \text{(Eq. 3-10)}$$

where P is the unit stream power, τ is the shear stress, U is the velocity, ρ is the density of water, and C_f is the coefficient of friction. Re-writing (Eq. 3-9) for the stream power using $U = \sqrt{\frac{\tau}{\rho C_f}}$ yields:

$$P = \tau U = \tau \sqrt{\frac{\tau}{\rho C_f}} \quad \text{(Eq. 3-11)}$$

$$P = \frac{1}{C_f} \tau \sqrt{\frac{\tau}{\rho}} = \frac{1}{C_f} \frac{\tau^{1.5}}{\sqrt{\rho}} \quad \text{(Eq. 3-12)}$$

The stream power equation (Eq. 3-12) is equivalent to the applied stream power equation (Eq. 3-6), the applied stream power equation was derived from the universal boundary layer theory. Comparing (Eq. 3-6) and (Eq. 3-12):

$$\frac{1}{C_f} = 7.853 \quad \text{(Eq. 3-13)}$$

$$C_f = 0.016 \quad \text{(Eq. 3-14)}$$

As can be seen, the calculated value for the coefficient of friction is an order of magnitude higher than the one used by Hanson and Cook (2004) (C_f=0.00416).

Two arguments need to be considered. First, the value of the friction coefficient (C_f=0.00416) was determined through a series of jet experiments by Hanson *et al.,* (1990) that acted on a smooth and flat boundary. It should be noted that this value might be different in the case of a soil sample (which is not completely smooth and flat). Second, the friction coefficient (C_f = 0.016) was calculated using the boundary layer theory and turbulence production near the bed region, which is universal, widely accepted, and applicable to any kind of turbulent flow (Schlichting and Gersten, 2000).

Furthermore, the coefficient of friction for the plane turbulent wall jet was experimentally investigated by Myers *et al*. (1963), who reported a range of friction coefficient values (0.0003-0.03) along the impact length of the jet for Reynolds numbers between 60000 and 70000.

So, based on the calculations, the coefficient of friction used by Hanson and Cook (2004) to calculate the applied stress on the soil sample (C_f=0.00416) seems to be low and leads to an underestimation of the stress values. This argument can also explain why the erodibility index of the GB-15 and GB-14 mixtures, respectively, with 3.85% and 5.78% bentonite clay content were less than the one for the gravel material without any bentonite clay content.

Consider the case in which we use C_f=0.016 instead of C_f=0.00416 in the calculation of critical stress. Table 3-11 provides the erodibility index of the simulated bedrock mixtures in which C_f=0.016 was utilized to determine the critical stress value. Figure 3-41 shows the variation of erodibility index values with the bentonite clay content of the mixtures. Using C_f =0.016 resulted in larger calculated values of the erodibility index. Moreover, these values are larger than the erodibility index of the gravel material. The results agree with the observations made during the experiments.

Table 3-11. Erodibility index of the simulated bedrock mixtures (C_f=0.016)

Mixture	Gravel	Bentonite	Water	τ_c (Pa)	P_c (KWatt/m^2)	K
GB-15	89.45%	3.85%	6.70%	23.05	2.75E-02	1.50E-03
GB-14	87.52%	5.78%	6.70%	34.42	5.01E-02	5.89E-03
GB-13	85.60%	7.70%	6.70%	65.14	1.31E-01	5.19E-02
GB-12	83.68%	9.62%	6.70%	75.10	1.62E-01	8.43E-02
GB-16	81.75%	11.55%	6.70%	105.33	2.68E-01	1.73E-01

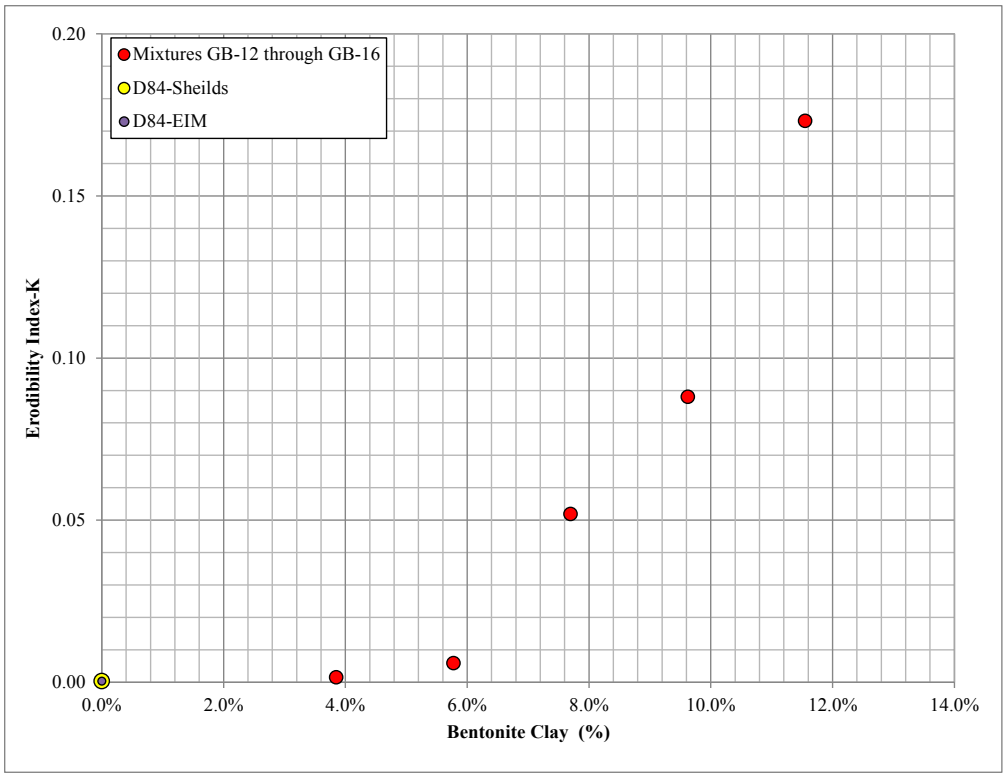

Figure 3-41. Variation of erodibility index with bentonite clay content (C_f=0.016)

As was previously demonstrated, using C_f=0.00416 (Hanson and Cook, 2004) seems to underestimate the erodibility index, whereas using C_f=0.016 (Annandale, 2006) resulted in more reasonable outcomes. However, the coefficient of friction value reported by Annandale (2006) is mathematically driven and requires experimental

verification. Henceforth, in the present study, a coefficient of friction equal to 0.016 is utilized for any calculations, and all the results are based on this value. The erosion threshold relationship for the simulated bedrock mixtures is developed and presented in Figure 3-42.

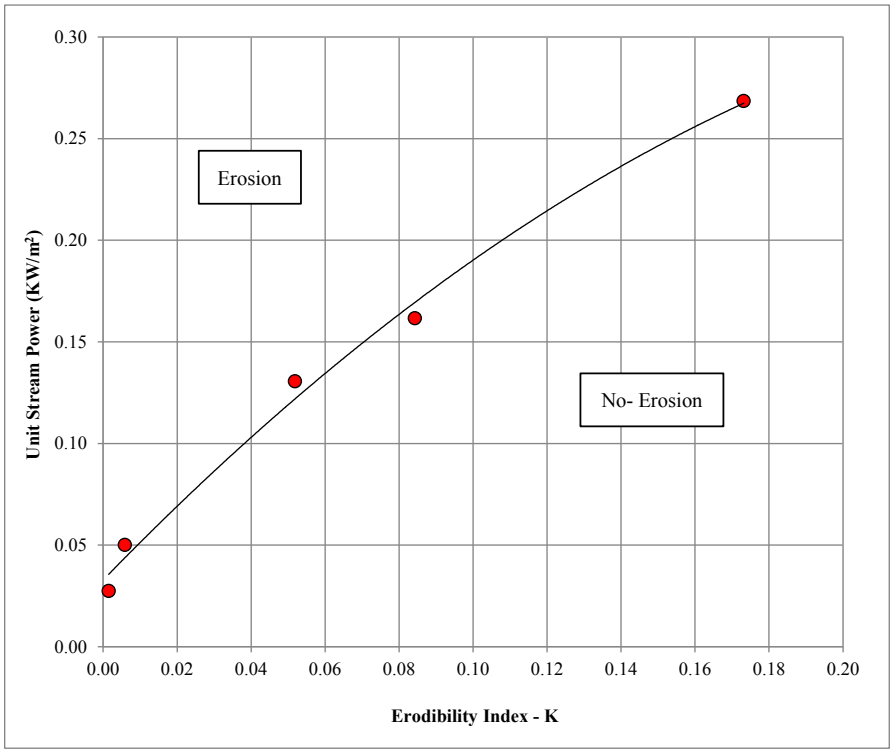

Figure 3-27. Erosion threshold relationship for the simulated bedrock mixture

3.4. Summary

This chapter summarized the rock scour simulation at the Priest Rapids Dam using the analog laboratory model, the Jet Erosion Test experimental setup and its measurements. The first part of this chapter presents the use of weakly cohesive material to study scour in the Priest Rapids Dam laboratory scaled model. This project is part of a series of projects at IIHR sponsored by the Public Utility District No. 2 of Grant County,

Ephrata, Washington (GCPUD) in order to investigate juvenile salmonid migration at the Wanapum/Priest Rapids Development. Three physical models were constructed and tested to support the design of Priest Rapids Dam's fish bypass. As part of the last phase of the project, it was important to determine the effect of the newly designed fish bypass system on the downstream rock foundation scour. To assess the scour process, we utilized the 1:64 Froude scale tailrace model of the dam.

In a series of tests, we attempted to establish an appropriate gravel/bentonite/water mixture to replicate an existing scour hole downstream of spillbay 22. The appropriate weakly cohesive substrate was determined as 9 parts gravel to 1 part bentonite clay and 1 part water expressed in term of volume (85.6% gravel, 7.70% bentonite clay, and 6.70% water expressed in term of mass). After finding the appropriate mixture, we utilized it in the model in order to evaluate the scour potential downstream of the fish bypass units and under the PMF condition.

The second part of this chapter presents the fundamental experiments and results. We used weakly cohesive substrate to simulate the rock formation. Bentonite clay was added as a cohesive additive to granular sediment and water to simulate rock formation. Various combinations of gravel, cohesive bentonite clay, and water were mixed in a rotary mixer, placed into the sample box layer by layer, and compacted to achieve the greatest possible degree of homogeneity. We then tested the samples using the laboratory JET apparatus to examine their resistance to the erosion process.

The JET apparatus was designed based on the one developed by Hanson and Hunt (2007) and was built at the IIHR-Hydroscience & Engineering, The University of Iowa.

The JET apparatus can produce a range of velocities up to 15.2 m/s. The calculated Reynolds number indicates that the jet is fully turbulent (Re>>2300).

Simulated bedrock samples- weakly cohesive substrate which is mixture of gravel, bentonite clay, and water- were tested using the JET apparatus. The results showed that the erosional strength of the substrate is mainly affected by the percentage of bentonite clay content. The mixtures with a higher percentage of bentonite clay are more resistant and less susceptible to erosion.

The initial data analysis using C_f=0.00416 resulted in low critical stress values. Following the argument made by Annandale (2006) and using C_f=0.016 yields more realistic results.

In order to correlate the erosional strength of simulated rock- weakly cohesive substrate- and prototype rock formation, we used Annandale's erodibility index method. The threshold of the erosion plot for the weakly cohesive substrate, similar to Annandale's plot for earth material, was then developed.

CHAPTER 4 MODEL AND PROTOTYPE ROCK

This chapter, which is based on the premise that the jointed rock formation can be considered pre-fractured, explains the method we developed to simulate the prototype bedrock for the laboratory hydraulic models. This premise allows the use of a mixture of gravel, water, and bentonite clay as a cohesive additive to simulate the jointed rock formation. Gravel represents the rock block, and the cohesive additive holds the modeled rock block together.

The erosional strength of the weakly cohesive substrates - simulated bedrock mixtures - was determined through a series of experiments using a JET device. The example of the Priest Rapids Dam project illustrates the method we used to simulate the strength of the prototype bedrock for use in the laboratory model.

4.1. Simulating the Erosional Strength of Prototype Bedrock using the Weakly Cohesive Substrate

In the present study, the weakly cohesive substrate is comprised of gravel, water, and bentonite clay as a cohesive additive. As previously discussed, the amount of adhesive additive that is used is the key variable that affects the strength of the simulated bedrock mixture. While the gravel size distribution plays some role in the strength of the mixture, it is much less significant than the amount of cohesive additive. Moreover, the process of selecting an appropriate gravel type is site specific and was not investigated in the present study. When we investigated the effect of the amount of water used to build the samples, we determined that the strength of the mixture does not depend on the water

content. Since the important variable is the amount of bentonite clay, choosing an appropriate mixture in this study signifies using the appropriate amount of bentonite clay.

4.1.1. Determining the Erosional Strength of the Prototype Bedrock

The first step in selecting an appropriate weakly cohesive substrate entails evaluating and examining the strength and resistance against erosion of the prototype bedrock. This can be achieved by using Annandale's erodibility index (See Section 2.4.2).

As an example, the erodibility index of the bedrock formation at the Priest Rapids Dam site project will be determined in the following section. A full description of the project site's geology with its bedrock formation characteristics is provided in Section 3.1.2, which will be used to examine the erodibility index.

- Mass strength number (M_s)

The Priest Rapids dam bedrock formation is classified as a very strong and dense rock, whose mass strength number (M_s) value is determined using

Table A-1. According to GeoEngineers, Inc. (2005), the bedrock formation is classified using the Unified Rock Classification System (URCS) as BBEAe to CBEAe. Based on the URCS classification the bedrock formation is "visually fresh state" to "stained state" in terms of the degree of weathering, " pit quality" in terms of strength (estimated UCS=55-103 MPa), "Open 3-D planes of separation" in terms of discontinuities, and unit weight greater than 2550 Kg/m^3. Therefore, based on the available information, the mass strength number of rock at the Priest Rapids dam is estimated to be M_s=70.0.

- Particle/block size number (K_b)

The block size number depends on the joint spacing and number of joints set in the rock formation. Joint spacing is determined by the Rock Quality Designation (RQD). The RQD of the rock formation at the Priest Rapids site project is unavailable and needs to be estimated using the following equations (Annandale, 2006):

$$RQD = \left(115 - 3.3\, J_c\right) \quad \text{(Eq. 4-1)}$$

where J_c is the number of joints in a volume of one cubic meter and can be measured or estimated with the equation:

$$J_c = \left(\frac{3}{D}\right) + 3 \quad \text{(Eq. 4-2)}$$

where D is the mean block diameter that can be calculated by:

$$D = \left(J_x J_y J_z\right)^{0.33} \quad \text{for} \quad \text{D>0.10 m} \quad \text{(Eq. 4-3)}$$

where J_x, J_y, and J_z are the average joint spacing in meters in three perpendicular directions.

Also, another equation can be used:

$$RQD = (105 - \frac{10}{D}) \quad \text{(Eq. 4-4)}$$

According to the GeoEngineers (2005), the bedrock formation at the project site is characterized by open three-dimensional planes of separation that are estimated to form blocks of 0.5-1'x 1-2'x 1-3'. The RQD value of the rock formation can be calculated using the above mentioned equation. The joint set number (J_n) was determined to be equal to 3.34 using Table A-2. Table 4-1 presents the RQD value of the rock formation.

Table 4-1. RQD of the
Priest Rapids dam project site
rock formation

$D_{smallest}$ (m)	0.24
$D_{largest}$ (m)	0.55
$D_{average}$ (m)	0.40
$J_{c\text{-}ave}$	10.54
RQD_{ave} (Eq. 4-1)	80.2
RQD_{ave} (Eq. 4-4)	79.9

Consequently, the block size number can be determined using (Eq. 4-5), which yields (K_b=23.95) for the rock formation.

$$K_b = \frac{RQD}{J_n} \quad \text{(Eq. 4-5)}$$

- Discontinuity/bond shear strength number (K_d)

The discontinuity/shear strength number represents the resistance of the rock formation due to its discontinuities and is defined by the following equation:

$$K_d = \frac{J_r}{J_a} \quad \text{(Eq. 4-6)}$$

where J_r and J_a represent joint wall roughness and joint wall alteration, respectively.

Based on the photos provided by GeoEngineers (2005) (Figure 3-2), the rock formation was assessed with open joints/fissures. This assessment yields a joint wall roughness (J_r) value that is equal to 1.0. The joint alteration number was considered to be the average value for the joint separation of 1 mm to 5 mm (J_a =6.0). The values of joint

alteration numbers are provided in Table A-4. The discontinuity shear strength number of the Priest Rapids project site was estimated to be K_d=0.167.

- Orientation and shape number (J_s)

The orientation and shape number depends on the structure and orientation of the rock formation joints. The GeoEngineers (2005) reported that the rock formation joints at the project site are nearly horizontal and gently dip southeast in the direction of flow. Since there is not enough information available regarding the ratio of joint spacing, the average value is considered here. Using Table A-5, the orientation number is estimated to be equal to 1.3.

The erodibility index of the rock mass formation at the Priest Rapids Dam site project can now be determined using:

$$K = M_s \,.K_b \,.K_d \,.J_s \qquad \text{(Eq. 4-7)}$$

Using the values obtained above, the erodibility index of the rock formation is K=364. Moreover, the minimum erodibility index of the Priest Rapids rock formation was determined to be K_{min}=146.

4.1.2. Developing the Prototype Erodibility Index Plot

The second step is to use the model length scale in order to upscale the erodibility index of the weakly cohesive substrates to the prototype. To do this, the critical stream power of the simulated bedrock mixture is upscaled to the prototype using (Eq. 4-6), and the associated erodibility index is subsequently determined using (Eqs. 4-7 and 4-8).

$$P_{c-proto} = P_{c-model} \times length\ scale^{1.5} \qquad \text{(Eq. 4-6)}$$

$$P_c = 0.48\,K^{0.44} \quad \text{for} \quad K \leq 0.1 \qquad \text{(Eq. 4-7)}$$

$$P_c = K^{0.75} \quad \text{for} \quad K > 0.1 \qquad \text{(Eq. 4-8)}$$

Table 4-2 shows the calculation for the Priest Rapids project for the 1:64 Froude scale laboratory model. The erodibility index of the mixture that is associated with the prototype was plotted against the bentonite clay content (Figure 4-1), and the strength of the prototype rock formation (See Section 4.1.1) was identified (dashed line). Then, the appropriate bentonite clay content of the mixture to simulate the strength of the prototype rock formation for use in the 1:64 scale model was determined (6.70%-9.25%). The mixtures containing higher and lower percentages of bentonite clay contents are labeled as not erodible enough and too erodible, respectively. The use of mixtures with bentonite clay contents outside of the appropriate BCC zone yields unrealistic results.

Table 4-2. Erodibility index of the simulated bedrock-model and prototype value (Priest Rapids Project)

Mixture	**Material (%)**			$\tau_{cr\text{-}m}$ (Pa)	$P_{cr\text{-}m}$ (KW/m^2)	K_{model}	$P_{cr\text{-}p}$ (KW/m^2)	K_{proto}
	Gravel	**Bentonite**	**Water**					
GB-15	89.45%	3.85%	6.70%	23.05	0.0275	0.0015	14.1	33.95
GB-14	87.52%	5.78%	6.70%	34.42	0.0501	0.0059	25.7	75.75
GB-13	85.60%	7.70%	6.70%	65.14	0.1306	0.0519	66.8	271.29
GB-12	83.68%	9.62%	6.70%	75.10	0.1616	0.0843	82.8	360.62
GB-16	81.75%	11.55%	6.70%	105.33	0.2685	0.1732	137.4	709.32

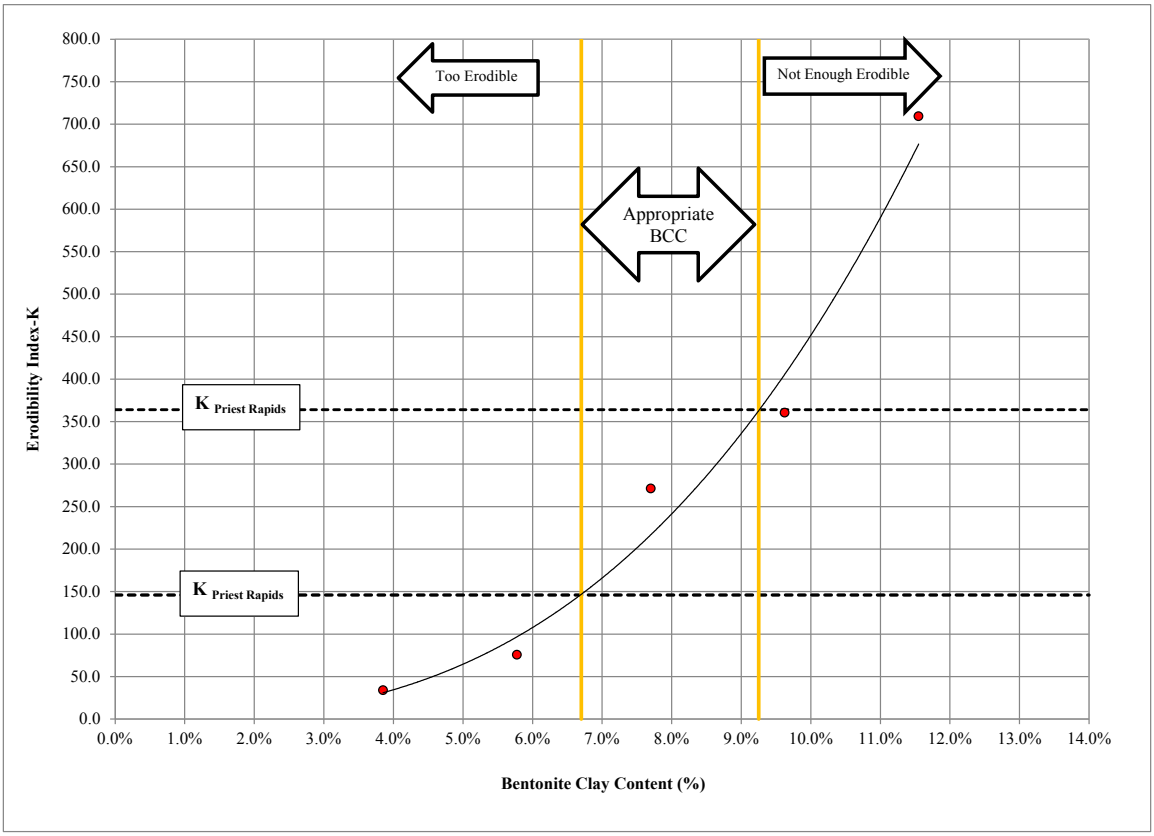

Figure 4-1. Erodibility index of the mixtures (prototype value) against the bentonite clay content (Priest Rapids Project)

4.1.3. Evaluating the Erodibility of the Selected Mixture

After examining the appropriate bentonite clay content zone for simulating the strength of the prototype rock, the selected mixture should be evaluated to ensure that the erosion process will occur in a reasonable timeframe in the scaled laboratory model. The selected mixture should be tested in the scaled laboratory model. To validate the mixture, the resultant model scour data should be verified with the field scour data, if there is any available.

For instance, in the case of the Priest Rapids dam scour tests, the final erodible mixture contained 7.70% bentonite clay which locates in the appropriate bentonite clay

content region (Figure 4-1) was evaluated in the model. The mixture was utilized in the 1:64 scale model to replicate an existing scour hole that occurred at the Priest Rapids dam project site (See Section 3.1.4). Figure 4-2 shows the existing scour hole at the downstream of the bay 22, resultant scour hole after the model test and the comparison between the two bathymetry datasets. The selected mixture containing 7.70% bentonite clay was able to replicate the existing scour hole observed at the project site. The scour hole reached the target scour depth of ~ 357.7 after 10.25 model hours. The mixture was able to simulate the scour hole shape and side slope similar to the prototype case.

Choosing mixture outside of the appropriate bentonite clay content yields to inaccurate results. Figure 4-3 shows pictures of the resultant model scour holes using various mixtures. Mixtures with low bentonite clay contents (Figure 4-3-a and b) are too erodible to replicate the scour hole shape and the mixture with high bentonite clay content (Figure 4-3-d) is not erodible enough and does not even reach the target scour depth.

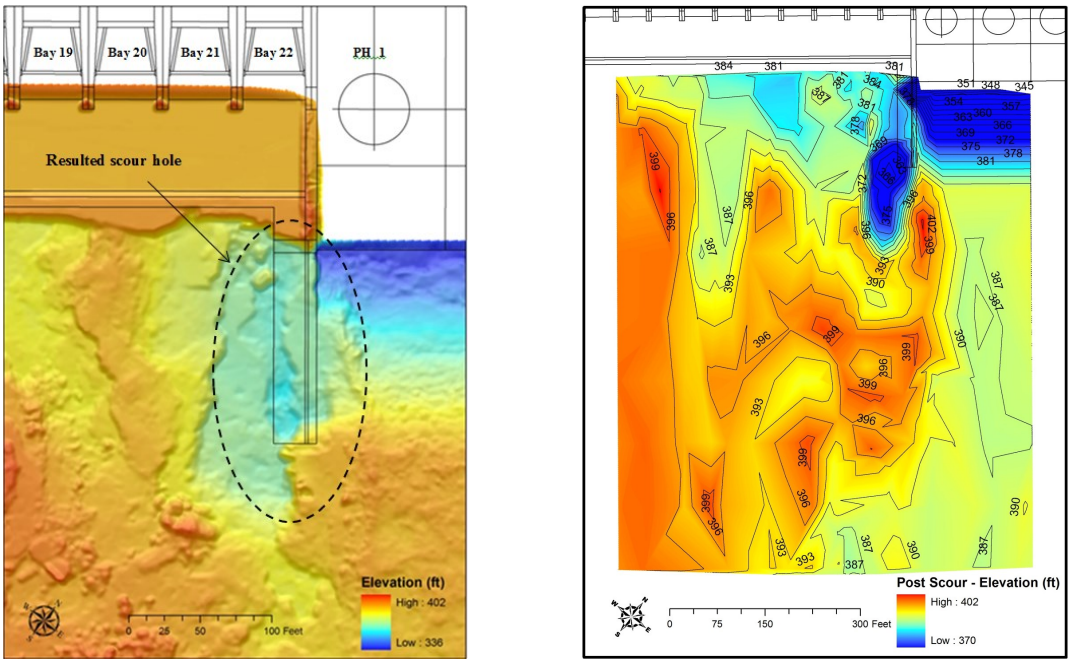

a) b)

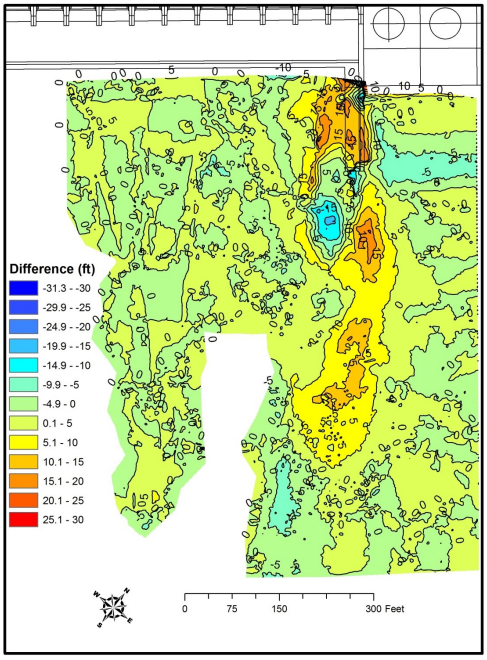

c)

Figure 4-2. Evaluating the selected mixture (7.7% BCC) for the Priest Rapids dam scour tests: a) Resultant scour hole (field dataset); b) Resultant scour hole (model dataset); c) Difference plot– final model bathymetry minus field bathymetry

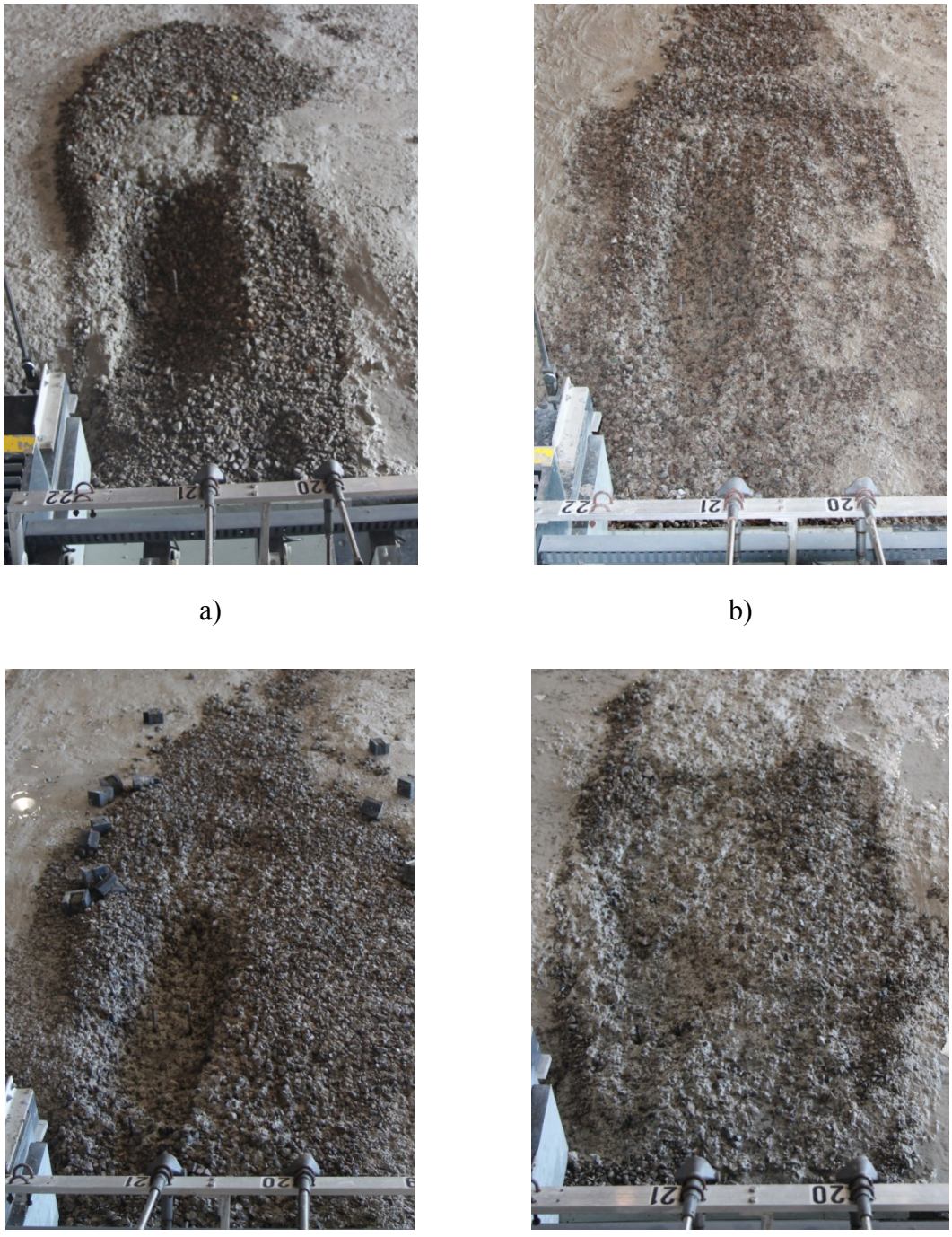

a) b)

c) d)

Figure 4-3. Resultant scour holes for the Priest Rapids dam full open gate 22 release for various mixtures: a) No Bentonite clay content (gravel only); b) 6.0% bentonite clay content; c)7.70% bentonite clay content; and d) 10.80% bentonite clay content

4.2. Brownlee Dam Rock Scour Simulation

The hydraulic model study of the Brownlee dam was conducted at the IIHR-Hydroscience & Engineering to investigate spillway deflector design to reduce total dissolved gas below the dam (Lyons and Weber, 2005). To investigate the scour potential downstream of the spillway for the Probable Maximum Flood (PMF) the tests were conducted in the 1:48 Froude scale model on a weakly cohesive substrate bed material. The simulated bedrock was a mixture of 3/8-inch crushed gravel, bentonite clay, and water. The erodible mixture contained 79.3% gravel and 11.1% bentonite clay.

The developed method in the current study was utilized to assess the appropriateness of the weakly cohesive mixture used for simulating the bedrock formation for the Brownlee dam project. Based on the available geology information of the project site (Stearns, 1954), the bedrock formation is very hard, fine grained, closely jointed basalt, with three joint sets and random fissures, dipping 13 degree towards west. The estimated erodibility index of the bedrock formation is ranging between 239 to 351.

After determining the erodibility index of the prototype rock formation, we use the model length scale in order to upscale the erodibility index of the weakly cohesive substrates to the prototype.

Table 4-2 shows the calculation for the Brownlee project for the 1:48 scale laboratory model. The erodibility index of the mixture that is associated with the prototype was plotted against the bentonite clay content (Figure 4-4), and the strength of the prototype rock formation was identified (dashed line). Then, the appropriate bentonite clay content of the mixture to simulate the strength of the prototype rock formation for use in the 1:48 scale model was determined (9.75%-11.25%). The mixtures

containing higher and lower percentages of bentonite clay contents are labeled as not erodible enough and too erodible, respectively.

It is observed that the chosen mixture containing 11.1% bentonite clay is within the appropriate bentonite clay content zone.

Table 4-3. Erodibility index of the simulated bedrock-model and prototype value (Brownlee Project)

Study	Sample	Material (%)			$\tau_{cr\text{-}m}$ (Pa)	$P_{cr\text{-}m}$ (kW/m^2)	K_{model}	$P_{cr\text{-}p}$ (kW/m^2)	K_{proto}
		Gravel	Bentonite	Water					
Currnet Study	GB-15	89.5%	3.9%	6.7%	23.05	0.0275	0.0015	9.1	19.10
	GB-14	87.5%	5.8%	6.7%	34.42	0.0501	0.0059	16.7	42.61
	GB-13	85.6%	7.7%	6.7%	65.14	0.1306	0.0519	43.4	152.60
	GB-12	83.7%	9.6%	6.7%	75.10	0.1616	0.0843	53.8	202.85
	GB-16	81.8%	11.6%	6.7%	105.33	0.2685	0.1732	89.3	398.99

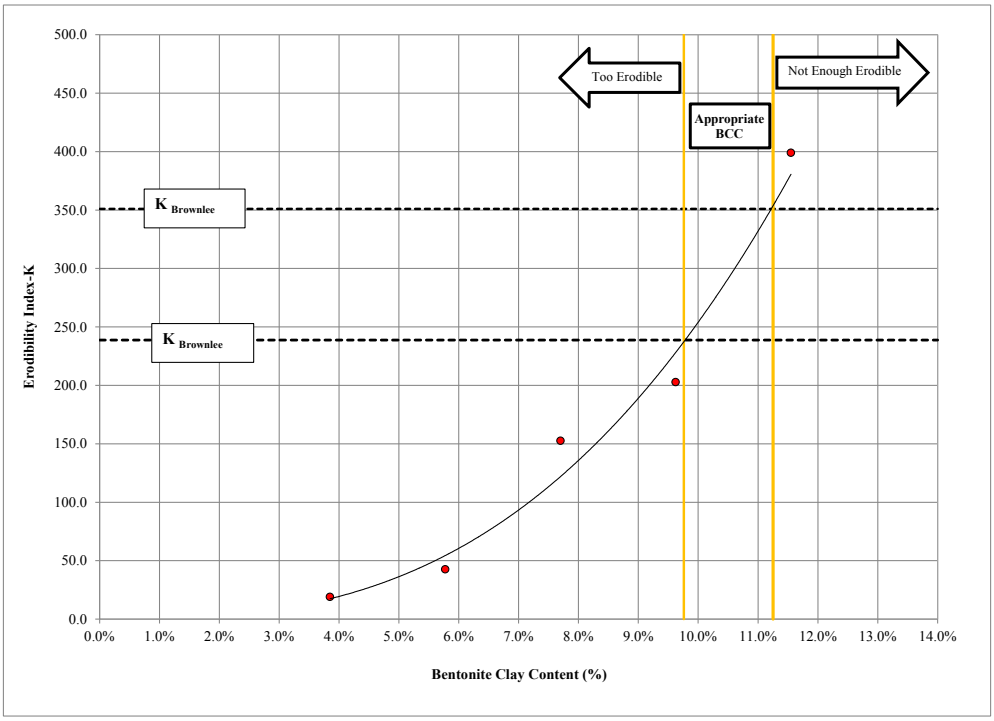

Figure 4-4. Erodibility index of the mixtures (prototype value) against the bentonite clay content (Brownlee Project)

4.3. Summary

This chapter explained the method to simulate the prototype bed rock formation to use in the laboratory analog models. A step-by-step method was developed to determine the appropriate combination of weakly cohesive substrate in order to simulate the strength of the prototype bedrock. The method is based on the Annandale's erodibility index method and requires information about the prototype bedrock strength (erodibility index). The method is explained in conjunction with the Priest Rapids Dam project example. The method's reliability depends on the reasonable estimation of the prototype rock strength. It should be noted that it is reasonable to choose a more erodible mixture within the appropriate zone in order to expedite the scour test and eliminate the hindrance of time.

CHAPTER 5 SUMMARY, CONCLUSION AND FUTURE WORKS

5.1. Summary and Conclusion

The rock scour that occurs downstream of a dam as a result of a high velocity impinging jet is a very complex, three-dimensional process. Underestimating the process may compromise a dam's stability and structural integrity and threaten public safety. Moreover, it can endanger the stability of the downstream river bed and side slope. Therefore, having deeper insight into the key mechanisms of the rock scour process is crucial in terms of predicting its extent. While hydraulic laboratory models have proven to be reliable tools for investigating hydraulic and sedimentology processes, conducting a rock scour study using laboratory models poses some challenges. A weakly cohesive substrate (i.e., a mixture of granular sediment and cohesive additive) has been employed to investigate the rock scour process (i.e., Johnson, 1977; Shepherd and Schumm, 1974; Wohl and Ikeda, 1997). These studies have all used a bedrock formation that was simulated using a trial and error method to produce a substrate that qualitatively represents the rock formation. There has not yet been a robust study to systematically scale down the strength of the prototype rock for use in laboratory models.

The main objective of the present experimental study was to develop a method to systematically and dynamically simulate the jointed rock formation for use in the laboratory analog scaled models.

As part of the current study, we investigated the scour process downstream of the Priest Rapids dam with laboratory scaled models that used a weakly cohesive substrate. This project is part of a series of projects at IIHR, which is sponsored by the Public Utility District No. 2 of Grant County, Ephrata, Washington (GCPUD), to investigate

juvenile salmonid migration at the Wanapum/Priest Rapids Development. As part of the last phase of the project, it was crucial to determine the effect of the newly-designed fish bypass system on the downstream rock foundation scour. To assess the scour downstream of the dam, we used the 1:64 Froude scale tailrace model of the dam.

To simulate the bedrock formation downstream of the Priest Rapids dam, we added bentonite clay to gravel and water and tested it in a series of experiments that were designed to ascertain the appropriate mixture by replicating an existing scour hole downstream of the dam. The appropriate weakly cohesive substrate was determined to be 9 parts gravel to 1 part bentonite clay and 1 part water by volume (85.60% Gravel, 7.70% bentonite Clay, and 6.70% water by weight). After identifying the appropriate mixture, we utilized it in the model in order to evaluate the scour potential downstream of the fish bypass units and under the PMF condition.

This trial and error method to establish an appropriate mixture is problematic since several attempts must be made to determine the proper combination of gravel, bentonite clay, and water. This process is also costly and time consuming, especially in the case of large scale models. Moreover, the applicability of the method would be questionable when there is not enough information or a past data set that can be used as a baseline (witness) test. Consequently, this suggests the need to develop a systematic method to scale down the strength of the rock formation for use in the laboratory models.

To develop this method, we used the vertical JET device to test various combinations of gravel, bentonite clay, and water and examined the critical stress of the mixtures. The results revealed that the resistance of the mixture to erosion primarily depends on the bentonite clay content (i.e., the adhesive part of the mixture). It should be

noted, however, that the gravel size distribution (i.e., the non-cohesive part) does affect the critical stress of the mixture, but it is negligible compared to the role of the cohesive part (bentonite clay). Also, the selection of the appropriate gravel size distribution depends upon the rock's characteristics at the project site.

We then developed the threshold relationship of the erosion for the weakly cohesive substrates. This relationship was similar to the one presented by Annandale (1995) for the earth material. We also employed Annandale's erodibility index technique in order to develop a method to scale down the strength of the prototype bedrock.

We subsequently introduced a step-by-step procedure to systematically simulate the prototype rock formation for use in the laboratory analog scour models. As an example, we described the procedure to choose an appropriate weakly cohesive substrate for the Priest Rapids project. The appropriate mixture for the Priest Rapids project site was found to contain (6.70%-9.25%) bentonite clay, which agrees with the mixture established by the trial and error method (7.7% bentonite clay).

The main findings of this experimental study can be summarized as follows:

1- The prototype rock formations can be modeled using a weakly cohesive substrate to investigate the rock scour process in laboratory models.
2- The weakly cohesive substrate can simulate the scour mechanisms in a jointed rock mass formation.
3- A step-by-step method was developed to assist with scaling the strength of the prototype rock formation by determining the appropriate combination of weakly cohesive substrate.

5.2. Recommendation for Future Works

As we investigated only one type of non-cohesive material in the current study, it would be interesting to explore the effects of gravel size distribution, uniformity, and angularity in future studies. While the erosional strength of the simulated rock mixture correlates with the characteristics of the non-cohesive component, its impact is less significant compared to the cohesive component's impact. Investigating the effects of the other properties of the non-cohesive component enables the development of nomographs that will be used according to the properties of the prototype rock mass formation (i.e., block size).

The weakly cohesive substrate developed in the current study (a combination of gravel, bentonite clay, and water) replicates a jointed rock mass formation. Adding sand to the mixture fills the existing voids and creates a more homogenous structure in the substrate that can replicate jointed and intact rock mass formations. Therefore, the study of a weakly cohesive substrate containing sand should be conducted.

The preliminary results of this study reveals that the friction coefficient value used by Hanson and Cook (2004) to determine the stress of the jet is low, and an argument was made that the value can be an order of magnitude larger. Since the JET device method is being extensively used to determine the erodibility of cohesive soils, it is necessary to re-evaluate the coefficient. Consequently, an experimental study to determine the friction coefficient of submerged impinging jet acting on a soil sample should be conducted.

APPENDIX A

ERODIBILITY INDEX METHOD TABLES

Table A-1. Mass strength number for rock (M_s) (Annandale, 1995)

Hardness	Identification in Profile	Unconfined Compressive Strength (MPa)	Mass Strength Number (M_s)
Very soft rock	Material crumbles under firm (moderate) blows with sharp end of geological pick and can be peeled off with a knife; is too hard to cut triaxial sample by hand.	Less than 1,7 1,7 - 3,3	0,87 1,86
Soft rock	Can just be scraped and peeled with a knife; indentations 1 mm to 3 mm show in the specimen with firm (moderate) blows of the pick point.	3,3 - 6,6 6,6 - 13,2	3,95 8,39
Hard rock	Cannot be scraped or peeled with a knife; hand-held specimen can be broken with hammer end of geological pick with a single firm (moderate) blow.	13,2 - 26,4	17,70
Very hard rock	Hand-held specimen breaks with hammer end of pick under more than one blow.	26,4 - 53,0 53,0 - 106,0	35,0 70,0
Extremely hard rock	Specimen requires many blows with geological pick to break through intact material.	Larger than 212,0	280,0

Table A-2. Rock joint set number (J_n) (Annandale, 1995)

Number of Joint Sets	Joint Set Number (J_n)
Intact, no or few joints/fissures	1,00
One joint/fissure set	1,22
One joint/fissure set plus random	1,50
Two joint/fissure sets	1,83
Two joint/fissure sets plus random	2,24
Three joint/fissure sets	2,73
Three joint/fissure sets plus random	3,34
Four joint/fissure sets	4,09
Multiple joint/fissure sets	5,00

Table A-3. Joint roughness number (J_r) (Annandale, 1995)

Joint Separation	Condition of Joint	Joint Roughness Number
Joints/fissures tight or closing during excavation	Discontinuous joints/fissures Rough or irregular, undulating Smooth undulating Slickensided undulating Rough or irregular, planar Smooth planar Slickensided planar	4,0 3,0 2,0 1,5 1,5 1,0 0,5
Joints/fissures open and remain open during excavation	Joints/fissures either open or containing relatively soft gouge of sufficient thickness to prevent joint/fissure wall contact upon excavation. Shattered or micro-shattered clays	1,0 1,0

Table A-4. Joint alteration number (J_a) (Annandale, 1995)

Description of Gouge	Joint Alteration Number (J_a) for Joint Separation (mm)		
	1,0[1]	1,0 - 5-0[2]	5,0[3]
Tightly healed, hard, non-softening impermeable filling	0,75	-	-
Unaltered joint walls, surface staining only	1,0	-	-
Slightly altered, non-softening, non-cohesive rock mineral or crushed rock filling	2,0	2,0	4,0
Non-softening, slightly clayey non-cohesive filling	3,0	6,0*	10,0*
Non-softening, strongly over-consolidated clay mineral filling, with or without crushed rock	3,0*	6,0**	10,0
Softening or low friction clay mineral coatings and small quantities of swelling clays	4,0	8,0*	13,0*
Softening moderately over-consolidated clay mineral filling, with or without crushed rock	4,0*	8,0**	13,0
Shattered or micro-shattered (swelling) clay gouge, with or without crushed rock	5,0*	10,0**	18,0

Note: 1. Joint walls effectively in contact.
2. Joint walls come into contact after approximately 100 mm shear.
3. Joint walls do not come into contact at all upon shear.
4. * Values added to Barton et al's data.
5. ** Also applies when crushed rock occurs in clay gouge without rock wall contact.

Table A-5. Orientation and shape number (J_s) (Annandale, 1995)

Dip Direction of Closer Spaced Joint Set (degrees)	Dip Angle of Closer Spaced Joint Set (degrees)	Ratio of Joint Spacing, r			
		1:1	1:2	1:4	1:8
180/0	90	1,14	1,20	1,24	1,26
In direction of stream flow	89	0,78	0,71	0,65	0,61
	85	0,73	0,66	0,61	0,57
	80	0,67	0,60	0,55	0,52
	70	0,56	0,50	0,46	0,43
	60	0,50	0,46	0,42	0,40
	50	0,49	0,46	0,43	0,41
	40	0,53	0,49	0,46	0,45
	30	0,63	0,59	0,55	0,53
	20	0,84	0,77	0,71	0,67
	10	1,25	1,10	0,98	0,90
	5	1,39	1,23	1,09	1,01
	1	1,50	1,33	1,19	1,10
0/180	0	1,14	1,09	1,05	1,02
Against direction of stream flow	-1	0,78	0,85	0,90	0,94
	-5	0,73	0,79	0,84	0,88
	-10	0,67	0,72	0,78	0,81
	-20	0,56	0,62	0,66	0,69
	-30	0,50	0,55	0,58	0,60
	-40	0,49	0,52	0,55	0,57
	-50	0,53	0,56	0,59	0,61
	-60	0,63	0,68	0,71	0,73
	-70	0,84	0,91	0,97	1,01
	-80	1,26	1,41	1,53	1,61
	-85	1,39	1,55	1,69	1,77
	-89	1,50	1,68	1,82	1,91
180/0	-90	1,14	1,20	1,24	1,26

Notes: 1. For intact material take $K_s = 1,0$
2. For values of r greater than 8 take K_s as for r = 8

Table A-6. Mass strength number for granular sediment (M_s) (Annandale, 1995)

Consistency	Identification in Profile	SPT Blow Count	Mass Strength Number (M_s)
Very loose	Crumbles very easily when scraped with geological pick	0-4	0,02
Loose	Small resistance to penetration by sharp end of geological pick	4-10	0,04
Medium dense	Considerable resistance to penetration by sharp end of geological pick	10-30	0,09
Dense	Very high resistance to penetration of sharp end of geological pick - requires many blows of pick for excavation	30-50	0,19
Very dense	High resistance to repeated blows of geological pick - requires power tools for excavation	50-80	0,41

APPENDIX B

CRITICAL STRESS OF THE SIMULATED BEDROCK MIXTURES

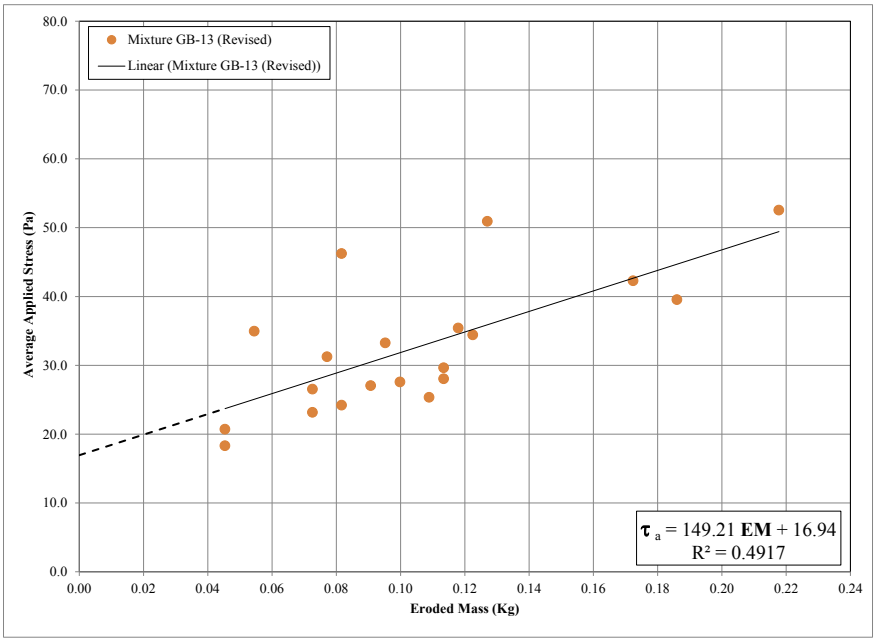

Figure B-1. Eroded mass vs. average applied stress for mixture GB-13

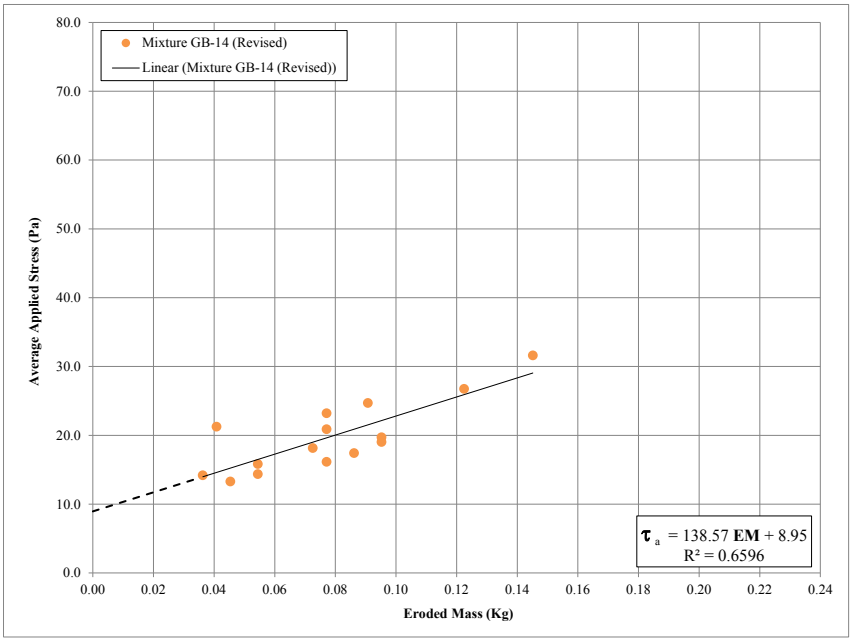

Figure B-2. Eroded mass vs. average applied stress for mixture GB-14

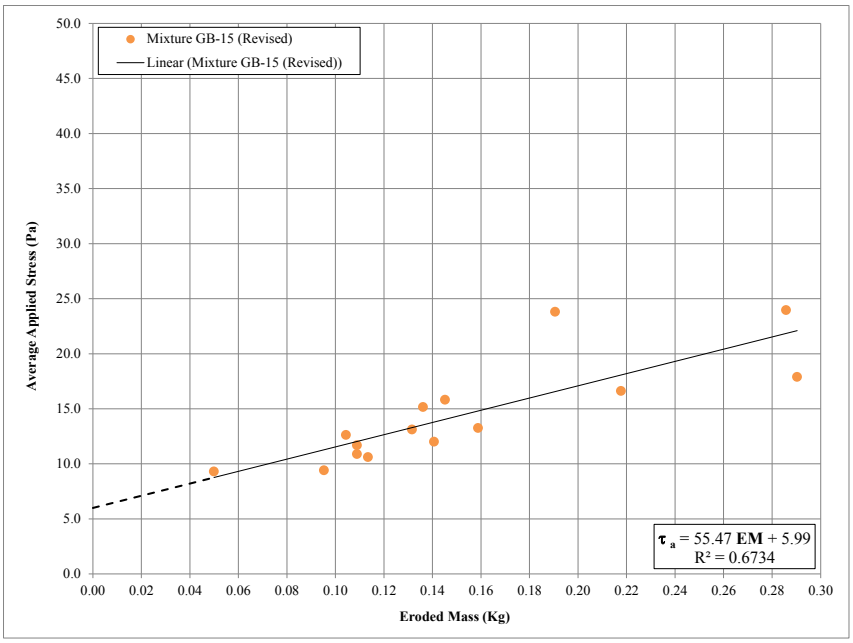

Figure B-3. Eroded mass vs. average applied stress for mixture GB-15

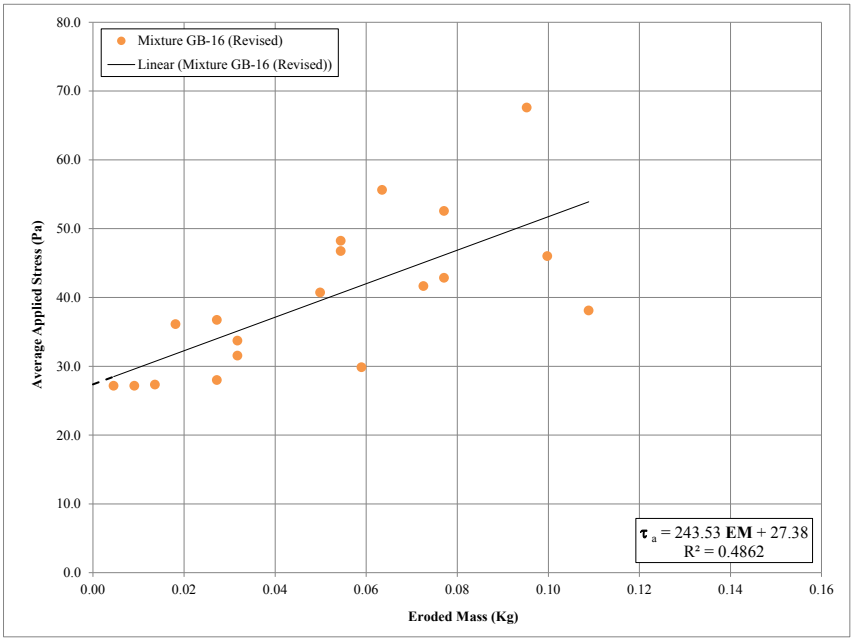

Figure B-4. Eroded mass vs. average applied stress for mixture GB-16

REFERENCES

Akhmedov, T. K. (1988). Calculation of the depth of scour in rock downstream of a spillway. *International Water and Power and Dam Construction, 40*(12), 25-27.

Albertson, M. L., Dai, Y. B., Jenson, R. A., & Rouse, H. (1950). Diffusion of submerged jets. *Proceedings ASCE*, *74*.

Annandale, G. W. (1995). Erodibility. *Journal of Hydraulic Research, 33*(4), 471-494. doi:10.1080/00221689509498656.

Annandale, G. W. (2006). *Scour Technology.* New York: McGraw-Hill.

Annandale, G. W. (2007). Current state-of-the-art rock scouring technology. *Geotechnics of Soil Erosion*, (pp. 1-12). doi:10.1061/40911(230)2.

Atkinson, B. K. (1987). *Fracture mechanics of rock.* Orlando, Florida: Academic Press Inc.

Barani, G., Kamalipoor Azad, Z., & Torbati, M. (2008). Scour resistance simulation of stone materials using hydraulic modeling, Case study: Plunge pool of Karoon-III Dam. *Iran Water Resources Research, 4*(1), 40-49.

Beltaos, S., & Rajaratnam, N. (1973). Plane turbulent impinging jets. *Journal of Hydraulic Research, 11*(1), 29-59.

Beltaos, S., & Rajaratnam, N. (1974). Impinging circular turbulent jets. *Journal of the Hydraulic Division, 100*(HY10), 1313-1328.

Blaisdell, F. W., Clayton, L. A., & Hebaus, G. G. (1981). Ultimate dimenssion of local scour. *Journal of Hydraulic Division, 107*(HY3), 327-337.

Bollaert, E. (2002). *Transient water pressures in joints and formation of rock scour due to high-velocity jet impact.* Ph.D. Dissertation, Ecole Polytechnique Fédérale de Lausanne, Lausanne.

Bollaert, E. (2010). Physics of rock scour: the power of the bubble. *International Conference on Scour and Erosion 2010 (ICSE-5)*, (pp. 21-40). San Francisco, CA.

Bollaert, E., & Schleiss, A. (2001). A new approach for better assessment of rock scouring due to high velocity jets at dam spillways. *The 5th ICOLD European Symposium.* Geiranger, Norway.

Bollaert, E., & Schleiss, A. (2003). Scour of rock due to the impact of plunging high velocity jets Part I: A state-of-the-art review. *Journal of Hydraulic Research, 00*(0), 1-14.

Bormann, E., & Julien, P. Y. (1991). Scour downstream of grade-control structures. *Journal of Hydraulic Engineering, 117*(5), 579-594.

Breusers, H., & Raudkivi, A. J. (1991). *Scouring.* Rotterdam, Netherlands: A.A. Balkema.

Briaud, J. L., Ting, F., Chen, H. C., Cao, Y., Han, S. W., & Kwak, K. (2001). Erosion Function Apparatus for scour rate predictions. *Journal of Geothechnical and Geoenvironmental Engineering, 127*(2), 105-113.

Bribiesca, S. J., & Viscaino, A. C. (1973). Turbulent effects on the lining of stilling basin. *ICOLD 11th Congress*, *2*, pp. 1575-1592.

Chatanantavet, P. (2007). *Physically-based models of bedrock incision processes in mountain streams.* Ph.D. Dissertation, University of Minnesota.

Chee, S. P., & Yuen, E. M. (1985). Erosion of unconsolidated gravel beds. *Canadian Journal of Civil Engineering, 12*, 559-566.

Cola, R. (1965). Energy dissipation of a high-velocity jet entering a basin. *Proceedings of the 11th Congress of the IAHR.* Leningard.

Cossette, D., Mazurek, K., & Rennie, C. (2012). Critical shear stress from varied method of analysis of a submerged circular turbulent impinging jet test for determining erosion resistance of cohesive soils. *The Sixth International Conference on Scour and Erosion (ICSE-6)*, (pp. 11-18). Paris.

D698-07, A. S. (2007). *Standard test methods for laboratory compaction characteristics of soil using standard effort.* West Conshohocken, PA: ASTM International.

Ervine, D. A., & Falvey, H. R. (1987). Behavior of turbulent jets in the atmosphere and in plunge pools. *Proceedings of the Institution of Civil Engineers*, *83*, pp. 295-314.

Ervine, D. A., Falvey, H. R., & Withers, W. (1997). Pressure fluctuations on plunge pool floors. *Journal of Hydraulic Research, 35*(2).

GeoEngineers, Inc. (2005). *Geologic and underwater video consultation service. Priest Rapids juvenile fish bypass system, Priest Rapids Project.*

Gleason, M. H., Daniel, D. E., & Eykholt, G. R. (1997). Calcium and sodium bentonite for hydraulic containment application. *Journal of Geothechnical and Geoenvironmental Engineering, 123*(5), 438-445.

Grim, R., & Guven, N. (1978). *Bentonites: geology, mineralogy, properties and uses.* New York, N.Y.: Elsevier Science Publishing Co., Inc.

Hanson, G. J. (1990). Surface erodibility of earthen channels at high stresses: Part I-Open channel testing. *Transaction of the ASAE, 33*(1), 127-131.

Hanson, G. J. (1991). Development of a jet index to characterize erosion resistance of soils in earthern spillways. *Transaction of the ASCE, 33*(1), 2015-2020.

Hanson, G. J., & Cook, K. R. (1997). Development of excess shear stress parameters for circular jet testing. *ASAE Annual International Meeting.* Minneapolis, Minnesota.

Hanson, G. J., & Cook, K. R. (2004). Apparatus, test procedures, and analytical methods to measure soil erodibility in situ. *Applied Engineering in Agriculture, 20*(4), 455-462.

Hanson, G. J., & Hunt, S. L. (2007). Lessons learned using laboratory JET method to measure soil erodibility of compacted soils. *Applied Engineering in Agriculture, 23*(3), 305-312.

Hanson, G. J., Robinson, K. M., & Temple, D. M. (1990). Pressure and stress distributions due to a submerged impinging jet. *Proceeding of 1990 National Conference, Hydraulic Engineering American Society of Civil Engineers*, (pp. 525-530).

Hartung, F., & Hausler, E. (1973). Scours, stilling basins and downstream protection under free overfall jets at dams. *Proceedings of the 11th Congress on Large Dams*, (pp. 39-56). Madrid, Spain.

Harza Engineering Company. (1959). *Priest Rapids hydroelectric project, Wanapum development, geologic graphic core logs.*

Homma, M. (1953). An experimental study on water fall. *Proceedisngs of the Minnesota International Hydraulic Conference.* Minnesota, USA.

Johnson, G. (1977). Use of a weakly cohesive material for scale model scour studies in flood spillway design. *17th Congress of the IAHR*, *4.* Baden-Baden.

Kirsten, H. (1982). A classification system for excavation in natural materials. *The Civil Engineer in South Africa*, 292-308.

Lyons, T. C., & Weber, L. J. (2005). *Hydraulic modeling for Brownlee dam spillway deflector design: Phase two- 3D model.* Limited Distribution Report No. 328. IIHR-Hydroscience & Engineering, the University of Iowa.

Mackin, H. J. (1961). *A stratigraphic section in the Yakima Basalt and the Ellensburg Formation in South-Central Washington.* Washington Division of Mines and Geology.

Mason, P., & Arumugam, K. (1985). Free jet scour below dams and flip buckets. *Journal of Hydraulic Engineering, 111*(2), 220-235.

Mazurek, K. A. (2001). *Scour of clay by jets.* Ph.D. Dissertation, Department of Civila and Environmental Engineering, University of Alberta, Edmonton, Alberta.

Moore, W. L., & Masch, F. D. (1962). Experiments on the scour resistance of cohesive sediments. *Journal of Geophysical Research, 64*(4), 1437-1449.

Myers, G., Schauer, J., & Eustis, R. (1963). Plane Turbulent Wall Jet Flow Development and Friction Factor. *Journal of BAsic Engineering*, 47-53.

Papanicolaou, A. N., Elhakeem, M., & Hilldale, R. (2007). Secondary current effects on cohesive river bank erosion. *Water Resources Research, 43*(12), W12418.

Poreh, M., & Hefez, E. (1967). Initial scour and sediment motion due to an impinging submerged jet. *Proceedings of the 12th IAHR Congress.* Fort Collins.

Rajaratnam, N. (1981). Erosion by plane turbulent jets. *Journal of Hydraulic Research, 19*(4), 339-358.

Ramos, C. (1982). Energy dissipation on free jet spillways. Bases for its study in hydraulic models. *Transaction of the International Symposium on the Layout of Dams in NArrow Gorges, ICOLD*, *1*, pp. 263-268. Rio de Janeiro, Brazil.

Schlichting, H., & Gersten, K. (2000). *Boundary Layer Theory.* Springer.

Schmitt, C. K., Guill, C., & Drossel, B. (2012). The robustness of cyclic dominance under random fluctuations. *Journal of Theoretical Biology, 308*, 79-87.

Schumm, S. A., Paul Mosley, M., & Weaver, W. (1987). *Experimental fluvial geomorphology.* New York: John Wiley and Sons.

Shepherd, R., & Schumm, S. (1974). Experimental study of river incision. *Geological Society of America Bulletin, 85*, 257-268. doi:10.1130/0016-7606(1974)85<257:ESORI>2.0.CO;2

Standard, A. (1995). *Measurement of fluid in pipes using orifice, nozzle, and venturi.* The American Society of Mechanical Engineers, ASME MFC-3M-1989, Reaffirmed 1995.

Stearns, H. T. (1954). *Geology of the Brownlee damsite Snake River, Idaho-Oregon.* Hope, Idaho.

Stein, O. R., Julien, P. Y., & Alonso, C. V. (1993). Mechanics of jet scour downstream of a headcut. *Journal of Hydraulic Research, 31*(6), 723-738.

Tetra Tech Inc. (2010). *Final survey report: Multibeam sonar bathymetry survey report Wanapum and Priest Rapids Dam, Grant County, Washington.*

Thompson, D., & Wohl, E. E. (2013). Flume experimentation and simulation of bedrock channel processes. In K. J. Tinkler, & E. E. Wohl (Eds.), *Rivers Over Rock: Fluvial Processes in Bedrock Channels* (pp. 279-296). Washington, D. C.: American Geophysical Union. doi:10.1029/GM107p0279.

Van Schalkwyk, A., Jordaan (Jnr.), J. M., & Dooge, N. (1994). Erosion of rock in unlined spillways. *International Commission on Large Dams*, (pp. 555-572). Paris, France.

Wahl, T. L. (2010). Relating HET and JET test results to internal erosion field tests. *Joint Federal Interagency Conference on Sedimentation and Hydrologic Modeling.* Las Vegas, NV.

Wan, C. F., & Fell, R. (2002). *Investigation of internal erosion and piping of soils in embankment dams by the Slot Erosion Test and Hole Erosion Test.* The University of New South Wales, Sydney, Australia.

Whittaker, J. G., & Schleiss, A. (1984). *Scour related to energy dissipators for high head structures.* Zürich.

Wohl, E. E., & Ikeda, H. (1997). Experimental simulation of channel incision into a cohesive substrate at varying gradients. *Geology, 25*, 295-298. doi:10.1130/0091-7613(1997)025<0295:ESOCII>2.3.CO;2